Assessment of Mission Design Including Utilization of Libration Points and Weak Stability Boundaries

Authors: Franco Bernelli Zazzera, Francesco Topputo, Mauro Massari.
Academic Institution: Dipartimento di Ingegneria Aerospaziale, Politecnico di Milano.
Approved by: Dario Izzo, Advanced Concepts Team (ESTEC)

Contacts:

Franco Bernelli Zazzera
Tel: +39-02-23998328
Fax: +39-02-23998334
e-mail: franco.bernelli@polimi.it

Dario Izzo
Tel: ++31 (0)71565 – 3511
Fax: ++31 (0)71565 – 8018
e-mail: act@esa.int

Ariadna id: 03/4103
Study length: 2 months.
Contract Number: 18147/04/NL/MV

Available on the ACT net (www.esa.int/act)

Contents

List of Figures

List of Tables

List of Symbols and Acronyms

Symbols

ΔV	Instant velocity variation
Δt	Time interval
$\Phi(\mathbf{x}, t)$	Flow associated to the initial condition $\mathbf{x}$ at the time t
μ	Mass parameter of the three-body system
$\lambda_{s,u}$	Stable and unstable eigenvalues
A_x	Halo in-plane x-amplitude
A_y	Halo in-plane y-amplitude
A_z	Halo out-of-plane z-amplitude
C	Jacobi constant
M	Monodromy matrix
T	Orbital period
h	Altitude of a circular Earth's orbit
i	Inclination of an Earth's orbit
k	Gravitational constant
l	Distance between the primaries
$m_{1,2}$	Masses of the primaries
n	Angular velocity of the primaries
$\mathbf{v_{s,u}}$	Stable and unstable eigenvectors

Acronyms

2PBVP	Two-Point Boundary Value Problem
3BP	Three-Body Problem
CR3BP	Circular Restricted Three-Body Problem
EML1	Earth-Moon $L1$
EML2	Earth-Moon $L2$
EMrf	Earth-Moon rotating frame
ER3BP	Elliptic Restricted Three-Body Problem
GEO	Geostationary Earth Orbit
GTO	Geostationary Transfer Orbit
HEO	High Earth Orbit
LEO	Low Earth Orbit
L3BP	Lambert's Three-Body Problem
MJD	Modified Julian Date
R3BP	Restricted Three-Body Problem
SEL1	Sun-Earth $L1$
SEL2	Sun-Earth $L2$
SErf	Sun-Earth rotating frame
SJrf	Sun-Jupiter rotating frame
SMrf	Sun-Mars rotating frame
SVrf	Sun-Venus rotating frame
TCM	Trajectory Correction Manoeuvre

Abstract

This work has been carried out in a two-month study (from April to June 2004) within the Ariadna context, under ESA contract, with the intention to assess the uses of the libration points and generic non-linear chaotic trajectories for space applications.

In this study several possibilities for the exploitation of the libration points dynamics for space missions are given. The spatial circular restricted three-body problem has been used to evaluate the performances of the proposed concepts. This model presents a high non-linear behavior, a chaotic dynamics and does not allow any analytic solution. Therefore, the approach to the problem has followed the dynamical system theory and the invariant manifolds technique since they provide for additional structures within the restricted problem.

Missions to the halo orbits about both the Sun-Earth and Earth-Moon system, interplanetary, lunar and generic orbital transfers have been analyzed. Since a systematic approach to the design of libration point missions does not exist, the mathematical tools necessary to analyze these space applications have been developed within this work. Then, based on the results obtained for each application, some considerations from the authors' point of view are given about the potential use for future space missions. Finally, some implications of these trajectories upon the whole space system are discussed together with the possible drawbacks associated to this kind of missions.

Introduction

This work has been carried out in a two-month study (from April to June 2004) within the Ariadna context, under ESA contract, with the intention to assess the uses of the libration points and generic non-linear chaotic trajectories for space applications.

In the last years, the interest concerning the libration points for space applications has risen within the scientific community. This is because the libration points, natural equilibrium solutions of the restricted three-body problem (R3BP), offer the unique possibility to have a fixed configuration with respect to two primaries. Therefore, a libration point mission could fulfill a lot of mission constraints that are not achievable with the classical Keplerian two-body orbits. Moreover, exploiting the stable and unstable part of the dynamics concerning these equilibria, low-energy interplanetary, lunar, moon-to-moon transfers of practical interest can be obtained.

Although several n-body models are available in literature, in this work the *spatial* and *circular* restricted three-body problem has been assumed to study the features of the libration point missions. This model, that takes into account two gravitational attractions acting simultaneously upon the spacecraft, turns out to be very appropriate for the preliminary analysis since the libration points are defined in this frame with autonomous equations of motion.

Nevertheless, in the step from the two-body to the three-body problem, some "information" concerning the motion are lost since in this new model the orbital elements, integral of motion for conic orbits, no longer exist. In the R3BP, the only constant available is the Jacobi integral that represents a constraint, as the conservation of the energy, for the states of the problem. But, only one fixed parameter with respect to six states makes the problem difficult to treat.

Associated to the equilibrium points and to the periodic orbits around them, there is a family of *invariant manifolds*, stable and unstable, that replaces the lost information: in the phase space, the invariant manifolds provide for additional structures that may be exploited in the R3BP frame

and applied in order to design trajectories for future space missions.

The trajectories obtained within the R3BP turn out to be accurate first guess solutions for the estimations of the mission performances. Anyway, the authors want to stress that all the results presented throughout this report need to be corrected in more refined models that take into account second order effects as the eccentricity of the orbits, the perturbations of other bodies and the solar wind.

The first chapter presents a qualitative description of the dynamics, the libration points, the halo orbits and the invariant manifolds of the R3BP. These concepts are further analyzed, from a computational point of view, in the second chapter. Here, the method that allows to obtain generic halo orbits is given together with a deep investigation on their parameters (i.e. amplitudes and period). Then, the developed method for the solution of the Lambert's three-body problem is presented in the last section.

The main part of the present report is enclosed in chapters from 3 to 6. Here, four different uses of the libration points for space missions have been considered:

- *missions on orbits around $L1$ and $L2$ in the Sun-Earth system.* This chapter contains a qualitative study on the trajectories belonging to the stable manifolds associated to the halo orbits around $L1$ and $L2$. Even if a simplified approach has been undertaken, the results found within this model represent an important tool when some preliminary and accurate features concerning the transfer trajectories are needed (e.g. in a concurrent design environment);

- *missions on orbits around $L1$ and $L2$ in the Earth-Moon system.* Here a combined approach, based on the target of a piece of stable manifold by using a Lambert's arc, has been developed in order to design transfers to these halo. It has been found that cheaper and short-time transfers can be accomplished by starting from both GTOs and LEOs;

- *interplanetary missions through libration points.* In this context a model to link the inner planets with three-body trajectories is presented. The features of these transfers, with a special emphasis to trajectories to Venus and Mars, show that cheap interplanetary missions could reach these two planets. Nevertheless, the high times of transfer represent the main drawback for these possible missions;

- *missions to the Moon through the point $L1$.* These missions aim to reach the Moon with the lowest energy level allowed. The idea has been to pass through the small neck opened at $L1$ by targeting an arc of stable

manifold associated to $L1$. The results indicate that the Moon could be approached with very low-cost missions departing again from LEOs and GTOs.

Any of these chapters contains first an analysis of the actual state of the art, known to the authors, concerning both the concepts for future missions and the design of libration point trajectories. Then, the problem approach is shown and the tools necessary to analyze the missions are developed. Later, some considerations on the outcomes and the potential uses for space missions are given. The critical discussion concerns also the evaluation of the drawbacks associated to the applications and generic reflections at the whole system level.

The last chapter evaluates the possibility to use the non-linear Moon assisted trajectory for the common transfers between two orbits around the Earth. This approach aims to reduce the cost of these orbital manoeuvres and can be used to provide for a transfer after a launch failure or in recovery conditions by simply exploiting the Moon's gravitational attraction.

The authors believe that libration points and invariant manifolds could represent a powerful tool to carry out future space missions with unique performances. Here, the intention has been to demonstrate that such studies, aimed to assess the effectiveness of these concepts, are on the right way for a complete characterization of their potential uses. Nevertheless, in order to have a full scenario of all the features concerning specific missions, further and more intensive studies are necessary.

Chapter 1

Dynamics, Libration Points, Halos and Invariant Manifolds

This chapter introduces the dynamics of the circular restricted three-body problem (CR3BP) that will be used throughout the present work. First, the equations of motion will be given in both the Lagrangian and Hamiltonian formulation. Then the manifold of the states of motion, represented by the Jacobi integral, will be introduced and the nature of the equilibrium points, defined as the singular points of this manifold, will be analyzed. In the second part of the chapter the halo orbits and their associated invariant manifolds will be treated since they are the basics of this study. Nevertheless, a deep characterization of the halo orbits is given in the next chapter.

1.1 Equations of motion

The problem is the evaluation of the motion of a negligible mass (m_3) under the gravitational attractions of two *primaries* (m_1 and m_2) that move in circular Keplerian orbits due to their interaction (see figure 1.1). The problem is *restricted* to the third mass, here generically called *spacecraft*, since it does not influence the motion of the primaries[1]. While in the planar problem the third mass is constrained to stay in the same plane of the primaries, the *spatial* (3D) problem, assumed for this study, leaves the spacecraft free to move in the whole physical space.

Since the two main bodies revolve in circular orbits, the gravitational and centrifugal forces must balance, so:

$$k\frac{m_1 m_2}{l^2} = m_1 a n^2 = m_2 b n^2 \tag{1.1}$$

[1] This hypothesis involves that, as stated above, $m_3 \ll (m_1, m_2)$.

where the distances a, b and l are shown in figure 1.1, k is the Gaussian gravitational constant and n is the angular velocity of the two bodies around their center of mass. Manipulating the equations 1.1, the following relations can be obtained:

$$k(m_1 + m_2) = n^2 l^3, \qquad a = \frac{m_2 l}{m_1 + m_2}, \qquad b = \frac{m_1 l}{m_1 + m_2} \tag{1.2}$$

The *sideral* system (X,Y,Z) is an inertial frame with the origin in the center of mass and the X-axis aligned with the primaries at initial time. The Y-axis is in the orbital plane of the primaries and the Z-axis is bi-normal to X and Y (figure 1.1). In this system the equations of motion are:

$$\begin{aligned}
\frac{d^2X}{dt^{*2}} &= -k\Big[\frac{m_1(X + a\cos nt^*)}{R_1^3} + \frac{m_2(X - b\cos nt^*)}{R_2^3}\Big] \\
\frac{d^2Y}{dt^{*2}} &= -k\Big[\frac{m_1(Y + a\sin nt^*)}{R_1^3} + \frac{m_2(Y - b\sin nt^*)}{R_2^3}\Big] \\
\frac{d^2Z}{dt^{*2}} &= -k\Big[\frac{m_1 Z}{R_1^3} + \frac{m_2 Z}{R_2^3}\Big]
\end{aligned} \tag{1.3}$$

where:

$$\begin{aligned}
R_1^2 &= (X + a\cos nt^*)^2 + (Y + a\sin nt^*)^2 + Z^2 \\
R_2^2 &= (X - b\cos nt^*)^2 + (Y - b\sin nt^*)^2 + Z^2
\end{aligned} \tag{1.4}$$

are the distances between the spacecraft and the primaries and t^* is the dimensional time.

In the sideral system the location of the primaries is not fixed, so the equations 1.3 turn out to be non-autonomous because they include the time explicitly. This is the reason why the sideral system is not a useful frame for a qualitative description of the dynamics. Indeed, when fixed quantities such as integral of motion and equilibrium points are needed, the dynamical system must be autonomous.

Looking at the figure 1.1, the choice of an appropriate system is spontaneous: since in the equations 1.3 the time is introduced by the motion of the primaries, one can observe that they are always aligned and choosing this line as the x-axis of the new system, taken from the greater toward the smaller primary, the time can be removed. The y-axis is again in the orbital plane of the primaries and the z-axis is bi-normal to both x and y. This system is said *synodic*.

Another observation comes directly from the equations 1.1. Since the primaries revolve in circular orbits under their mutual gravitational attractions,

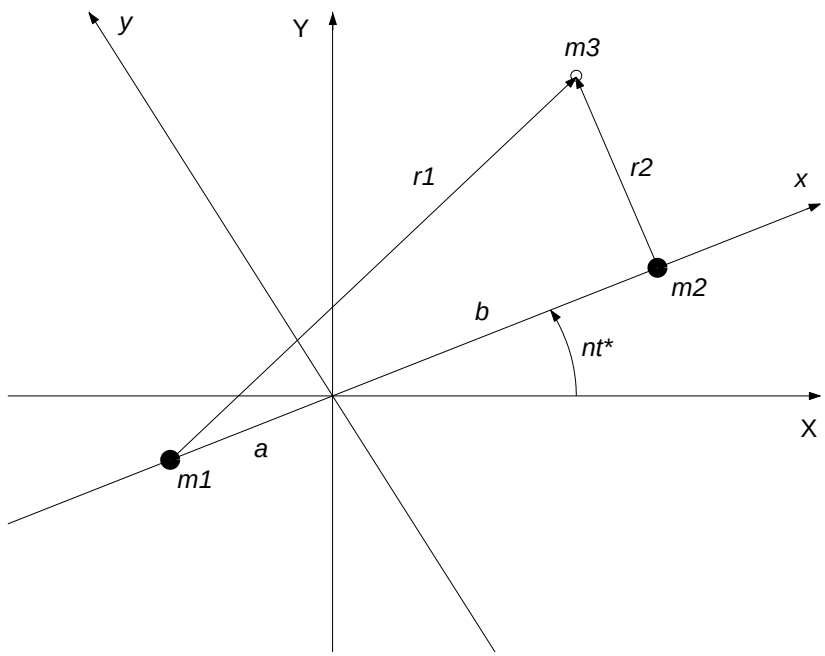

Figure 1.1: Geometry of the problem, the sideral (X, Y) and the synodic (x, y) planes.

the constants a, b, l, n, m_1 and m_2 are not independent but can be related to only one parameter. Defining the *mass parameters* as:

$$\mu_{1,2} = \frac{m_{1,2}}{m_1 + m_2} \tag{1.5}$$

and taking $\mu = \mu_2$ and $1 - \mu = \mu_1$, the Lagrangian dimensionless equations in the synodic system are[2]:

$$\begin{aligned} \ddot{x} - 2\dot{y} &= \Omega_x \\ \ddot{y} + 2\dot{x} &= \Omega_y \\ \ddot{z} &= \Omega_z \end{aligned} \tag{1.6}$$

where the subscripts denote partial derivatives of the function:

$$\Omega(x, y, z) = \frac{1}{2}(x^2 + y^2) + \frac{1-\mu}{r_1} + \frac{\mu}{r_2} + \frac{1}{2}\mu(1-\mu) \tag{1.7}$$

[2]For an excellent explanation and derivation of all the equations contained in this section the classical book of Szebehely [68] is recommended.

and:

$$\begin{aligned} r_1^2 &= (x+\mu)^2 + y^2 + z^2 \\ r_2^2 &= (x-1+\mu)^2 + y^2 + z^2 \end{aligned} \tag{1.8}$$

Equations 1.6 imply the following conventions:

(i) the sum of the masses of the two primaries is normalized to one;

(ii) the distance between the two primaries is normalized to one;

(iii) the angular velocity of the primaries around their center of mass is normalized to one (the period is equal to 2π);

It can be noted that, since the equations 1.6 are written in a rotating system, the first term in Ω (equation 1.7) is the centrifugal potential of the spacecraft while the second term in the first two equations 1.6 is the Coriolis force.

The system has a first integral of motion, called *Jacobi integral*, equal to:

$$C = 2\Omega(x,y,z) - (\dot{x}^2 + \dot{y}^2 + \dot{z}^2) \tag{1.9}$$

The Jacobi integral represents a 5-dimensional manifold for the states of the problem because the full 6-dimensional phase space is restricted to the submanifold $C(x,y,z,\dot{x},\dot{y},\dot{z}) = const$. Moreover, since $\dot{x}^2 + \dot{y}^2 + \dot{z}^2 \geq 0$, the equation 1.9 can be rewritten as:

$$2\Omega(x,y,z) \geq C \tag{1.10}$$

Thus, given an initial condition $\mathbf{x_0} = \{x_0, y_0, z_0, \dot{x}_0, \dot{y}_0, \dot{z}_0\}$ and its associated Jacobi integral $C = C(\mathbf{x_0})$, some allowed and forbidden regions, in the configuration space, can be set with the respect of the equation 1.10. When the kinetic energy is zero, equation 1.9 becomes:

$$2\Omega(x,y,z) = C \tag{1.11}$$

and defines the zero velocity surfaces in the configuration space. These surfaces projected in the synodic plane (x,y) generate some lines called zero velocity curves or *Hill's curves*. Figure 1.2 shows the forbidden regions and the Hill's curves for different values of the Jacobi constant.

The energy of the spacecraft and the Jacobi constant are related by:

$$C = -2E \tag{1.12}$$

which states that a high value of C is associated to a low energy of the spacecraft. This is the case when the spacecraft is bounded to orbit around

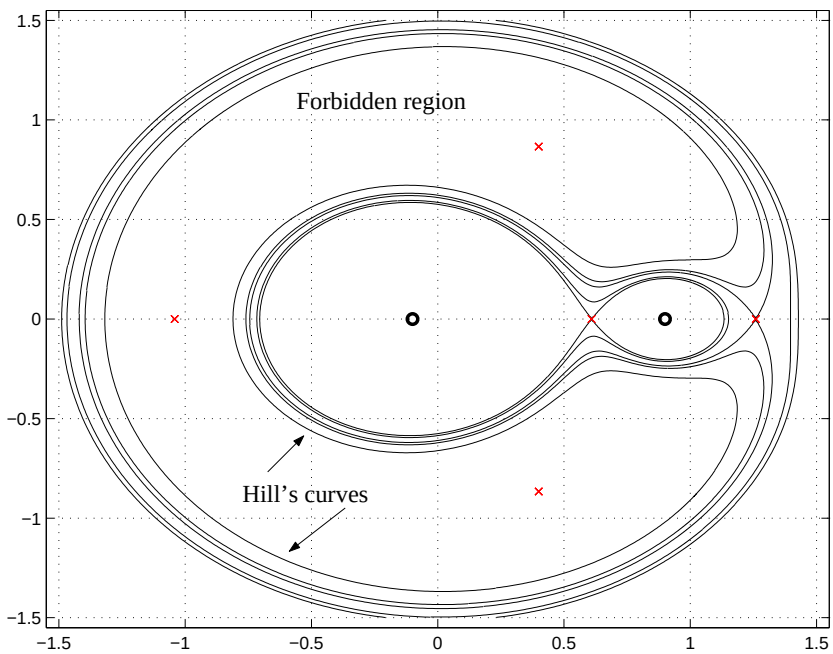

Figure 1.2: Forbidden regions and Hill's curves for several values of C, $\mu = 0.1$.

one of the two primaries. If the energy is increased (or the Jacobi constant is lowered) the allowed regions of motion enlarge and the spacecraft is free to leave one of the two primaries.

By introducing momenta as $p_x = \dot{x} - y$, $p_y = \dot{y} + x$ and $p_z = \dot{z}$, the problem can be written in Hamiltonian form with Hamiltonian function [27]:

$$H(x, y, z, p_x, p_y, p_z) = \frac{1}{2}(p_x^2 + p_y^2 + p_z^2) - xp_y + yp_x - \frac{1-\mu}{r_1} - \frac{\mu}{r_2} \quad (1.13)$$

The differential equations are:

$$\begin{aligned} \dot{x} &= \frac{\partial H}{\partial p_x} & \dot{p_x} &= -\frac{\partial H}{\partial x} \\ \dot{y} &= \frac{\partial H}{\partial p_y} & \dot{p_y} &= -\frac{\partial H}{\partial y} \\ \dot{z} &= \frac{\partial H}{\partial p_z} & \dot{p_z} &= -\frac{\partial H}{\partial z} \end{aligned} \quad (1.14)$$

and the Hamiltonian is related to the Jacobi constant by:

$$C = -2H + \mu(1-\mu) \quad (1.15)$$

1.2 Libration points

Since the spacecraft has three degrees of freedom, its motion is described by a sixth-order differential system (equations 1.6) that can be solved if an initial condition is specified. This condition is a point in the six-dimensional *phase space* and could be also a solution of the system. The Jacobi constant (equation 1.9) represent a manifold for the states of the problem:

$$F(x, y, z, \dot{x}, \dot{y}, \dot{z}) = 2\Omega(x, y, z) - (\dot{x}^2 + \dot{y}^2 + \dot{z}^2) = C \tag{1.16}$$

and its singular points are given by:

$$\begin{aligned} \frac{\partial F}{\partial x} &= 0 \Rightarrow \Omega_x = 0, & \frac{\partial F}{\partial \dot{x}} &= 0 \Rightarrow \dot{x} = 0 \\ \frac{\partial F}{\partial y} &= 0 \Rightarrow \Omega_y = 0, & \frac{\partial F}{\partial \dot{y}} &= 0 \Rightarrow \dot{y} = 0 \\ \frac{\partial F}{\partial z} &= 0 \Rightarrow \Omega_z = 0, & \frac{\partial F}{\partial \dot{z}} &= 0 \Rightarrow \dot{z} = 0 \end{aligned} \tag{1.17}$$

With these quantities, the equations 1.6 become:

$$\ddot{x} = 0, \qquad \ddot{y} = 0, \qquad \ddot{z} = 0 \tag{1.18}$$

which means that the singularities of the manifold of the states of motion are equilibrium points for the dynamical system. These points are called Lagrangian or *libration* points and are represented in figure 1.3. There are three *collinear* ($L1$, $L2$ and $L3$) and two *triangular* ($L4$ and $L5$) points.

System	μ	$L1$	$L2$
Sun-Venus	0.0000024510	0.9906782924	1.0093750674
Sun-(Earth+Moon)	0.0000030359	0.9899909371	1.0100701875
Sun-Mars	0.0000003233	0.9952484658	1.0047659847
Sun-Jupiter	0.0009538754	0.9323655863	1.0688305221
Sun-Saturn	0.0002855022	0.9547609794	1.0460572665
Earth-Moon	0.0121409319	0.8369626376	1.1556450246

Table 1.1: Position of the libration points $L1$ and $L2$ for some problems in the solar system.

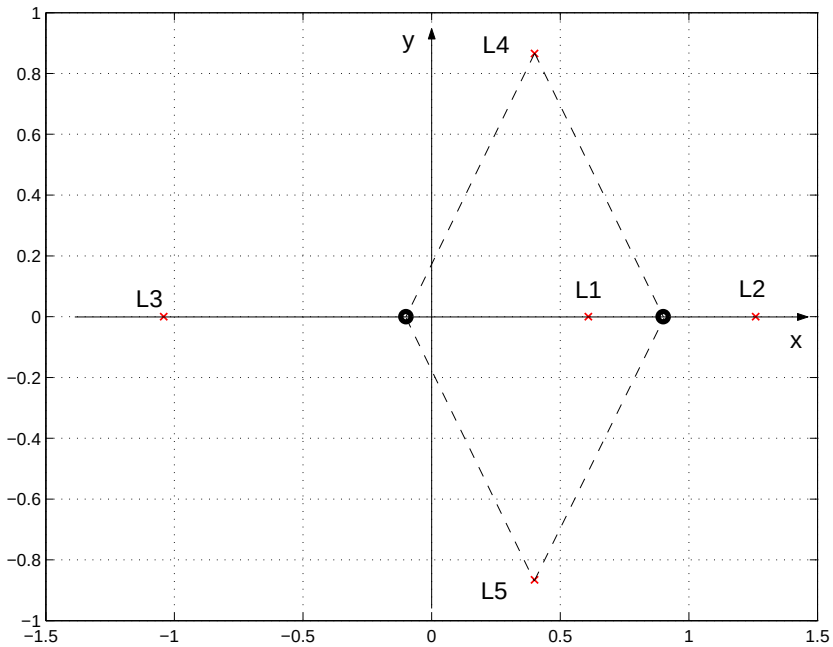

Figure 1.3: Libration points representation, $\mu = 0.1$.

While the triangular points are at the vertex of two equilateral triangles with the primaries, found assuming $r_1 = r_2 = 1$, the position of the collinear points can be located by solving a five-degree polynomial given by the first of the equations 1.17. Table 1.1 summarizes the location of the points $L1$ and $L2$ for some practical problems in the solar system.

1.2.1 Phase space around $L1$ and $L2$

In this work, the possibility to exploit the nature of the libration points for space applications must be analyzed. In particular, this study aims to investigate the stable and unstable dynamics associated to these points. Aiming to do this, only $L1$ and $L2$ must be considered since $L3$ has a slow dynamics and a mild instability [27]. The triangular points $L4$ and $L5$ are always stable for the Sun-Planet-Spacecraft problems in the solar system, therefore they are not suitable in this context. Furthermore, low energy levels, or high values of the Jacobi constant in equation 1.12, are associated to $L1$ and $L2$. This means that already for low levels of the energy E, Hill's curves opens at $L1$ and $L2$ allowing the motion of the spacecraft outside the forbidden regions or between the primaries.

From the analysis of the equations 1.6 the linearized dynamics around the collinear points is that of the product of a *saddle* (two real opposite eigen-

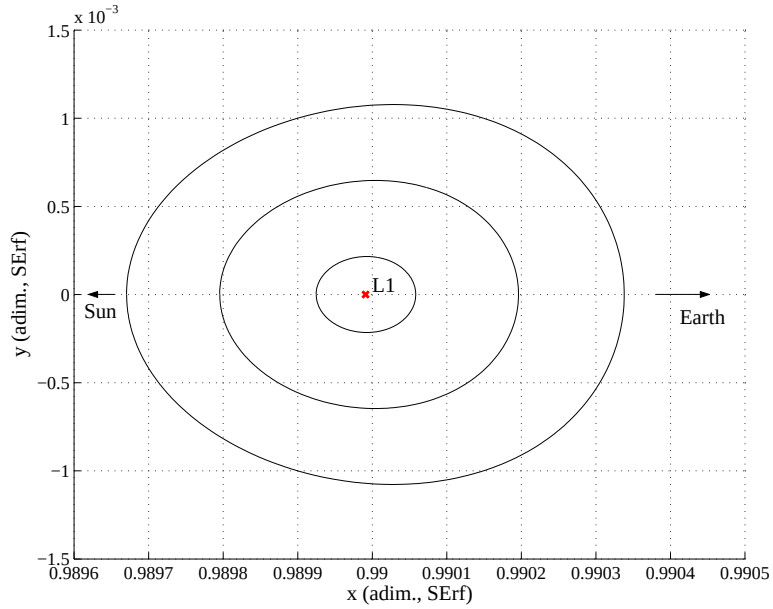

Figure 1.4: Three finite-size Lyapunov orbits ($A_x = 10000\ km$, $A_x = 30000\ km$ and $A_x = 50000\ km$) around $L1$ in the Sun-Earth rotating frame (SErf).

values) times a 4D *center* (periodic motion given by two pairs of imaginary eigenvalues) [36].

Thus, in a small neighborhood of $L1$ and $L2$ points, giving an appropriate initial condition only in the direction of the center branch [68], it is possible to obtain some infinitesimal or *Lyapunov* orbits. These planar orbits can be numerically continued [70] until the desired finite size is reached. Figure 1.4 shows three different finite-size planar Lyapunov orbits around $L1$ in the Sun-Earth system. A complete description of the Lyapunov orbits and their features will be given in the next chapter.

1.3 Halo orbits

Although finite-size periodic Lyapunov orbits can be obtained in the CR3BP, these orbits are not suitable for space applications since they do not allow the out-of-plane motion. For instance, a spacecraft placed in the Sun-Earth $L1$ point must have an out-of-plane amplitude in order to avoid the solar exclusion zone (dangerous for the downlink [23]); a relay satellite around the point $L2$ in the Earth-Moon system should have an out-of-plane motion to assure a direct link between the far side of the Moon and the Earth (see figure 4.1); finally, a space telescope around the Sun-Earth $L2$ point must

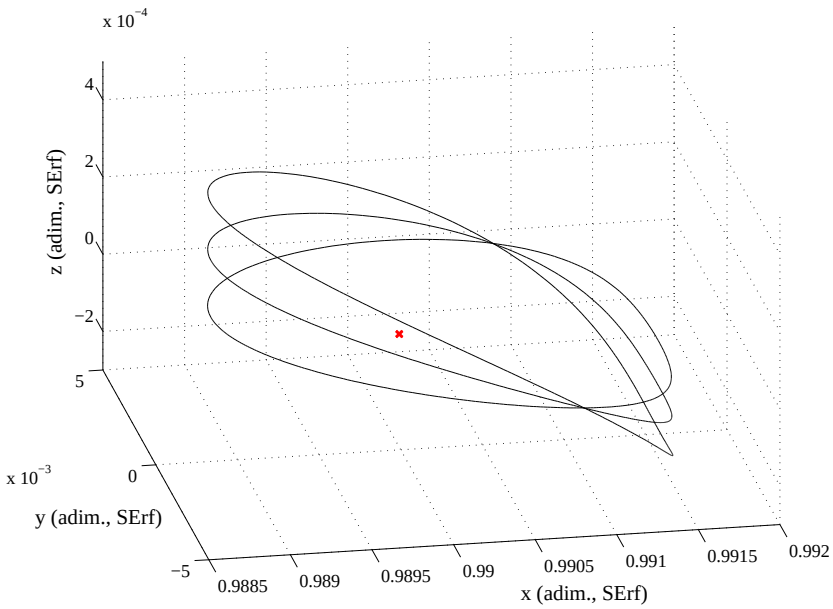

Figure 1.5: Three halo orbits ($A_z = 10000\ km$, $A_z = 30000\ km$ and $A_z = 50000\ km$) around $L1$ in the Sun-Earth rotating frame.

avoid the eclipses and so requires a 3D periodic orbit [12].

In the mid 60's Farquhar [17] discovered that when the out-of-plane (A_z) amplitude is greater than a fixed value $\bar{A}_z$, the in-plane on out-of-plane frequencies match and full 3D periodic *halo* orbits can be generated. In figure 1.5 three halos have been generated with different A_z.

Since the R3BP does not have any analytic solution, the halo orbits are difficult to obtain because the problem is highly non-linear and small changes in the initial conditions break the periodicity of the orbits. Richardson [57] [58] [60] developed a systematic approach, based on a semi-analytical formulation, that allows to generate halo orbits with desired amplitudes. This method, together with an accurate analysis of the characteristics of the halo orbits, will be described in the next chapter.

1.4 Invariant manifolds of the CR3BP

The stable and unstable dynamics of a libration point Li can be exploited using either the 1D manifolds associated to the point (W_{Li}) or the 2D manifolds associated to the periodic orbits around that point ($W_{Li,p.o.}$) for $i = 1, 2$. While the formers can be obtained directly from the eigenvalues and the

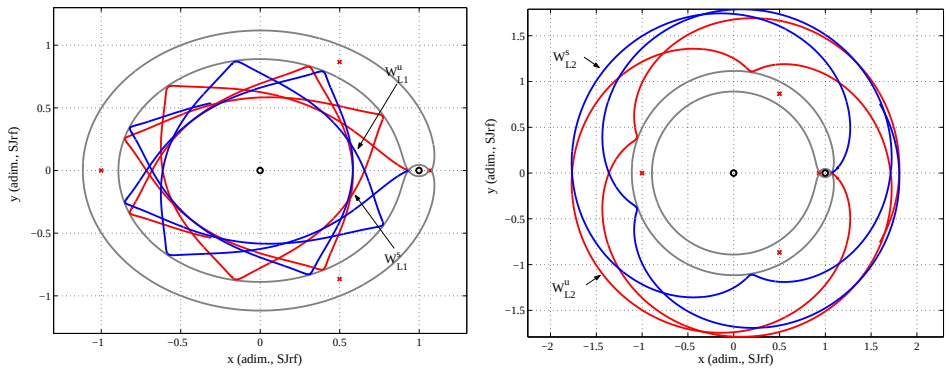

Figure 1.6: Invariant manifolds associated to $L1$ (left) and $L2$ (right) in the Sun-Jupiter system.

eigenvectors of the Jacobian matrix associated to the equations 1.6, the stable and unstable manifolds associated to the periodic orbits require the computation of the monodromy matrix associated to the orbit.

1.4.1 Invariant manifolds associated to the points

The saddle part of the dynamics is represented by one stable eigenvalue and another unstable. This means that the manifolds associated to the points are two 1D lines: W^s_{Li} and W^u_{Li} for $i = 1, 2$.

Rewriting the system 1.6 in six first order equations $\dot{\mathbf{x}} = \mathbf{f}(\mathbf{x})$, with $\mathbf{x} \in \Re^6$, and linearizing these equations at each equilibrium point, the following linear system can be easily obtained:

$$\dot{\mathbf{x}} = A\mathbf{x} \tag{1.19}$$

where A represents the Jacobian matrix of the dynamics. Now, let λ_s and λ_u be respectively the stable and the unstable eigenvalue of A ($\lambda_s < 0$ and $\lambda_u = -\lambda_s$); if $\mathbf{v_s}$ and $\mathbf{v_u}$ are the corresponding eigenvectors, the computation of the manifolds associated to the points requires only the propagation of a perturbation given in the direction of the stable or the unstable eigenvector [70].

Thus, if d is the size of this perturbation and if $\mathbf{x_0}$ are the states associated to the equilibrium point, in order to obtain W^s_{Li} it is necessary to integrate backward the following initial condition:

$$\mathbf{x_0^s} = \mathbf{x_0} \pm d\mathbf{v_s} \tag{1.20}$$

while for W^u_{Li}:

$$\mathbf{x_0^u} = \mathbf{x_0} \pm d\mathbf{v_u} \tag{1.21}$$

must be integrated forward. The signs $\pm$ indicate that there are two legs for each manifold. Figure 1.6 illustrates the stable and unstable manifolds associated to $L1$ and $L2$ of the Sun-Jupiter system.

1.4.2 Invariant manifolds associated to the halo orbits

The manifolds associated to the periodic orbits are centered on the manifolds of the points. These 2-dimensional subspaces are here called $W^s_{Li,p.o.}$ and $W^u_{Li,p.o.}$ $(i = 1, 2)$, according to the notation introduced by Llibre et al [45]. If the spacecraft is on a stable manifold, its trajectory winds onto the orbit and, if it is on the unstable one, it winds off the orbit [43]. This aspect is very important for the design of missions about the libration points, for instance, in the Sun-Earth or Earth-Moon systems (chapters 3 and 4).

It is important to observe that in the planar problem, since the Jacobi constant is a 3-dimensional surface, the manifolds are separatrices and they split different regimes of motion. Gómez et al [28] extended these results to the spatial problem and showed that the invariant manifolds associated to the periodic orbits still act as separatrices for two types of motion: orbits inside the invariant manifolds "tubes" are transit orbits and those outside the tubes are non-transit orbits. Thus, it is not accidental that the transit trajectory shown in figure 1.7 passes through the periodic orbit and remains within the regions delimited by the manifolds. This is due to the initial condition of the transit orbit which lies inside the curve associated to the Poincaré section of the manifold. Indeed, figures 1.8, using the Poincaré sections, shows that the transit orbit is located *inside* the manifold, while the asymptotic orbit lies *on* the manifold.

Since the monodromy matrix represents the first order approximation of the flow mapping for a point of the orbit $\mathbf{x_0}$ into a point $\mathbf{x}$ of an arbitrary Poincaré section:

$$\mathbf{x} \mapsto \mathbf{x_0} + M(\mathbf{x} - \mathbf{x_0}) \tag{1.22}$$

its eigenvectors give the direction of the 1-dimensional manifolds associated to each point of the orbit [27] [69] [70]. Hence, if $\mathbf{x_0^i}$ is a generic point of the orbit, its associated stable manifold can be obtained propagating backward the following initial condition:

$$\mathbf{x_{0,s}^i} = \mathbf{x_0^i} \pm d\mathbf{v_s^i} \tag{1.23}$$

where $\mathbf{v_s^i}$ is the eigenvector associated to the stable eigenvalue of the monodromy matrix evaluated in $\mathbf{x} = \mathbf{x_0^i}$. The parameter d represents the distance between the point of the orbit and the initial condition for the computation

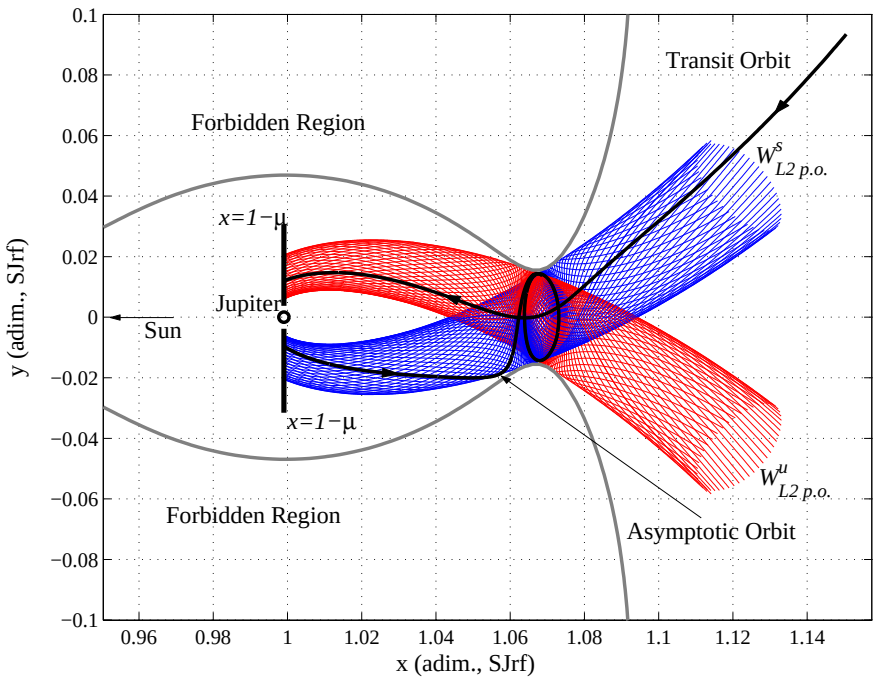

Figure 1.7: Transit and asymptotic orbits for the Sun-Jupiter $L2$ [71].

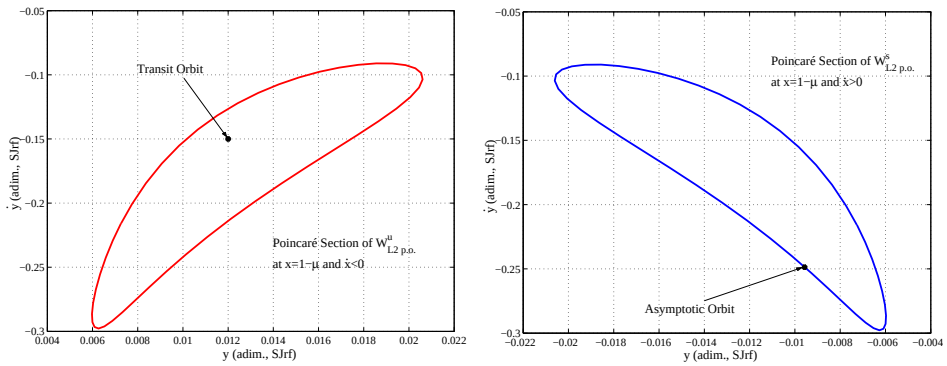

Figure 1.8: Poincaré sections of the unstable (left) and stable manifolds (right) [71].

of its associated manifold, taken in the direction of the eigenvector. It is clear that, the smaller is the value of d, the better is the approximation of the manifold that this first order method could yield. The signs $\pm$ indicate that there are again two different branches of the manifold. In the same way, the unstable manifold associated to the considered point can be achieved integrating forward the initial condition taken in the direction of the unsta-

ble eigenvector. Repeating this process for each point of the orbit, the two dimensional invariant manifolds associated to the orbit have been obtained.

In this study both the manifolds associated to the equilibrium points and to the periodic orbits have been generated by using the process described in the two sections above. For the sake of clarity, the authors suggest the reader to see the work of Thurman and Worfolk [69] (for the manifolds associated to the orbit) and Topputo [70] (for both the manifolds of the points and of the orbits).

Chapter 2

Lyapunov and Halo Orbits of the CR3BP

As seen in the previous chapter, around each of the three collinear equilibrium points a family of unstable orbits exists. Since the spacecraft ISEE-3 inserted into a Sun-Earth $L1$ halo [23], these orbits have proved to be useful for many space applications requiring a fixed configuration with respect to two primaries. Moreover, when ballistically captured transfers are needed [42] [71], the computation of planar Lyapunov orbits is necessary.

In the present chapter, the $L1$ and $L2$ Lyapunov and halo orbits belonging to both the Sun-Earth and Earth-Moon systems are analyzed. Since the R3BP have no analytic solutions, their computation is possible only by combining successive approximations with differential correction methods. This is the process developed by Richardson [60] for the design of the ISEE-3 mission. In the last section, with the use of the same numerical algorithm, an approach to the solution of the Lambert's three-body problem is presented.

2.1 The Richardson's approximation for halo orbits

In Hamiltonian systems the presence of a periodic orbit involves the characterization of the whole family since isolated periodic orbits do not exist in such systems. Hence, in order to identify a single orbit belonging to the family, one parameter must be introduced. This parameter is the in-plane "semi-amplitude" (A_x) for the Lyapunov orbits[1] and the out-of-plane amplitude (A_z) for the halos (see figures 1.4 and 1.5). The choice of A_z as the

[1] A_x is the distance, in the x-direction, between the orbit and the libration point. Strictly speaking, this is not a semi-amplitude because the orbits are distorted, so A_x is

parameter for the halos is important since through its value a lot of mission constraints can be formulated. For instance, the lunar communication station proposed by Farquhar (section 4.1) needs a minimum out-of-plane excursion to avoid the Moon's coverage; or a space telescope about the Sun-Earth $L2$ (section 3.1) requires a minimum A_z in order to avoid the eclipses.

Richardson [57], studying the nominal orbit for the ISEE-3 spacecraft, wrote the equations of motion, centered at the Sun-Earth $L1$, in a compact power series of the distance from the point. Thus, the first order equations of motion are [60]:

$$\begin{aligned} \ddot{x} - 2\dot{y} - (1 + 2c_2)x &= 0 \\ \ddot{y} + 2\dot{x} + (c_2 - 1)y &= 0 \\ \ddot{z} + c_2 z &= 0 \end{aligned} \tag{2.1}$$

where c_2 is a constant depending only on the masses [12]. As mentioned in the previous chapter, the solution to the characteristic equation for the x-y motion has two real and two imaginary roots. The two real roots are of opposite sign so, arbitrarily chosen initial conditions will give rise to unbounded motion as time increases. If, however, the initial conditions are restricted only to the center part, the solution is non-divergent and can be expressed as:

$$\begin{aligned} x &= -A_x \, cos(\lambda t + \phi) \\ y &= kA_x \, sin(\lambda t + \phi) \end{aligned} \tag{2.2}$$

with the frame centered on the equilibrium point and with the constants given is Richardson [60]. The out-of-plane motion is simply-harmonic:

$$z = A_z \, sin(\nu t + \psi) \tag{2.3}$$

Hence, the three dimensional motion is quasi-periodic since the in-plane and the out-of-plane frequencies λ and ν are generally different. This process generates the small-size *Lissajous* quasi-periodic orbits. These orbits do not allow big excursions in the out-of-plane direction, so, for the purposes of the present study, halo orbits are preferred.

In order to have large periodic orbits, the in-plane and the out-of-plane amplitudes have to be large enough to allow the non-linear contributions to

taken from the point toward the x-decreasing direction.

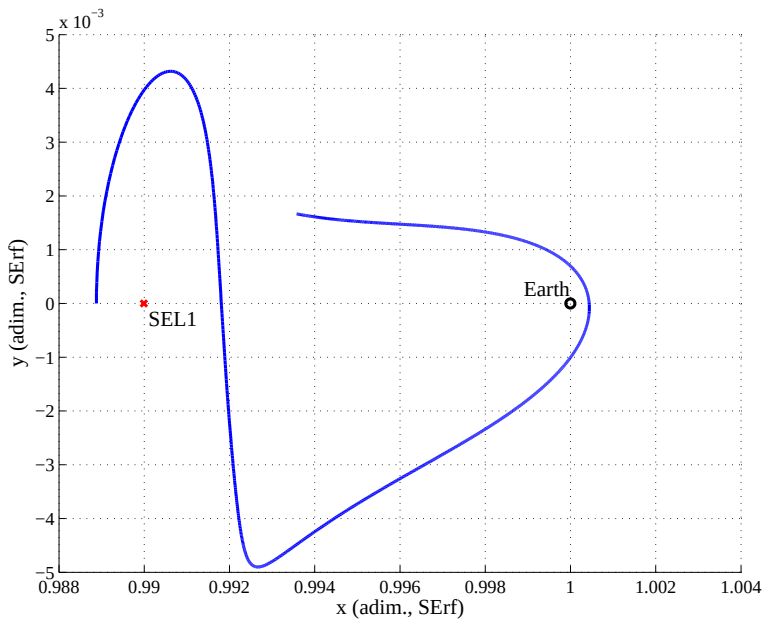

Figure 2.1: Propagation of the analytic initial condition for a halo orbit about the Sun-Earth $L1$ point (SEL1) with $A_z = 100000\ km$.

produce equal eigenfrequencies. Hence, the solution is *forced* to be:

$$\begin{aligned} x &= -A_x\ cos(\lambda t + \phi) \\ y &= kA_x\ sin(\lambda t + \phi) \\ z &= A_z\ sin(\lambda t + \phi) \end{aligned} \tag{2.4}$$

and a correction is introduced to avoid the secular terms [58]. This relations involves a constraint between A_x and A_z that will be shown later.

Taking the initial conditions associated to the equations 2.4 as a first guess solution and propagating in the full systems, no periodic motion is obtained (figure 2.1). Nevertheless, this initial condition represents a good starting point for further corrections because, as shown in the figure above, the semi-orbit is well approximated.

2.2 Numerical computation of halo orbits

In this section, the method of Thurman and Worfolk [69] will be applied for the correction of the first guess solution obtained with the analytic approximation. First, one has to observe that the full equations of motion 1.6 given

in section 1.1 present the following symmetry:

$$S: \ (x, y, z, \dot{x}, \dot{y}, \dot{z}, t) \ \rightarrow \ (x, -y, z, -\dot{x}, \dot{y}, -\dot{z}, -t) \tag{2.5}$$

thus, given a solution $\mathbf{x}(t) = \{x(t), y(t), z(t), \dot{x}(t), \dot{y}(t), \dot{z}(t)\}$ there is guaranteed another orbit $\mathbf{x}(-t) = \{x(-t), -y(-t), z(-t), -\dot{x}(-t), \dot{y}(-t), -\dot{z}(-t)\}$ [79]. Given this symmetry, a trajectory that crosses perpendicularly the $y = 0$ plane twice is a periodic orbit.

Let $\mathbf{x_0}$ be an initial guess, obtained through the previous method, located on the (x, z)-plane with a component of the velocity only in the y-direction:

$$\mathbf{x_0} \ = \ \{x_0, 0, z_0, 0, v_0, 0\} \tag{2.6}$$

where the symbols u, v and w are used instead of $\dot{x}$, $\dot{y}$ and $\dot{z}$. Flowing $\mathbf{x_0}$ under the equations 1.6, until the first return to the (x, z)-plane occurs (at time $t = T_{1/2}$), gives the flow:

$$\Phi(\mathbf{x_0}, T_{1/2}) \ = \ \{\tilde{x}, 0, \tilde{z}, \tilde{u}, \tilde{v}, \tilde{z}\} \tag{2.7}$$

and if $\tilde{u} = \tilde{w} = 0$ the periodic orbit is computed. So, the initial condition is corrected through a first order expansion:

$$\Phi(\mathbf{x_0}+\mathbf{\Delta x}, T_{1/2}+\Delta t) = \Phi(\mathbf{x_0}, T_{1/2}) + \left[\frac{\partial \Phi(\mathbf{x_0}, T_{1/2})}{\partial \mathbf{x}}\right] \cdot \mathbf{\Delta x} + \frac{\partial \Phi(\mathbf{x_0}, T_{1/2})}{\partial t} \cdot \Delta t \tag{2.8}$$

with:

$$\mathbf{\Delta x} = \{\Delta x, 0, \Delta z, 0, \Delta v, 0\} \tag{2.9}$$

and the periodicity is imposed by setting the flow equal to:

$$\Phi(\mathbf{x_0} + \mathbf{\Delta x}, T_{1/2} + \Delta t) = \{x^*, 0, z^*, 0, v^*, 0\} \tag{2.10}$$

that is still unknown.

Observing that $\partial \Phi / \partial \mathbf{x} = M$ is the state transition matrix, called *monodromy matrix* for the periodic orbits, the equation 2.8 can be rewritten as:

$$M \begin{Bmatrix} \Delta x \\ 0 \\ \Delta z \\ 0 \\ \Delta v \\ 0 \end{Bmatrix} + \mathbf{f}(\Phi)\Delta t = \begin{Bmatrix} x^* \\ 0 \\ z^* \\ 0 \\ v^* \\ 0 \end{Bmatrix} - \begin{Bmatrix} \tilde{x} \\ 0 \\ \tilde{z} \\ \tilde{u} \\ \tilde{v} \\ \tilde{w} \end{Bmatrix} \tag{2.11}$$

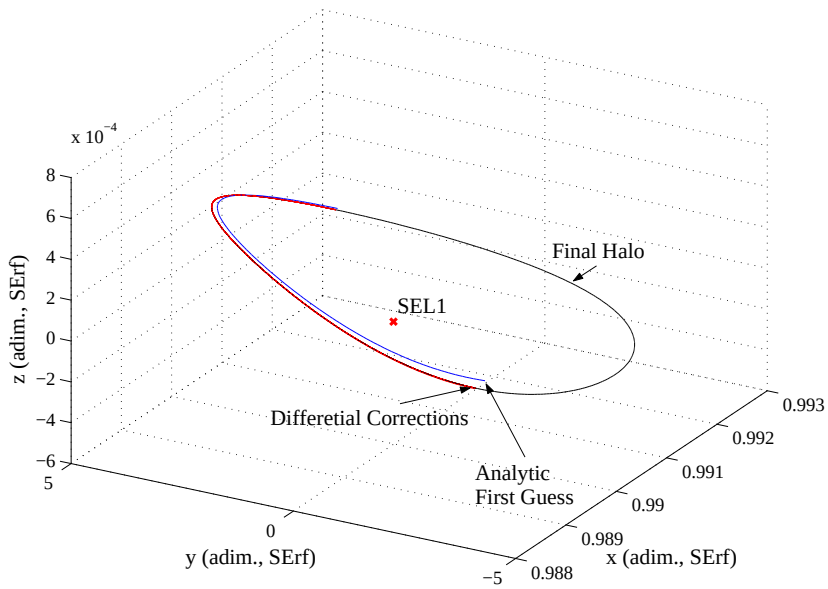

Figure 2.2: Differential correction of the analytic solution represented in figure 2.1.

where $\partial\Phi/\partial t$ has been replaced with the vector field of the system $\mathbf{f}(\Phi)$. Considering only the second, fourth and sixth rows, the system becomes:

$$\begin{aligned} m_{21}\Delta x + m_{23}\Delta z + m_{25}\Delta v + f_2\Delta t &= 0 \\ m_{41}\Delta x + m_{43}\Delta z + m_{45}\Delta v + f_4\Delta t &= -\tilde{u} \\ m_{61}\Delta x + m_{63}\Delta z + m_{65}\Delta v + f_6\Delta t &= -\tilde{w} \end{aligned} \tag{2.12}$$

that are three equations with four unknowns. This was expected since the family have to be parameterized by the out-of-plane amplitude. So, taking $\Delta z = 0$ the equations produce an iterative technique[2]. The new condition will be:

$$\mathbf{x}^{\mathbf{new}} = \mathbf{x}^{\mathbf{old}} + \mathbf{\Delta x} \tag{2.13}$$

and the method is applied again until the final accuracy is obtained. Figure 2.2 shows the corrections applied to the orbit represented in figure 2.1.

[2]For the Lyapunov orbits the system 2.12 has two equations and three unknowns since it lacks of the last equation and there is not an out-of-plane correction. In this case the system can be solved by taking $\Delta x = 0$ and parameterizing with A_x.

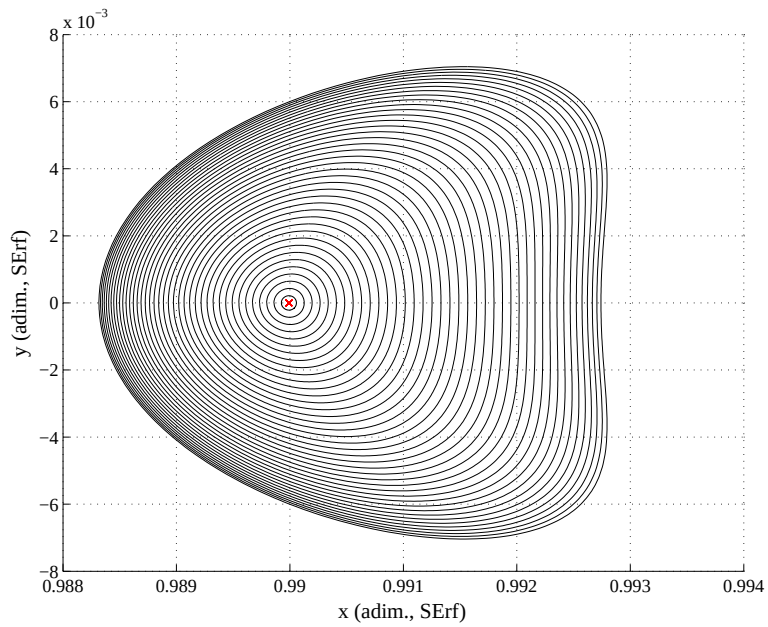

Figure 2.3: Lyapunov orbits around the Sun-Earth $L1$ with amplitudes $A_x = i \cdot 10000\ km$, $i = 1, ..., 40$.

The monodromy matrix is computed by integrating the system:

$$\begin{aligned} \dot{\mathbf{x}} &= \mathbf{f}(\mathbf{x}) \qquad , \quad \mathbf{x}(0) = \mathbf{x}_0 \\ \dot{M} &= \left[\frac{\partial \mathbf{f}}{\partial \mathbf{x}}\right] M \qquad , \quad M(0) = \mathbf{I} \end{aligned} \tag{2.14}$$

where $\mathbf{I}$ is the six-by-six unity matrix. The system 2.14 is a differential system with order $n + n^2$. For the halo orbits the full order is 42 (6+36) while for the Lyapunov it is equal to 20 (4+16).

2.3 Lyapunov orbits in the Sun-Earth system

The algorithm described in the previous section has been applied for the computation of the Lyapunov orbits about both $L1$ and $L2$ of the Sun-Earth system. Figure 2.3 and 2.4 shows forty orbits with increasing amplitudes. It can be observed that the larger the amplitude, the more the orbit becomes distorted due to the non-linearities. With this process, orbits of any size can be obtained until a collision with the Earth occurs.

The two figures below show the trend of the y-amplitude A_y and the orbital period T of the computed orbits with respect to the independent pa-

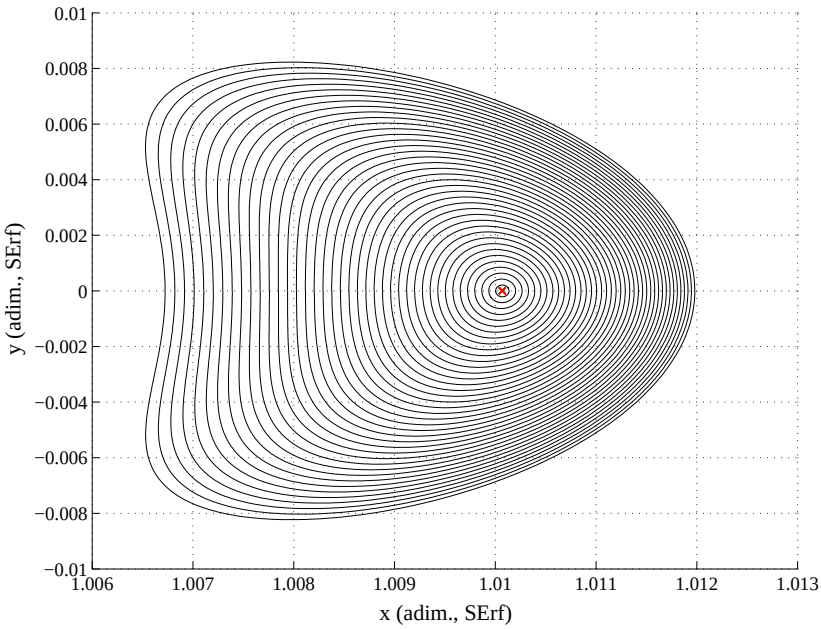

Figure 2.4: Lyapunov orbits around the Sun-Earth $L2$ with amplitudes $A_x = i \cdot 10000\ km$, $i = 1, ..., 40$.

rameter that is A_x. The first (A_y vs A_x) indicates that, as stated by the equations 2.2, there is a linear constraint between the two in-plane amplitudes: $A_y = kA_x$. The second figure shows that the orbital period is around six-months and it slightly changes with respect to the two points.

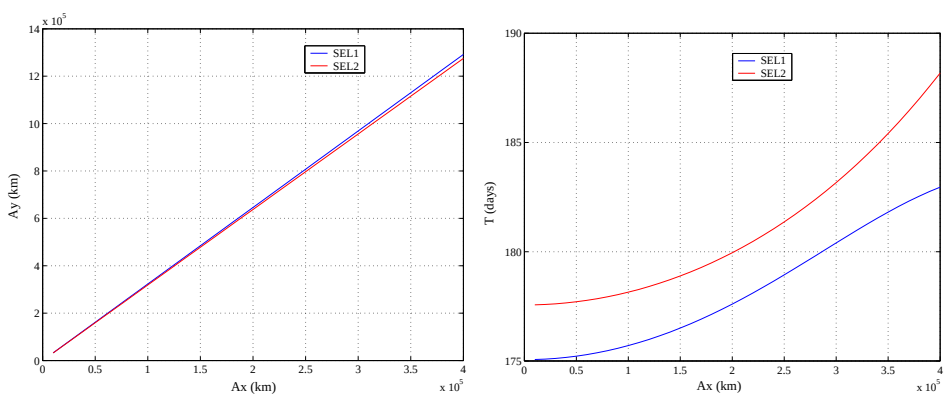

Figure 2.5: A_y amplitude (left) and period T (right) trend versus A_x for the Sun-Earth Lyapunov orbits in figures 2.3 and 2.4.

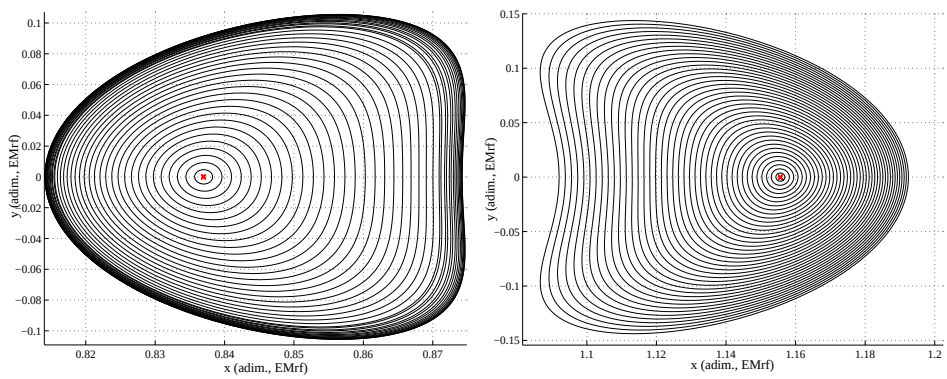

Figure 2.6: Lyapunov orbits around the Earth-Moon $L1$ (left) and $L2$ (right) with amplitudes $A_x = i \cdot 500\ km$, $i = 1, ..., 40$.

2.4 Lyapunov orbits in the Earth-Moon system

The method has been applied for the computation of Lyapunov orbits about $L1$ and $L2$ in the Earth-Moon system. In this system the mass parameter μ (table 1.1) is four orders of magnitude greater than the one of the Sun-Earth system. This produces large differences between the orbits around $L1$ and those around $L2$. This aspect is clear in figures 2.6 and and 2.7 that show respectively the two families of orbits and the trends A_y vs A_x and T vs A_x.

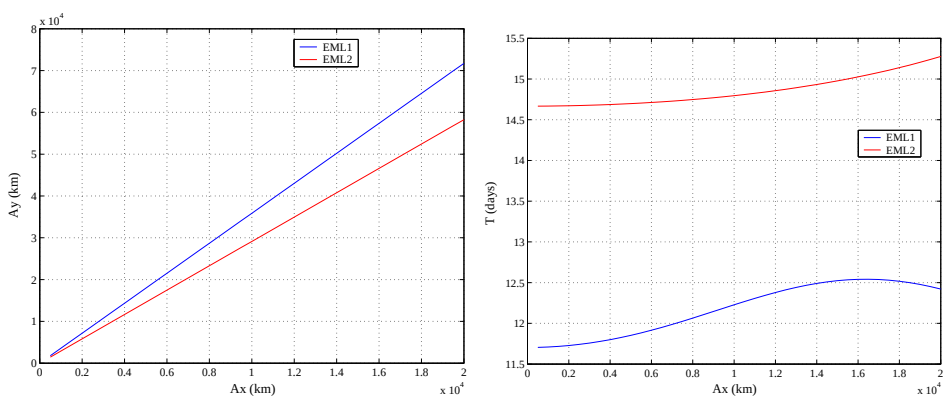

Figure 2.7: A_y amplitude (left) and period T (right) trend versus A_x for the Earth-Moon Lyapunov orbits in figures 2.6.

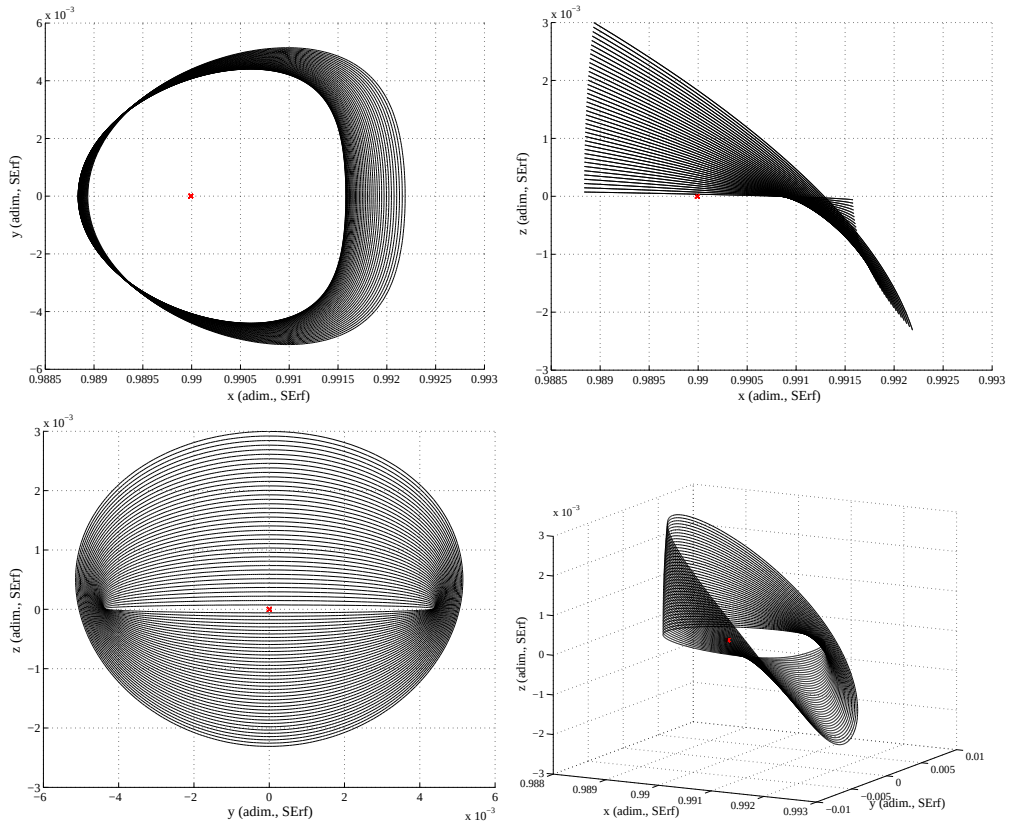

Figure 2.8: Halo orbits around the Sun-Earth $L1$.

2.5 Halo orbits in the Sun-Earth system

With the method described in the sections 2.1 and 2.2 a complete analysis of the halo orbits in the Sun-Earth system has been carried out.

Looking at the figures 2.8 and 2.9 the nature of these orbits is clear: when A_z is small they can be approximated by the Lyapunov orbits; large out-of-plane orbits have big excursions and are distorted by the non-linearities of the R3BP. Moreover, as observed by several authors [17] [24] [32] halo orbits do not exists below a certain in-plane amplitude $\bar{A}_x$ because they can be viewed as bifurcation of the planar orbits when A_x grows. The non-existence of halo orbits can also be viewed by equations 2.4 because the two frequencies do not match below certain values of the in-plane amplitude.

Figures 2.10 show the orbital parameters of the halo orbits in the Sun-Earth system: as stated analytically by Richardson [60] the relations $A_x =$

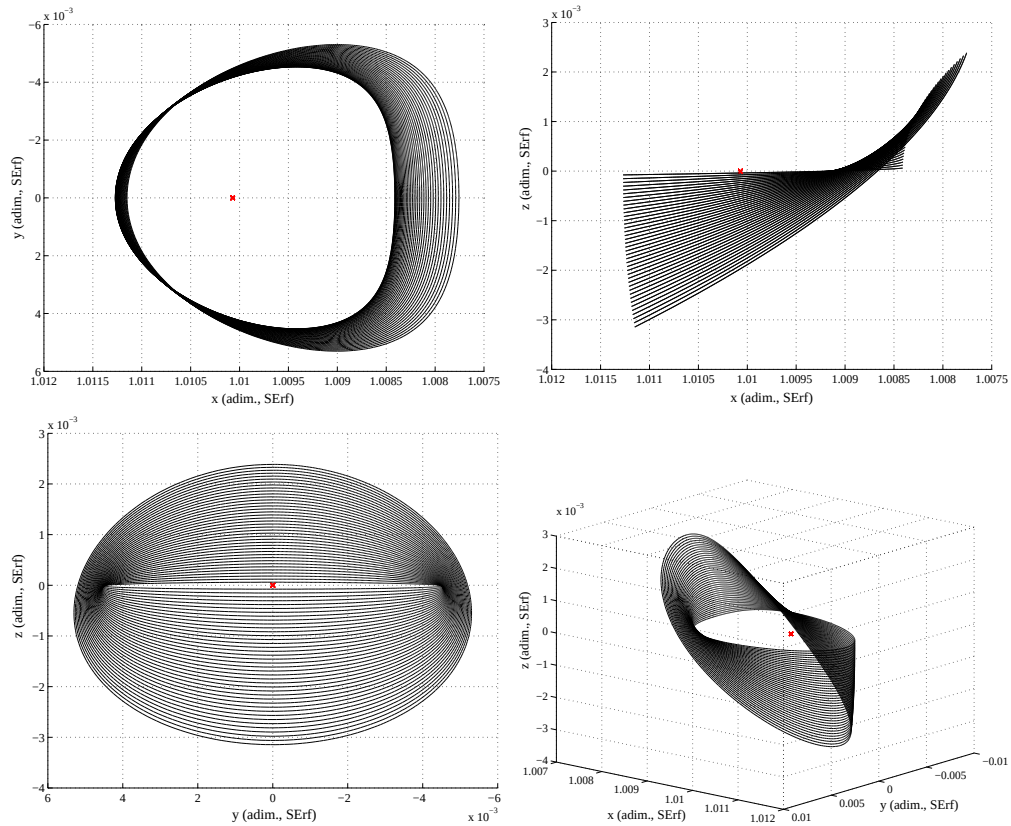

Figure 2.9: Halo orbits around the Sun-Earth $L2$.

$A_x(A_z)$ and $A_y = A_y(A_z)$ are parabolic and so they are also for the numerically computed orbits. Finally, the period of the Sun-Earth halos is around six months.

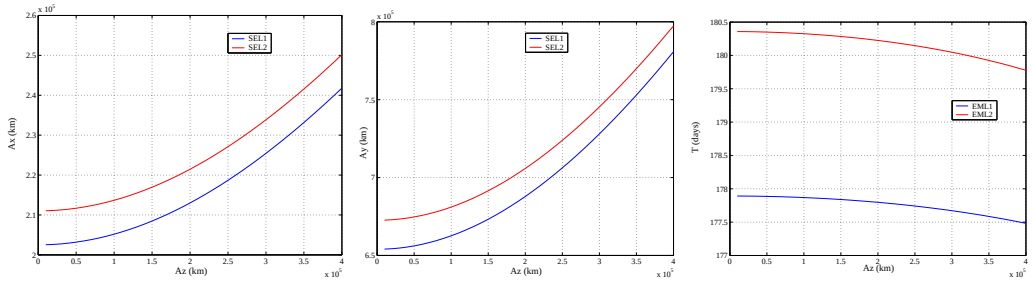

Figure 2.10: Orbital parameters of the Sun-Earth halo orbits.

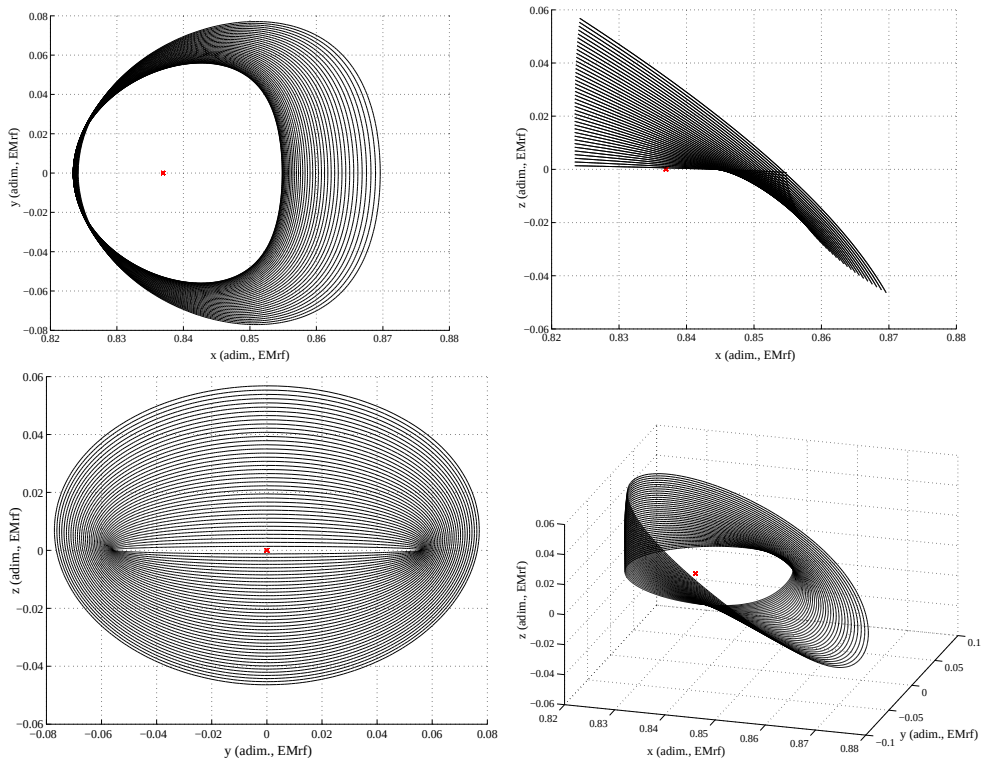

Figure 2.11: Halo orbits around the Earth-Moon $L1$.

2.6 Halo orbits in the Earth-Moon system

The developed tool for the fast analysis and computation of the halos has been applied for the orbits around $L1$ and $L2$ in the Earth-Moon system. Figures 2.11 and 2.12 represent the two families of orbits.

Again the distortion of the orbits when the out-of-plane amplitude increases is clear and, as for the Lyapunov orbits in this system, the differences between the $L1$ and $L2$ orbits are marked. In fact, if the same A_z excursion is imposed, the in-plane amplitude associated to $L2$ is greater than the one associated to $L1$. The same could be said for the maximum y-excursion due to the linear relation between A_x and A_y.

The orbital period is between 12 and 15 days. These values are almost equal to the half period associated to the revolution of the primaries around their center of mass (e.g. the Moon's period around the Earth). It is remarkable how this occurs also in the Sun-Earth system since the average period of the halos in this system is around six months.

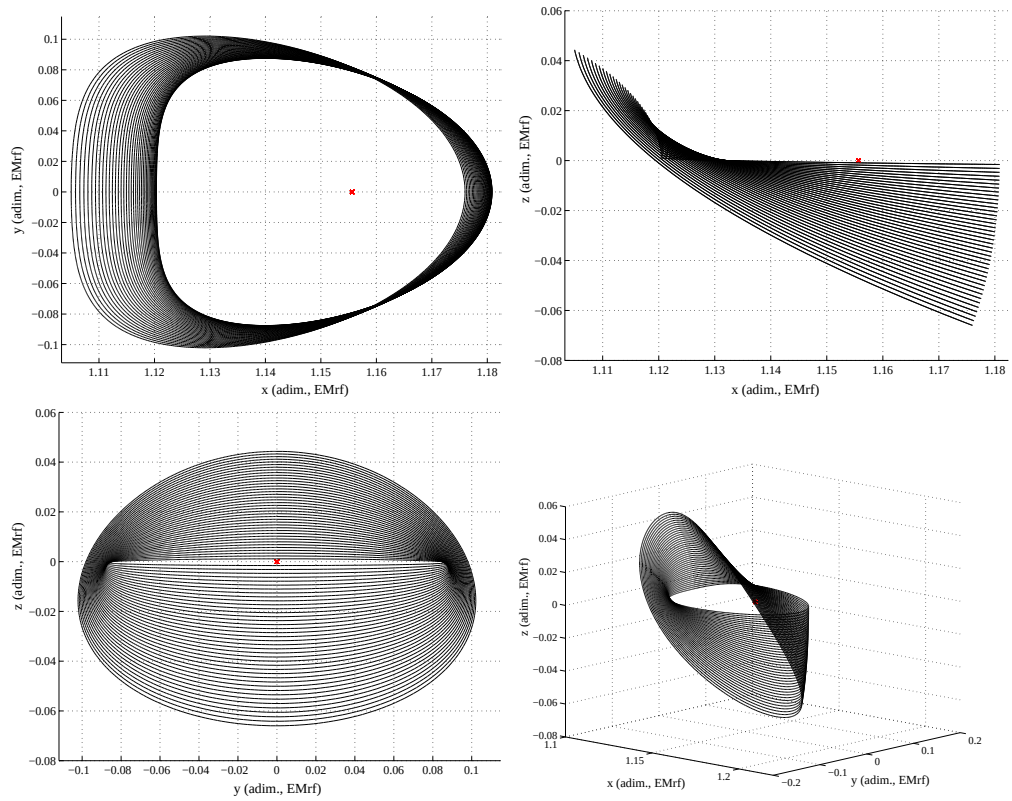

Figure 2.12: Halo orbits around the Earth-Moon $L2$.

The developed method has proven to be very fast and accurate for the computation of the halos and their orbital parameters. It could be a useful tool when the characteristics of the halo and Lyapunov orbits are needed.

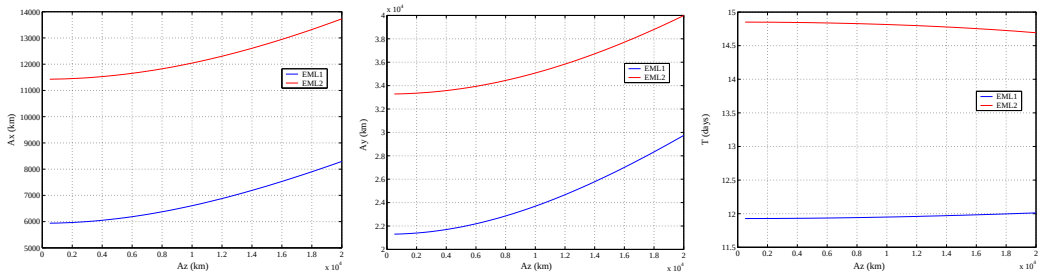

Figure 2.13: Orbital parameters of the Earth-Moon halo orbits.

2.7 The Lambert's three-body problem

The Lambert's problem is stated as the search of a path between two given points $\mathbf{r_1} = \{x_1, y_1, z_1\}$ and $\mathbf{r_2} = \{x_2, y_2, z_2\}$ with a time of flight equal to Δt. It is a typical differential problem where such mixed initial and final conditions are given. Even if the system is of the sixth order, the Lambert's problem requires seven conditions $(\mathbf{r_1}, \mathbf{r_2}, \Delta t)$ to be solved because, if for instance the time of flight is not given, there are infinite trajectories linking $\mathbf{r_1}$ and $\mathbf{r_2}$.

In the two-body model, the Lambert's problem is a well-known problem to the mission designers since it represents a basic tool for the preliminary analysis of transfer trajectories. In that system it can be solved analytically with fast algorithms [3].

In a three-body context, the Lambert's problem is no longer trivial. This happens because the R3BP problem does not have analytical solutions and so the Lambert's problem can be solved only through numerical techniques. In the past, several authors have studied this problem: both Broucke [10] and Prado [55] approached the problem with regularized coordinates to analyze free fall trajectories between the libration points and the primaries in the Earth-Moon system. D'Amario and Edelbaum [15] and Pu and Edelbaum [56] studied the optimal Lambert's arcs in the three and four-body model.

The algorithm developed from the authors, suitable in this work, is strictly related to the one described in section 2.2 for the correction of the analytical approximations of the halo orbits and represents a typical two-points boundary value problem (2PBVP). Indeed, if an initial velocity is guessed:

$$\mathbf{v_{1,g}} = \{u_{1,g},\ v_{1,g},\ w_{1,g}\} \tag{2.15}$$

a first guess trajectory can be propagated starting by:

$$\mathbf{x_0} = \{\mathbf{r_1},\ \mathbf{v_{1,g}}\} \tag{2.16}$$

and after Δt the flow is:

$$\Phi(\mathbf{x_0}, \Delta t) = \{\tilde{x},\ \tilde{y},\ \tilde{z},\ \tilde{u},\ \tilde{v},\ \tilde{z}\} \tag{2.17}$$

Thus, $\Phi(\mathbf{x_0}, 0)$ is expanded as in the equation 2.8 without applying any correction on the time of flight and assuming:

$$\mathbf{\Delta x} = \{0,\ 0,\ 0,\ \Delta u,\ \Delta v,\ \Delta w\} \tag{2.18}$$

so the first three rows of the 2.8 represents a system of three equations and three unknowns. The process is again iterative and the velocity corrections $\mathbf{\Delta v} = \{\Delta u, \Delta v, \Delta w\}$ are applied to the old velocity as:

$$\mathbf{v^{new}} = \mathbf{v^{old}} + \mathbf{\Delta v} \tag{2.19}$$

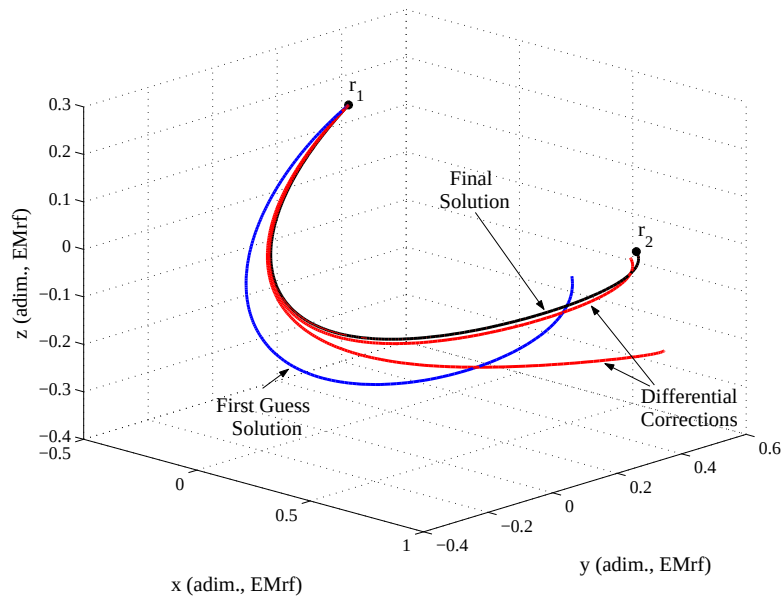

Figure 2.14: Solution example of the Lambert's three-body problem through the developed algorithm. The first guess trajectory (blue) is then corrected (red) until the final solution (black) is reached. In this example the algorithm converges with three iterations.

Figure 2.14 shows an example of solution through this method. In the Earth-Moon system, the dimensionless positions $\mathbf{r_1} = \{0.1, 0, 0.3\}$ and $\mathbf{r_2} = \{0.8, 0.4, 0\}$ must be linked in a dimensionless time equal to $\Delta t = 1$. The blue line is the first guess trajectory, while the red ones are the successive corrections computed by the algorithm. Finally, the black line is the exact solution. In this example, the convergence is achieved with only three iterations.

The algorithm has proven to be efficient, but in some cases, as for the target of a point belonging to a LEO (figure 2.15), the final solution could be an impact trajectory with one of the two primaries. This is due to the blindness of the algorithm with respect to the sizes of the primaries since the equations of motion 1.6 involves only point masses.

In order to avoid impacts, and so unfeasible trajectories, the algorithm has been further developed and figure 2.15 shows an example of the results obtained. This time the corrections are not applied after the time Δt, but when the path impacts the Earth. Although this process involves much computational time (more iterations), it gives accurate results.

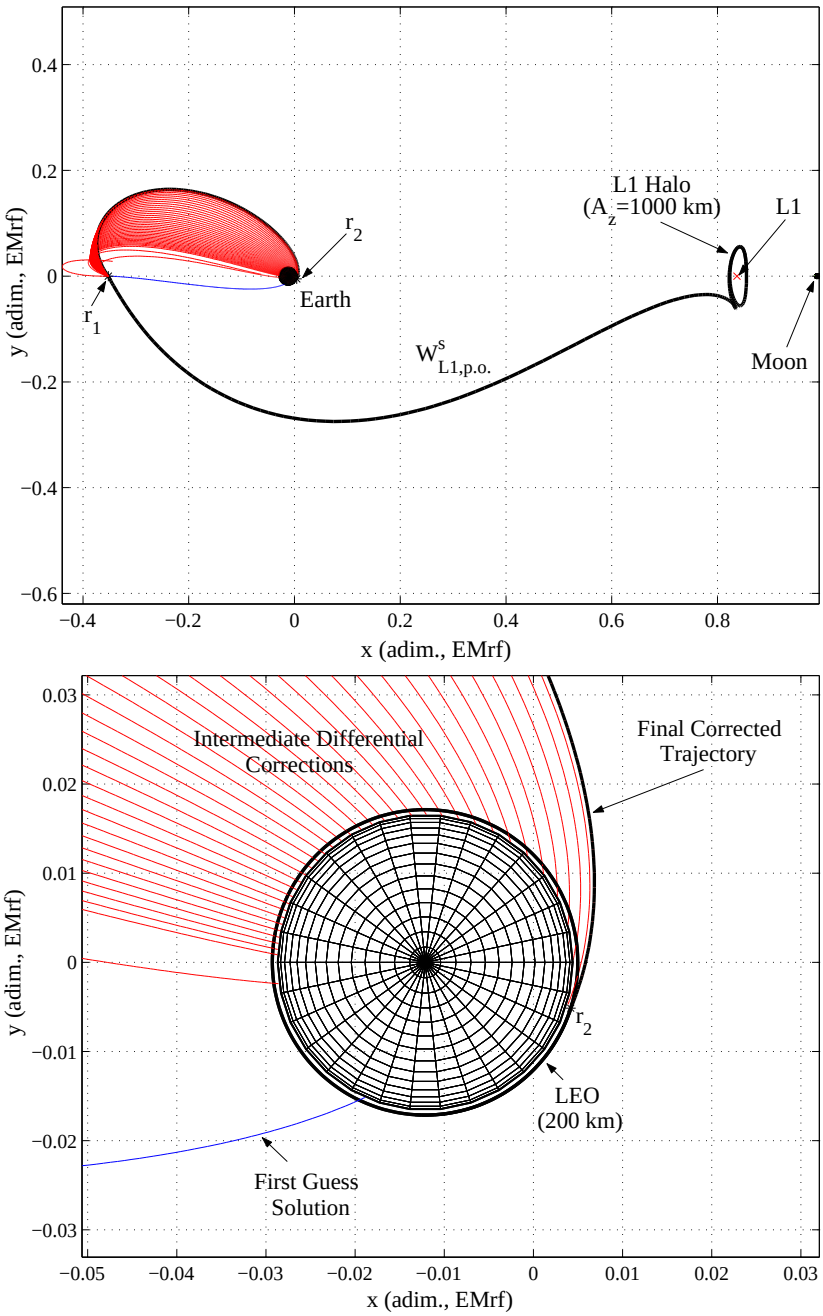

Figure 2.15: Modification of the algorithm to avoid Earth or Moon impacts. At the top the problem to target a piece of a stable manifold associated to a periodic orbit about $L1$ in the Earth-Moon system is presented. The Earth's neighborhood is enlarged at the bottom to show the modification of the algorithm that avoids Earth impact trajectories. In this case the algorithm convergence happens after thirty-eight iterations.

Chapter 3

Transfers to Halo Orbits in the Sun-Earth System

This chapter deals with the missions on halo orbits around $L1$ and $L2$ in the Sun-Earth system. Since here the Earth is the smallest primary, it is "close" to these points and the manifolds associated to the periodic orbits extend until they reach the Earth's neighborhood. Hence, in order to compute a libration point mission, in this system it is only necessary to target a point on the manifold by starting from a Keplerian orbit about the Earth.

In the first part of the chapter the state of the art, concerning libration point missions in the Sun-Earth system, will be analyzed. Then, the authors' approach to the problem and the results obtained will be presented together with some discussions upon the possible uses for space missions.

3.1 State of the art analysis

The trajectory design issues involved in libration point orbit missions go beyond the lack of preliminary baseline solutions since conic analysis fails in these regions of space. It is clear, indeed, that the use of a conic solution is forbidden a priori because libration points are defined as equilibrium solutions in the R3BP, while conic arcs are allowed only in a two-body model. So, one of the key drawbacks for mission design in the libration regime is the loss of orbital elements. Since libration orbits are nonlinear trajectories in the three-body problem, the Jacobi constant (section 1.1) is the only integral available and then the only in the R3BP formulation.

In this context, after that several speculations were made about the use of libration point orbits[13] [33], Farquhar [17], in the mid 60's, recognized that the Sun-Earth $L1$ point would have been an ideal location to continuously

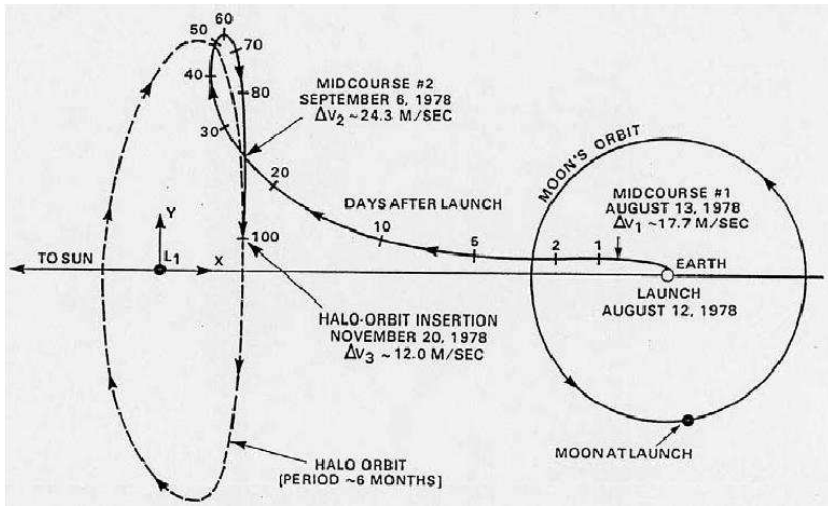

Figure 3.1: The ISEE-3 transfer trajectory to an $A_z = 120000\ km$ halo orbit [17].

monitor the interplanetary environment upstream from the Earth and out of Van Allen belts. So, Farquhar et al [23] designed the trajectory of ISEE-3, the first libration point satellite [81]. In this work the authors noted that a large halo orbit was suitable to avoid the solar exclusion zone during the downlink. Thus, they discovered that the ΔV costs for orbit insertion are smaller for large-amplitude halo orbits and they chosen an $A_z = 120000\ km$ halo orbit as the nominal one. Through numerical techniques, the full trajectory, represented in figure 3.1, was designed by assuming a pair of correction maneuvers (ΔV_1 and ΔV_2) and a final impulse (ΔV_3) necessary to insert the spacecraft into the final orbit.

In the years later, the concept of a libration point mission was discarded until early 90's when WIND [84] mission was planned. As can be observed by figure 3.2, its trajectory made several lunar swing-by's before having a large loop around the Sun-Earth $L1$ point. The spacecraft did not insert in a periodic orbit and its "acrobatic" path continued always below $L1$.

Then, the sophisticated ESA's solar observatory, SOHO [83], was injected into a transfer trajectory that guided it to an $A_z = 120000\ km$ $L1$ halo orbit. It was launched from a $h = 180\ km$ parking orbit with $\Delta V = 3200\ m/s$ and three mid course correction maneuvers were performed to assure the rendezvous with the final halo. The time of transfer was around $\Delta t \simeq 60\ days$ while the nominal halo orbit had a period equal to six months.

Another two libration point missions were ACE [77] and MAP (or WMAP) [82]. The former was the first spacecraft to enter in a $L1$ Lissajous quasi-periodic orbit ($A_z = 157000\ km$), while the latter was injected into a $L2$ halo

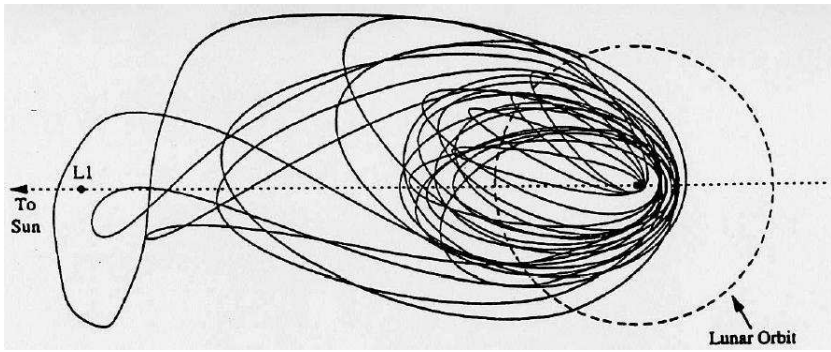

Figure 3.2: The WIND's full trajectory [17].

orbit.

All the missions above were designed using *ad hoc* numerical techniques that were developed on purpose for each mission. Anyway, the general concept that led the design of these trajectories was based on small perturbations given at a specific point of the nominal orbit. Starting from the perturbed point, the path was propagated backward until it reached the closest approach to the Earth. Then, the nominal trajectory was chosen, among those passing near the Earth, according to the minimum cost.

In the last years, the dynamical systems theory has given a great contribution to understand the structure of the phase space around the libration points. Thus, introducing the concept of stable and unstable manifolds associated to a periodic halo orbit, a systematic approach to design trajectories for libration point missions has been developed.

Howell et al [32] deeply investigated efficient trajectory options in the frame of the R3BP with the use of the dynamical system theory. They were able to find transfer trajectories from Earth parking orbits to large-amplitude halo orbits; heteroclinic connections between two orbits (one around $L1$ and the other around $L2$); return Earth-impact trajectories to bring the spacecraft back to the Earth.

Wilson and Howell [76] used these trajectories as first guess solutions in a Sun-Earth-Moon model and studied the use of Moon swing-by's to decrease the cost of these missions. Moreover, Barden and Howell [2] analyzed the issues involved in a formation flying around the libration points.

These studies were applied for the analysis of the Genesis mission [78]. Its full trajectory, shown in figure 3.3, can be separated into four legs: there is first a transfer path from a $h = 200\ km$ parking orbit to an $A_z = 320000\ km$ $L1$ halo orbit with a cost equal to $\Delta V = 3200\ m/s$ (red); then the spacecraft is injected into the halo orbit ,using $\Delta V = 12\ m/s$ and performing

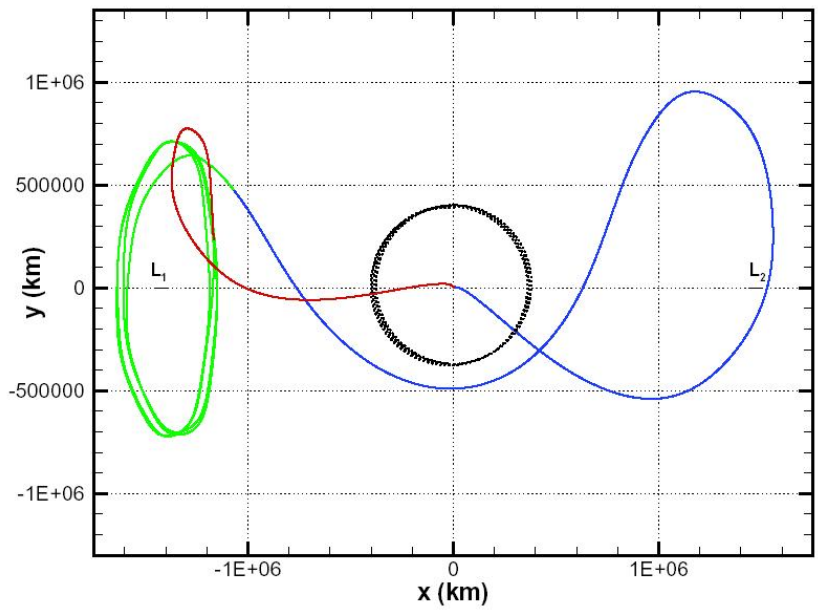

Figure 3.3: The Genesis' nominal trajectory [41].

almost four revolutions around $L1$ (green); the third phase is a heteroclinic connection between the halo and a Lissajous orbit around $L2$ with cost $\Delta V = 36\ m/s$ (blue); finally, with a low-cost maneuver ($\Delta V = 14\ m/s$) the spacecraft is placed on the unstable manifold associated to the $L2$ orbit and returns to the Earth (blue) [32].

Kechichian [39] applied the method of regularization to the equations of the R3BP centered at $L1$. He used an iterative process to generate transfer trajectories from a LEO to the vicinity of $L1$. He optimized this process and found that a cost around $\Delta V = 3300\ m/s$, involving also the halo injection, is enough to place a spacecraft on halo orbits.

Jenkin and Campbell [34] performed an insertion and dispersion error analysis assuming a generic halo orbit around $L2$ point. They found that such trajectories are extremely sensitive to the launch vehicle performance dispersions and, as previous libration point missions done, it is necessary to plan for trajectory correction maneuvers along the transfer and providing for additional propellant to enable such maneuvers. They showed that a ΔV budget around 180 m/s at a 99% confidence level should allow these corrections for generic halos around $L2$.

Cobos and Masdemont [12] applied the invariant manifolds technique to transfer a spacecraft between two Lissajous orbits around the same point. The authors state that such orbits are very suitable for future libration point

missions since, differently from the halos, they do not present big elongations around the point. Moreover, they developed also an optimal strategy for the eclipse avoidance around $L2$ allowing a six years free of eclipse for the ESA's missions FIRST and Planck.

3.1.1 Motivations for further studies

The state of the art analysis has shown that the history of libration point missions in the Sun-Earth system begun almost 25 years ago and, since now, six missions have been carried out. This represents the only case in this work where some missions have already been designed exploiting the libration points dynamics characteristics. Nevertheless, it seems that a general characterization of the transfer trajectories, by the technique of the manifolds, to these halos is still missing. For instance, when planning for a new libration point mission in the Sun-Earth system, a parametric study is required to analyze how changes in the final orbit, chosen according to the mission constraints, affect the parameters of the transfer trajectory. The authors mean, as an example, the concurrent design environments, like the ESA's CDF, where fast and well-approximated results have to be known to the designers. Many methods for the two-body analysis already exist, but, as known to the authors, the same is not yet true for the libration point mission analysis.

Thus, assuming a range of orbits, parameterized with the out-of-plane amplitude A_z, the orbital parameters have been analyzed in the previous chapter and now the objective is to study how the transfer trajectory between an Earth orbit to these halos changes with respect to the final orbit. Moreover, the orbit around the Earth could not have been completely fixed in a design process because it changes with respect to a lot of mission requirements.

Known this, the task of the present chapter can be summarized as: given a range of orbits about the Earth with altitudes $h \in [h_{min},\ h_{max}]$ and given a range of possible final halo orbits about $L1$ and $L2$ in the Sun-Earth system with amplitudes $A_z \in [A_{z,min},\ A_{z,max}]$, find the cost and the parameters (time of flight, insertion point, insertion cots, ...) of the possible transfer trajectories.

To simplify the work, only circular orbits about the Earth will be considered. This is not a great restriction since the case of elliptical orbits could be easily involved in a second step. In addition, no trajectory correction manoeuvres (TCMs) will be considered so the injection occurs directly on the stable manifold associated to the orbit. Even if with TCMs the total cost of the transfer can be reduced, here the interest is focused only on tra-

jectories lying on the manifolds. The mid-course manoeuvres improve the performances of the trajectory, but again could be added in a second step.

3.1.2 Space applications

The space applications concerning the libration point orbits in the Sun-Earth system are those missions that take advantage by holding a fixed configuration between the Earth and the Sun.

The $L1$ point is an ideal location for an uninterrupted observation of the Sun and its effects since this interior equilibrium is never covered by other bodies. Here, out of the Van Allen belts, a spacecraft could also study the interactions between the geomagnetic field and the solar wind. Due to the lack of eclipses, the power could be generated continuously by solar arrays. Moreover, at the $L1$ point a spacecraft could observe always the Earth or, as recently studied for the ESA's Space Weather Programme [73], it may be the location for a payload that studies the space weather.

The opposite exterior libration point $L2$, is a very suitable site for a space telescope since here the Earth, the Moon and the Sun are always behind the point and this means that there are stable thermal conditions, ideal for a telescope. But, a spacecraft in a halo orbit must have an appropriate out-of-plane motion in order to avoid the eclipses and so assure the power generation. From $L2$ also the observation of the other side of the Earth could be possible.

Finally, both points can be used for the location of relay satellites useful for the interplanetary navigation [72].

3.2 Selection of the appropriate Poincaré section

Starting from a circular parking orbit around the Earth, a spacecraft must be injected on the stable manifold associated to the a final halo orbit orbit $W^s_{Li,p.o.}$ $(i = 1, 2)$. Since the manifolds are two dimensional "tubes" in the six dimensional phase space, this task is not easy. In order to lower the dimensions of the problem, the Poincaré sections associated to the manifolds, a powerful tool in the dynamical system theory, have been introduced for the selection of the most appropriate injection point.

The equations of motion 1.6 are written in a rectangular coordinate system so it is usual to take the surface of section parallel to one of the three coordinate axes. When a manifold is cut by this section, one state is fixed by the location of the surface (e.g. $x = 1 - \mu$), four states are plotted (e.g.

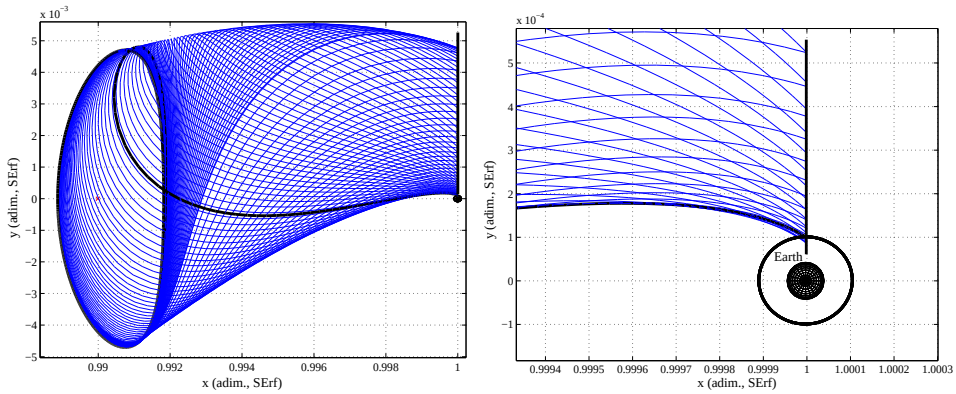

Figure 3.4: Poincaré section of $W^s_{L1,p.o.}$ at $x = 1 - \mu$ and $\dot{x} < 0$.

$\dot{y}$ vs y and $\dot{z}$ vs z) and the remaining ($\dot{x}$) is given by Jacobi constant (see equation 1.9) associated to the orbit.

The matter now, is the selection of the most appropriate section for the spacecraft injection. Three sections have been introduced for the transfer to a $L1$ halo orbit:

- $x = 1 - \mu$ and $\dot{x} < 0$ (figure 3.4);
- $y = 0$ and $\dot{y} > 0$ (figure 3.5);
- $x = 1 - \mu$ and $\dot{x} > 0$ (figure 3.6);

For all the three cases, a range of Earth orbits has been given with amplitudes $h \in [150,\ 10000\ km]$ and the algorithm has been left free to choose the cheaper insertion orbits. Figure 3.4 shows that the first Poincaré section

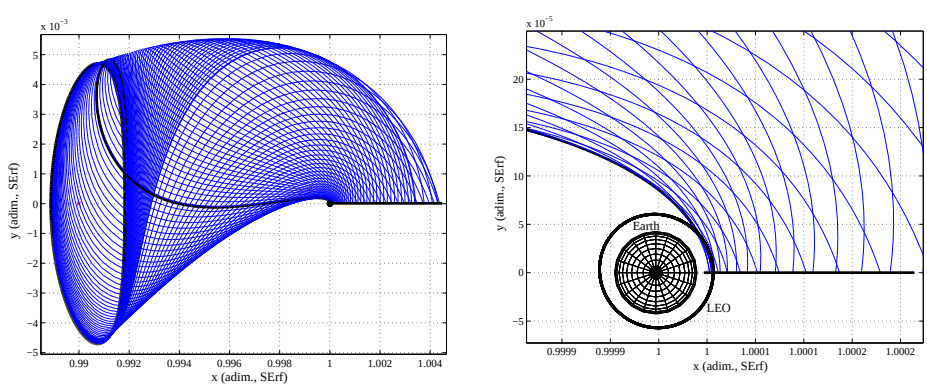

Figure 3.5: Poincaré section of $W^s_{L1,p.o.}$ at $y = 0$ and $\dot{y} > 0$.

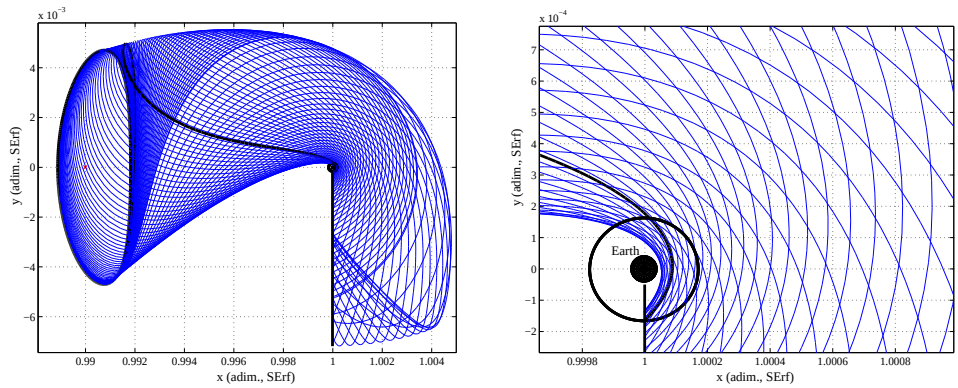

Figure 3.6: Poincaré section of $W^s_{L1,p.o.}$ at $x = 1 - \mu$ and $\dot{x} > 0$.

considered ($x = 1 - \mu$ and $\dot{x} < 0$) is not appropriate for a manifold injection since here the costs are elevated. It is known, indeed, that the optimum cost is associated to a tangential injection that is the one shown in figure 3.5 associate to a Poincaré section $y = 0$ and $\dot{y} > 0$.

In figure 3.6 the manifold reaches again the y-axis and the third section ($x = 1 - \mu$ and $\dot{x} > 0$) is considered. It is clear that this case is the worst since the injection happens inward to the Earth and high costs are required.

Figure 3.7 shows the same Poincaré section as in figure 3.5 (but with $\dot{y} < 0$) for the transfer to a $L2$ halo. This time the injection is perfectly tangential and the minimum cost for a $L2$ transfer is achieved.

The authors suspect that the selection of a Poincaré section at $y = 0$ and $\dot{y} > 0$ for $L1$ and $\dot{y} < 0$ for $L2$ involves minimum costs. In the present chapter these two sections have been chosen to study the transfer trajectories to the halos.

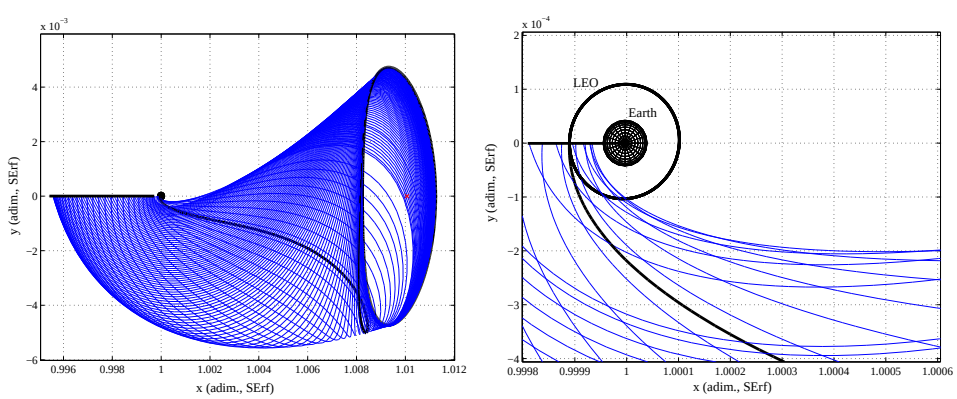

Figure 3.7: Poincaré section of $W^s_{L2,p.o.}$ at $y = 0$ and $\dot{y} < 0$.

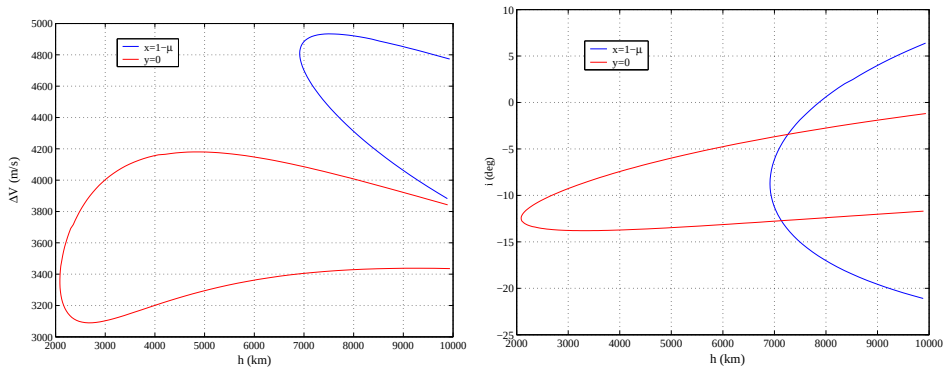

Figure 3.8: Δv vs h (left) and i vs h (right) for the first two sections considered.

Figure 3.8 shows the relation between the altitude of the parking orbit (h) and the cost of the transfer (Δv) for the first two sections. The assumptions are confirmed since the first figure shows that the Poincaré section at $y = 0$ assures at the same time a wide range of altitudes and reduced costs with respect to the section at $x = 1 - \mu$. On the contrary, this choice involves a restriction on the inclination (i) of the Earth's orbits for the manifold injection.

3.3 Problem approach

Without loosing of generality, let A_z be the out-of-plane amplitude of a halo orbit around $L1$. The extension to the $L2$ point and to all the amplitudes is straightforward. Associated to the j-th point of the orbit there is a one dimensional stable manifold $W^{s,\ j}_{L1,p.o.}$ that is propagated until the surface of section is reached (blue lines in figure 3.9).

On the surface of section, let the six state of $W^{s,\ j}_{L1,p.o.}$ be:

$$\mathbf{x_P^j} \ = \ \{x_P^j,\ y_P^j,\ z_P^j,\ \dot{x}_P^j,\ \dot{y}_P^j,\ \dot{z}_P^j\} \tag{3.1}$$

that are uniquely determined once the point on the orbit has been fixed. This means that there is a correspondence between the points on the orbit and the points on the surface of section.

When the states of equation 3.1 are known, the circular orbit required for the manifold injection must have an altitude equal to:

$$h \ = \ \sqrt{(x_P^j)^2 \ + (y_P^j)^2 \ + (z_P^j)^2} - R_E \tag{3.2}$$

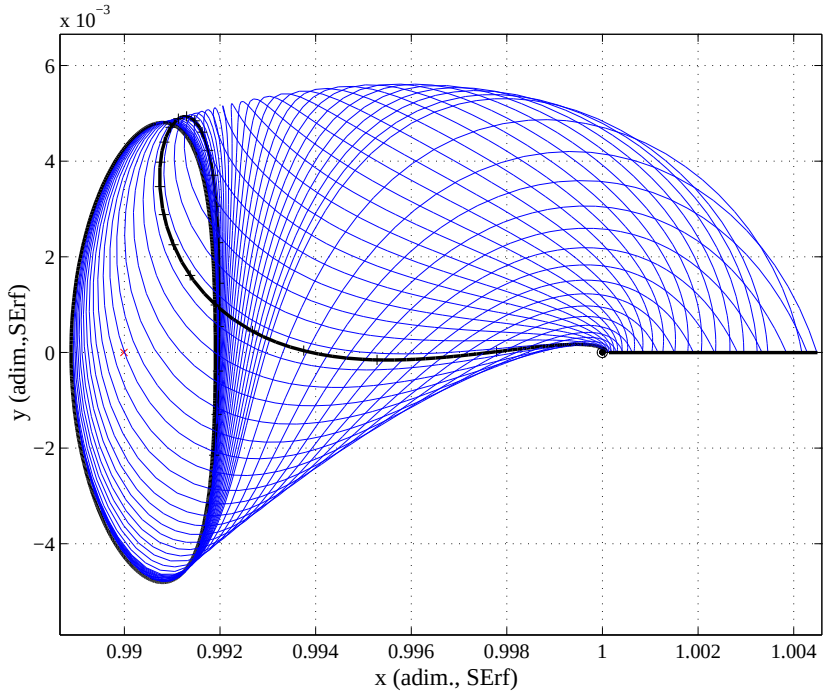

Figure 3.9: Example of transfer trajectory from an Earth's orbit to a $A_z = 290000\ km$ halo. The trajectory (black) is marked every ten days.

and an inclination (with respect to the ecliptic):

$$i \quad = \quad atan\left(\frac{z_P^j}{\sqrt{(x_P^j - 1 + \mu)^2 \ + (y_P^j)^2}}\right) \tag{3.3}$$

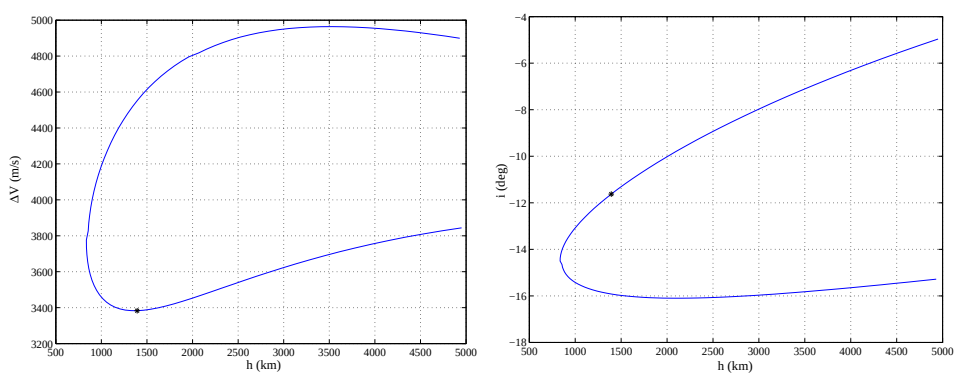

Figure 3.10: Δv vs h (left) and i vs h (right) for the example considered in figure 3.9. The marked point corresponds to the minimum cost trajectory.

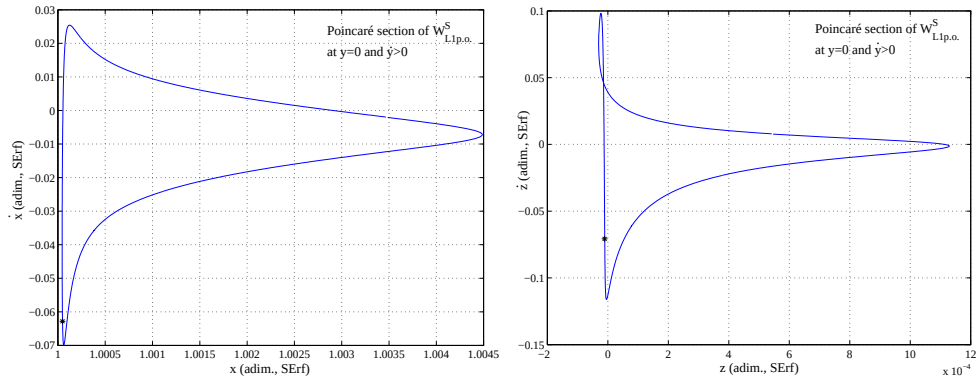

Figure 3.11: Poincaré sections $(x, \dot{x})$ (left) and $(z, \dot{z})$ (right) of the stable manifold in the example considered. The two marked points correspond to the minimum cost trajectory.

The cost necessary for the injection is:

$$\Delta v \quad = \quad \sqrt{(\dot{x}_P^j - v_{c,x})^2 \ + (\dot{y}_P^j - v_{c,y})^2 \ + (\dot{z}_P^j - v_{c,z})^2} \tag{3.4}$$

where $v_c = \sqrt{k_E/(R_E + h)}$ is the velocity on the circular orbit and R_E is the Earth's radius[1].

Repeating this process for each point of the halo, the relations among the parameters have been obtained. Figure 3.10 shows how the cost for the injection changes with the altitude of the orbits and the point corresponding to the minimum cost injection has been marked. The relation between the inclinations and the altitudes have been shown too.

Figure 3.11 represents the two Poincaré sections of the manifold considered. The marked point correspond to the minimum cost trajectory. The time of transfer of this example is $\Delta T = 122$ *days* and the cost for the orbit injection[2] is $\Delta v_{inj} \simeq 3$ m/s.

3.4 Transfer trajectories to the $L1$ halos

In order to study the properties of the transfer trajectories for missions around $L1$ in the Sun-Earth system, the minimum and maximum altitudes for the Earth's orbits have been fixed equal to $h_{min} = 200$ km and $h_{max} =$

[1]The values $k_E = 3.98 \cdot 10^{14}$ m^3/s^2 and $R_E = 6378$ km have been assumed.

[2]We remember that the manifolds computed here are only approximation and the trajectories must be forced to enter into the final orbit (see section 1.4.2).

5000 km. Several halos have been analyzed with amplitudes:

$$A_z = [140000 + (i-1)20000]\ km\ , \qquad i = 1, ..., 11 \tag{3.5}$$

and the obtained results are summarized in table 3.1. The table shows the best results obtained for each A_z halo with the altitudes in the given range.

It can be observed that the costs are slightly higher than the ones required for the previous missions. But, in this section the trajectory have not been optimized since the goal was the parametric study of the trajectories belonging to the manifolds. Indeed, if TCMs would have been introduced, the performances of the transfers could have been improved.

Figure 3.12 shows the trajectory analyzed with an emphasis on how the circular orbits about the Earth change with respect to the final halo transfer trajectory.

In figure 3.13 the locus of the minima Δv is plotted. Manifolds that goes beyond the minimum altitude $h_{min} = 200\ km$ have been cut since they represent Earth impact trajectories. Figure 3.14 represents the transfer departing from a GEO (last row in table 3.1) with an emphasis on the structure of the manifold near the Earth.

A_z (km)	h (km)	Δv (m/s)	i (deg)	ΔT $(days)$	Δv_{inj} (m/s)
140000	4987	2658	-6.7	120.3	2.8
160000	4954	2680	-6.6	120.6	2.8
180000	4806	2742	-6.9	120.8	2.9
200000	4219	2824	-7.8	121.0	2.9
220000	3605	2919	-8.7	121.1	2.9
240000	2984	3028	-9.6	121.3	2.9
260000	2344	3154	-10.4	121.5	3.0
280000	1711	3301	-11.2	121.8	3.0
300000	1004	3470	-12.2	122.0	3.0
320000	365	3668	-12.9	122.3	3.1
340000	224	4013	-11.9	122.7	3.1
100000	GEO	1456	-2.3	122.9	2.8

Table 3.1: Parameters of the transfer trajectories to the $L1$ halos in the Sun-Earth system.

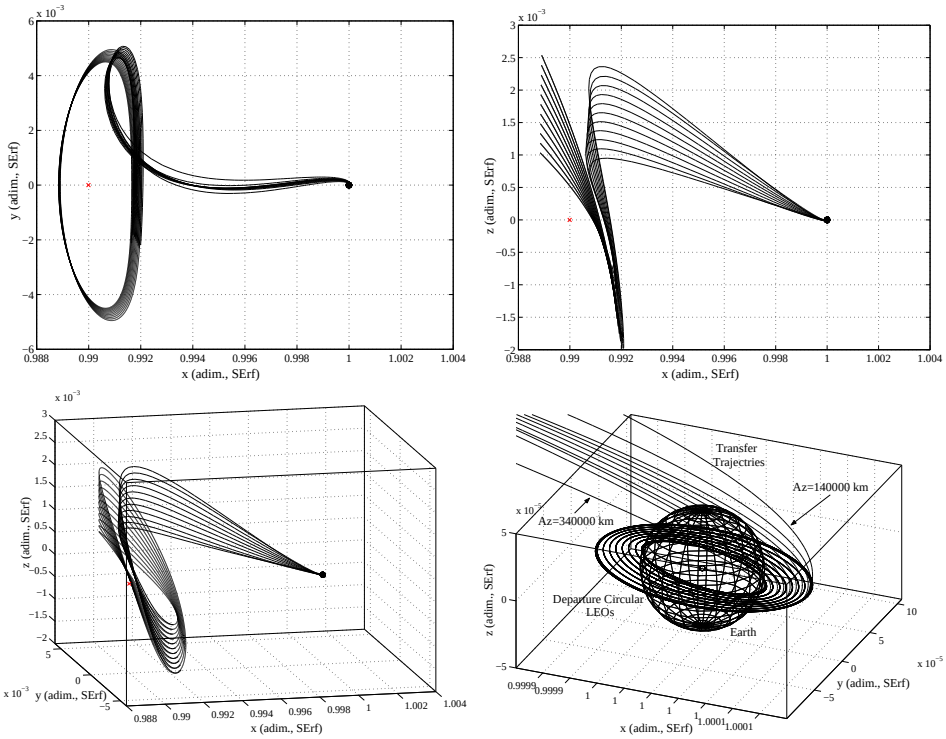

Figure 3.12: Transfers trajectories to the Sun-Earth $L1$ halos: (x, y) and (x, z) projections; the full 3D transfers and the circular Earth's orbits.

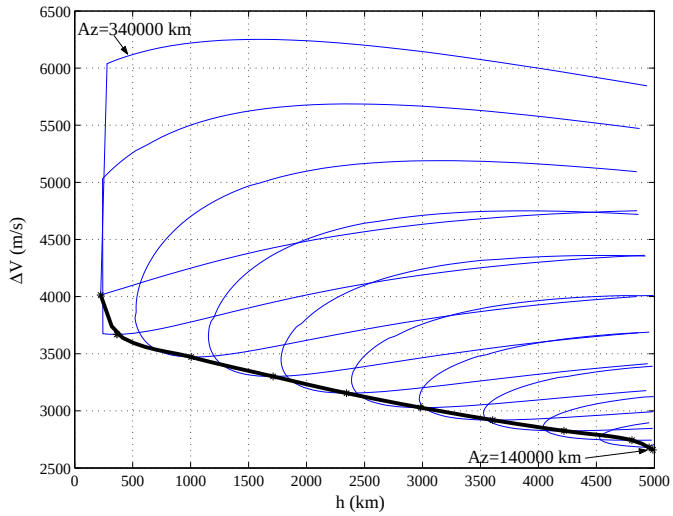

Figure 3.13: Δv vs h for the cases in table 3.1. The black line is the locus of the minima Δv's.

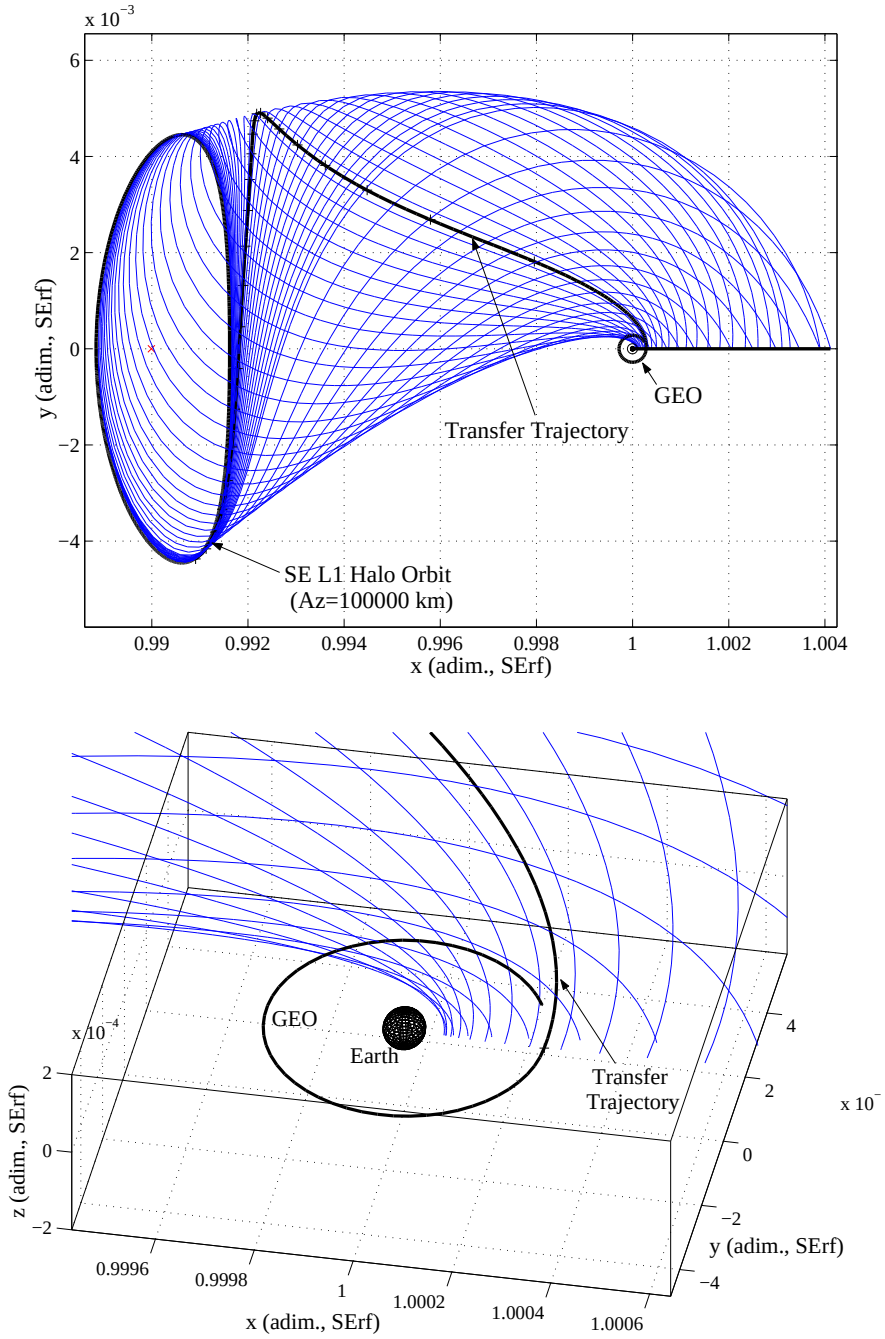

Figure 3.14: Transfer trajectory to an $A_z = 100000\ km$ departing from a GEO (top). This transfer requires a cost $\Delta v = 1456\ m/s$ and a time of flight equal to $\Delta T = 122.9\ days$. The structure of the manifold near the Earth (bottom). It is clear how the Earth's presence distorts the lines.

3.5 Transfer trajectories to the $L2$ halos

The transfer trajectories toward the Sun-Earth $L2$ orbits have been analyzed assuming the following amplitudes for the halos:

$$A_z = [130000 + (i-1)20000]\ km\ , \qquad i = 1, ..., 11 \tag{3.6}$$

and again the range of altitude is $h_{min} = 200\ km$ and $h_{max} = 5000\ km$.

Table 3.2 summarizes the results found in this case plus, in the last row, the parameters associated to a GEO departure. In this case, since the shape of the curves Δv vs h changes, the Earth's orbits associated to the minimum cost transfers have altitudes near the upper bound. Consequently, in this case the cost is lower than in the previous.

The time of transfers is again around four months and it is remarkable how, both for $L1$ and $L2$, the cost for the halo orbit injection Δv_{inj} does not vary with the size of the orbit and remains always around 3 m/s.

Also in this case, the model does not include neither optimized TCMs nor Moon swing-by's that are expected to further lower the total cost.

A_z (km)	h (km)	Δv (m/s)	i (deg)	ΔT $(days)$	Δv_{inj} (m/s)
130000	4991	2696	6.7	126.6	3.4
150000	4970	2598	8.2	126.7	3.5
170000	4938	2549	9.4	126.8	3.5
190000	4880	2517	10.5	127.0	3.6
210000	4838	2492	11.6	127.2	3.6
230000	4866	2474	12.7	127.4	3.7
250000	4983	2474	13.6	127.7	3.7
270000	4881	2521	14.5	128.0	3.7
290000	4825	2596	15.4	128.3	3.8
310000	4825	3997	16.3	128.6	3.8
330000	4901	2883	17.1	129.0	3.9
100000	GEO	1334	2.3	123.3	3.4

Table 3.2: Parameters of the transfer trajectories to the $L2$ halos in the Sun-Earth system.

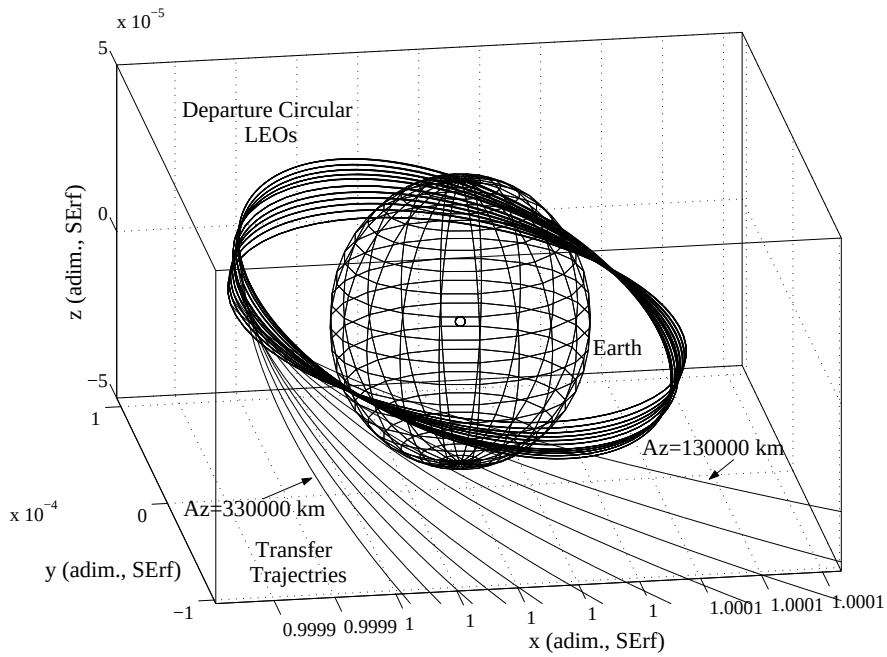

Figure 3.15: Earth's circular orbits for the Sun-Earth $L2$ transfers. Differently from the previous case, this time there is a broader excursion in the orbits' inclination (table 3.2).

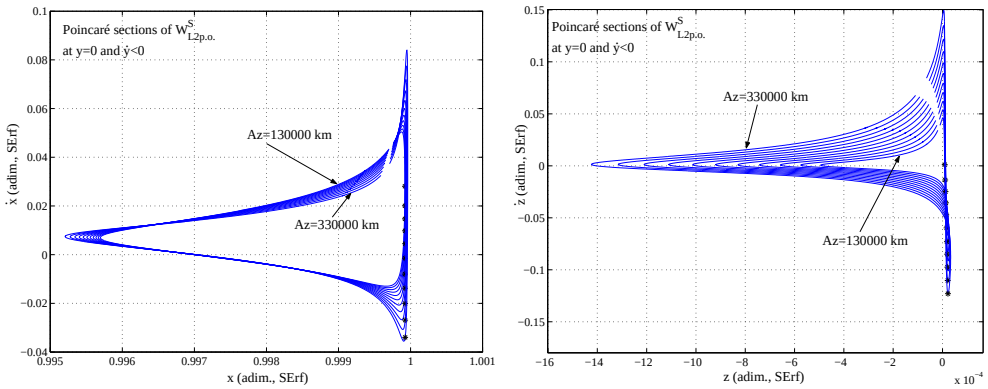

Figure 3.16: Poincaré section $(x, \dot{x})$ (left) and $(z, \dot{z})$ (right) for the transfers to $L2$. The marked points are associated to the minimum cost transfers.

3.6 Sun-Earth libration point orbits: uses for future space missions

This section has been prepared with the purpose to evaluate the properties associated to the trajectories belonging to the stable manifolds of $L1$ and $L2$ halos in the Sun-Earth system. The results found in this frame are here discussed together with the possible uses of these trajectories, the drawbacks and their implications at system level.

3.6.1 Remarks about the solutions

Missions about the halos of the Sun-Earth system are well known by the scientific community and a general method for their design has been established. In this section the intention has been to evaluate the performances of the transfer trajectories to these halos. So, neither trajectory correction manoeuvres nor Moon's swing-by's have been considered. The authors expect that the difference in the cost of about $300 \div 400$ m/s between the existing solutions and the ones found here is due to the lack of these two important phases.

Anyway, a trajectory belonging to the stable manifold can reach the final orbit by only waiting for the evolution of the dynamical system and about 3200 m/s are required to inject a spacecraft from a low Earth orbit on these stable manifolds. There are no sensible differences in these costs between orbits around $L1$ and around $L2$. The main differences, at a fixed point, concern the amplitudes of the halos. When the amplitude of the final orbit grows, indeed, the manifolds become larger and a great part of them approaches the Earth. So, in this case, it is easier to look for cheap solutions departing from Earth orbits.

The time required for these transfers is around four months for each of the two points considered while the cost for the orbit injection is always below 5 m/s. Furthermore, it has been calculated that the cost necessary to the stationkeeping is about 10 $m/s/year$.

These costs and times do not represent particular constraints for the missions on these halo. Maybe, this is the reason why only missions about these libration points have been done in the space activity. Nevertheless, the low number of these missions (six) indicates that a better knowledge of the mission design and the potential use of the libration points in the Sun-Earth system is necessary.

3.6.2 Uses for future space missions

The main uses of the libration points in the Sun-Earth system for future space missions are due to their fundamental property: a spacecraft placed around these points keeps its geometry fixed with respect to both the Earth and the Sun. It is clear that, with such a feature, a lot of missions can be planned in order to exploit this unique characteristic for space applications. The authors limits to only two of these.

Recently the $L2$ point has been established as a very appropriate location for a space telescope due to its stable thermal environment. These conditions are produced because the Sun, the Earth and the Moon are always aligned with that point. By placing a single satellite on this point half the sky could be observed and studied. The nominal orbit must of course avoid the Earth's disc in order to allow the power generation with the solar arrays.

Other uses of these orbits concern the scientific observation of the Sun and the Earth's monitoring from a fixed point: half the Earth is always visible from both $L1$ and $L2$. Finally, an interplanetary navigation system could be developed with several spacecrafts placed in the libration points of the Sun-Earth system (not only $L1$ and $L2$) [72].

3.6.3 Drawbacks

The times and costs associated to the transfers to the halos in the Sun-Earth system are not prohibitive. Thus, the only drawback associated to this kind of missions is represented by the navigation within this nonlinear environment. Nevertheless, the trajectory correction manoeuvres would be useful to avoid launch errors or dispersions.

When the Moon's swing-by's are considered, the launch windows are expected to be sensitive with respect to the Moon phase. Moreover, the Moon's perturbation must be considered in the cost and stationkeeping evaluation.

The analysis of the starting legs has sown that only a small range of inclinations allows a direct injection on the stable manifold.

3.6.4 Considerations at system level

Spacecrafts about the libration points in the Sun-Earth system do not require particular consideration concerning the whole space system. The power generation can be accomplished by using the solar arrays in both $L1$ and $L2$. Spacecrafts in the latter point must provide for an eclipse avoidance strategy in order to allow the power generation.

The continuous visibility of the Sun influences also the thermal subsystem that has to be designed in order to take into account this strong thermal source. The communication with the Earth is assured because the Earth is continuously in the field of view of the spacecraft. The propulsion is chemical and liquid engines are preferred due to their restartable properties. Nevertheless, if the spacecraft is placed on the transfer trajectories directly by the launcher, it could require only small engines to correct the trajectory.

Chapter 4

Transfers to Halo Orbits in the Earth-Moon System

Differently from the previous case, in the Earth-Moon system the Earth represents the largest primary and so this time $L1$ and $L2$ points are close to the Moon. This means that, as will be show in the present chapter, the manifolds associated to the periodic orbits around these libration points no longer approach the Earth. It could be that this is the reason why a libration point mission in this system has never been made. In order to overcome this problem, and at the same time exploit the feature of the invariant manifolds, an intermediate Lambert's R3BP arc has been introduced. By this arc, a point belonging to an orbit around the Earth and a point on the stable manifold associated to the final halo are linked together.

As done for the libration point missions in the Sun-Earth system, in the first part of this chapter the actual state of the art is analyzed. Later, the technical approach and the obtained results will be show together with the author's point of view concerning the uses for future space missions.

4.1 State of the art analysis

The idea of using the collinear libration points of the Earth-Moon system for space missions has a long history. Colombo [13] was the first who understood the high potential associated with these points and the importance to have a spacecraft in a fixed configuration with respect to the Earth and the Moon. He demonstrated that the collinear points ($L1$, $L2$ and $L3$) of the Earth-Moon system continue to be exact solutions of the R3BP even if no hypothesis are made on the motion of the primaries and when the perturbations of other bodies are considered. In this way, a point mass placed in

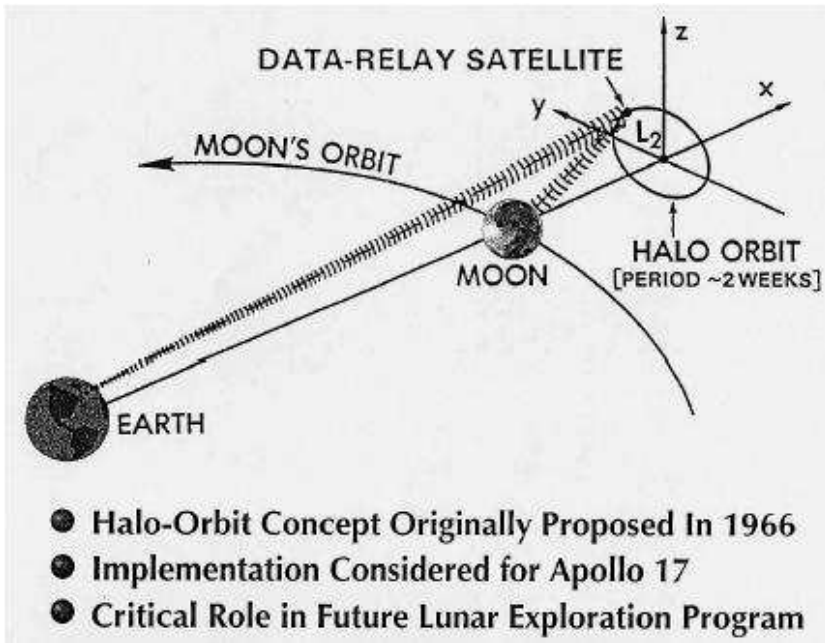

Figure 4.1: The lunar far-side communication concept proposed by Farquhar [17].

an equilibrium point with the appropriate velocity moves remaining aligned with the primaries.

Farquhar [22] proposed the use of a libration point satellite for lunar communications. He studied the possibility to have a real-time communication link between the far side of the Moon and the Earth by placing a *single* relay spacecraft in a halo orbit about $L2$ (figure 4.1). Moreover, he observed that by placing another single relay satellite at the cislunar libration point $L1$, a point-to-point communication network covering most of the lunar surface could have been also established. This libration point network concept was proposed as a navigation and control center for extensive lunar explorations.

These proposals were validated by Farquhar [19] [21] which estimated that the station-keeping cost required for such missions is around $\Delta V = 100\ m/s/year$ depending on the out-of-plane amplitude of the halo orbit considered.

Apart from the lunar far-side communications, Farquhar proposed also a deep space communication network by placing the relay satellites on the equilateral points ($L4$ and $L5$) of the Earth-Moon system in order to avoid the strong noise induced by clouds [20]. Recently, several studies deal with the development of this idea [72]. In the same work, Farquhar suggested the employment of a reusable spacecraft as a cycler between the libration points of the Sun-Earth and a Sun-Planet system. It is remarkable how, four

decades ago, Farquhar proposed such concepts that are being considered in these years.

In order to study a transfer trajectory between the Earth and the libration points of the Earth-Moon system a dedicated method must be developed in the R3BP frame. It is clear, indeed, that the conic analysis fails in these regions of space because the gravitational attractions of two bodies are comparable.

D'Amario and Edelbaum [15] developed a method to find optimal impulse transfers in the circular R3BP. This technique was based on the combination of a multiconic method with the primer vector theory and an accelerated gradient method of trajectory optimization. Their method was applied to the determination of optimal two and three-impulse transfers between circular orbits about the Moon and the translunar libration point $L2$.

Then, based on the previous study, Pu and Edelbaum [56] found two and three optimal impulse trajectories in a Sun-Earth-Moon environment where the three bodies all have a significant influence on the motion of the spacecraft. They applied this technique to analyze trajectories between the Earth and the $L1$ libration point and they estimated that a cost around $\Delta V = 3600\ m/s$ is necessary to reach that point departing from a circular orbit around the Earth with altitude $h = 185\ km$.

Broucke [10] computed free-fall trajectories from the Moon to the four Lagrangian points $L1$, $L2$, $L4$ and $L5$ and back from these points to the Moon. He considered in detail the problem of compromising short transit times and small residual velocity at the point. Broucke found several families of possible trajectories, depending on the time required for the transfer, for each of the four Lagrangian points.

Prado [55] completed the Broucke's work by analyzing transfers from the same points to the Earth. Both these studies, based on the solution of the Lambert's three-body problem in regularized coordinates, involve the transfer between a primary and a point. On the contrary, the present chapter analyzes the transfer trajectories from an orbit around the Earth to an orbit around the points $L1$ and $L2$.

Heppenheimer [30], in his study on the optimal location of a space colony, studied a transfer path from a high Earth orbit to the point $L2$. He observed that the nominal candidates were orbits found as periodic solutions in the R3BP and he chose a 2:1 resonant orbit as the baseline for his problem.

Jones and Bishop [35] developed a two-spacecraft terminal-phase rendezvous targeting in the circular R3BP. They used a small radius translunar halo orbit and ideal navigation to demonstrate the effectiveness of their technique.

In the last years, Starchville and Melton studied the transfer of a space-

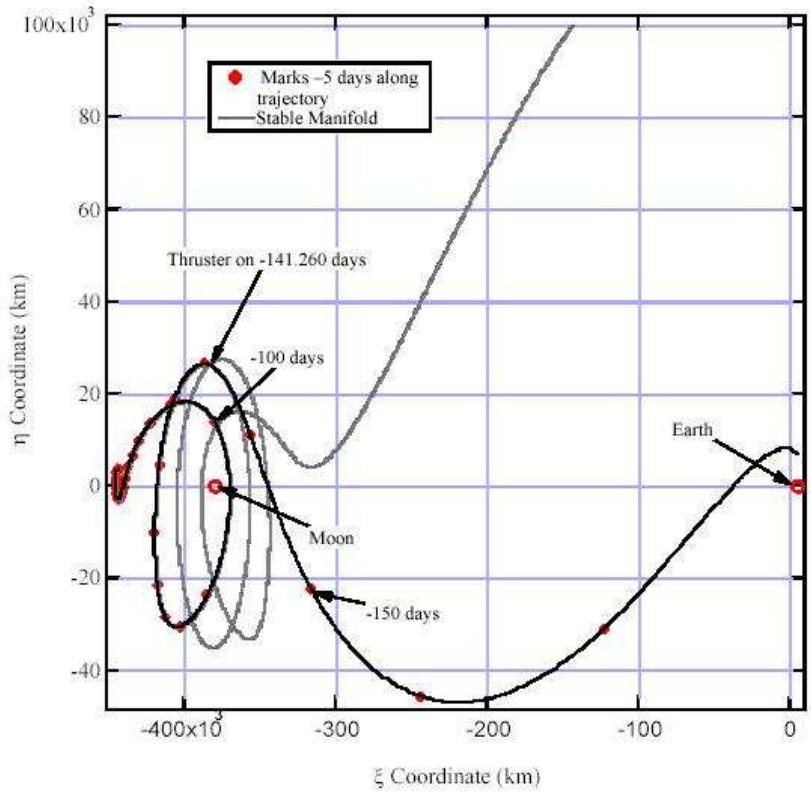

Figure 4.2: The translunar halo transfer computed by Starchville and Melton obtained combining invariant manifolds and low-thrust propulsion [66].

craft from an Earth orbit to a $L2$ halo orbit in both the circular [66] and elliptical problem [67]. Their works were innovative since the optimization of low-thrust trajectories and invariant manifolds technique were combined together. The full trajectory starts with a ΔV, provided from the launch vehicle, at an altitude above the Earth equal to h. Then, a thrust arc is used to target a piece of the stable manifold associated to the final halo around $L2$ (figure 4.2).

In the circular problem, the authors found that a halo orbit with $A_x = A_y = 7000\ km$ could be reached with a propellant mass fraction $m_p = 55 \div 60\ kg$ departing from an Earth orbit with altitude $h = 460 \div 500\ km$ and an initial burn equal to $\Delta V = 1700\ m/s$. A larger orbit with amplitudes $A_x = 25000\ km$ and $A_y = 70000\ km$ needs a propellant mass $m_p = 55 \div 80\ kg$ plus $\Delta V = 1700\ m/s$ at an altitude $h = 475 \div 500\ km$. In both the examples the time of flight was equal to $\Delta t = 365\ days$.

In the elliptical problem, the first halo requires $m_p = 55\ kg$ and $\Delta V =$

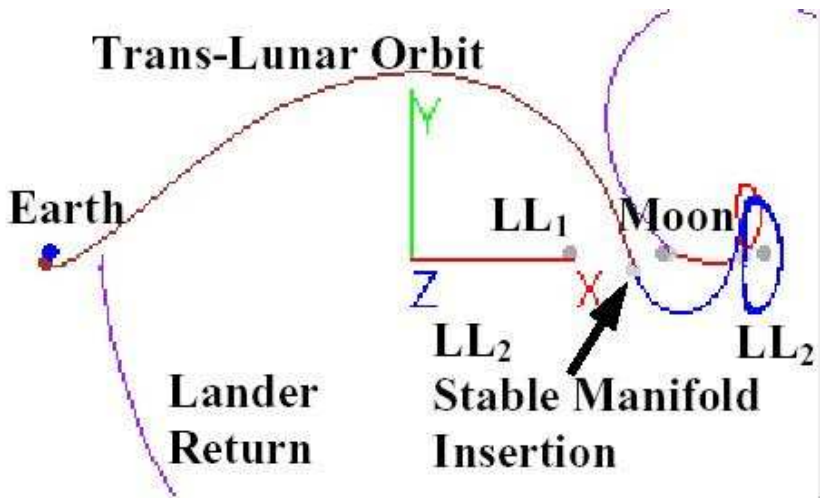

Figure 4.3: The direct transfer trajectory to the $L2$ halo orbit in Lo and Chung [48].

1700 m/s departing from $h = 465 \div 500$ km. In this model the larger orbit needs $m_p = 55 \div 60$ kg and $\Delta V = 1700$ m/s from $h = 420 \div 480$ km. These two cases have again a time of transfer equal to $\Delta t = 365$ $days$. In both cases, the final (in orbit) mass is equal to 1000 kg.

Finally, Lo and Chung [48], in a lunar sample return study, resumed the idea of Farquhar, cited above, to provide the communication between the Earth and the far side of the Moon. They studied three different scenarios to put a spacecraft about the Earth-Moon $L2$ departing from a 200 km circular orbit around the Earth.

In the first option, shown in figure 4.3, the spacecraft is transferred to the final halo by targeting the stable manifold associated to a point of this orbit. A first impulse equal to $\Delta V_1 = 3122$ m/s puts the spacecraft in a translunar trajectory, while a second maneuver with $\Delta V_2 = 570$ m/s forces the spacecraft to lay on the stable manifold. Thus, the total cost for this option is $\Delta V = 3692$ m/s and the time required is $\Delta t = 11$ $days$.

The second alternative they considered was a transfer to $L2$ via a heteroclinic connection with $L1$. The heteroclinic connection between these two orbits is shown in figure 4.4. In this case, with a first $\Delta V_1 = 3100$ m/s, the spacecraft is sent in a orbit that targets a piece of the stable manifold associated to the $L1$ halo. Here, with a second impulse equal to $\Delta V_2 = 600$ m/s, the spacecraft is injected in the $L1$ halo orbit. Then, a third $\Delta V_3 = 14$ m/s performs the heteroclinic connection and the spacecraft reach the final $L2$ halo. The overall cost for this option is $\Delta V = 3714$ m/s and the time of transfer is $\Delta t = 28$ $days$.

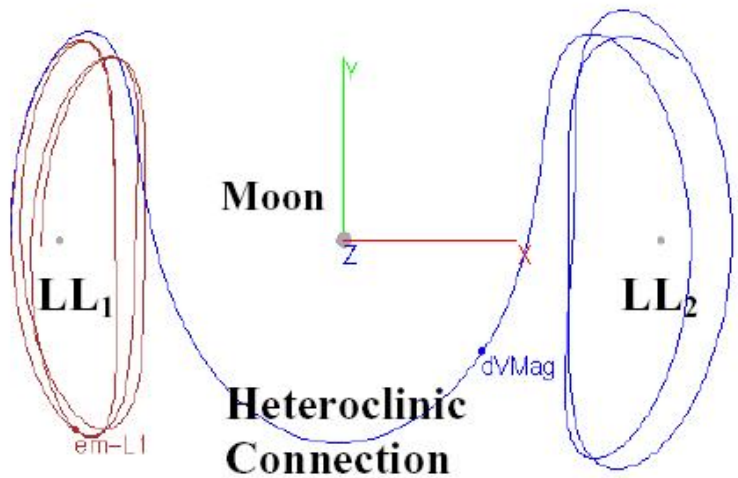

Figure 4.4: Terminal leg of the $L2$ halo transfer via a heteroclinic connection computed by Lo and Chung [48].

In the third option the spacecraft is sent on the final orbit by passing through the Sun-Earth $L1$ and exploiting the Moon capture mechanism (see section 6.1). The total cost for this scenario is $\Delta V = 3266\ m/s$ but the transfer time is $\Delta t = 391\ days$ that is sensibly higher than the previous two cases.

4.1.1 Motivations for further studies

From the analysis of the state of the art, it follows that a libration point mission in the Earth-Moon system has never been done. From the authors' point of view, this is the consequence of the increased difficult in trajectory design within this frame. In the Earth-Moon system, indeed, the Earth is the greatest primary so the two equilibrium points $L1$ and $L2$ are close to the Moon and the manifolds associated to the periodic orbits about these points no longer approach the Earth. Thus, departing from the Earth's neighborhood, there will be no *free* transport to the libration points as in the Sun-Earth system[1].

In the switch from the two-body to the three-body problem there is the loss of orbital elements, integral of motion in the 2BP, and the structure of the

[1]This case is qualitative analogous to a transfer toward the Sun-Earth $L1$ and $L2$ departing from the Sun.

trajectory is difficult to characterize. In the R3BP, the only integral available is the Jacobi constant, but one conserved quantity over six states of motion does not allow any quantitative useful information, apart from the forbidden regions. In this context, the manifolds provide for additional information within the R3BP since they represent a useful tool for the designers. This is the reason why the invariant manifolds must be considered also in this frame even if they only provide for *partial* free transport (i.e. the transfer from a given point far from the Earth to the final halo).

The works of Starchville and Melton [66] [67] and Lo and Chung [48] were aimed to target a piece of the stable manifold associated to the final periodic orbit. They used two different techniques to do this, but the former turned out to be a long-time transfer while the latter was short but quite expensive. The exploration of the intermediate possibilities is not easy since in the R3BP, given a time and two points, it is not easy to join these two points with the constraint on the time of flight. The reason is again the loss of a powerful tool used in the two-body environment: the Lambert's problem.

The authors suppose that when the time of transfer is free to vary, the trajectory could better exploit the Moon's resonances and cheaper transfers could be obtained. Aiming to do this, in the present study an algorithm for the solution of the Lambert's three-body problem (L3BP) has been developed (section 2.7) and so the task of the present chapter is the investigation on the existence of low-energy and mid-time transfers of practical interest. These transfers are based on the target of the stable manifold associated to the final orbit with a L3BP arc.

While the previous chapter was focused on a qualitative study of the trajectories belonging to the stable manifolds in the Sun-Earth system, here the approach is quite different since *quantitative* results are required to evaluate the feasibility of these transfers. Hence, the common LEO, GTO and GEO will be considered as starting orbit from the Earth.

4.1.2 Space applications

The high potential of the Earth-Moon equilibrium points for space applications is well-known in literature. Libration point orbits, indeed, have performances that cannot be achieved with the common Keplerian two-body orbits.

As an example, the concept proposed by Farquhar, for the communications between the far side of the Moon and the Earth through a single relay satellites placed in an Earth-Moon $L2$ halo, summarizes this statement. In this case, both the Moon's and Earth's disc can be covered always by the satellite and this feature is uniquely associated with a halo orbit. If Keplerian

orbits are considered, for instance polar orbits around the Moon, more than three satellites are required to achieve the same performances.

At the same time, a satellite on a $L1$ halo can assure the coverage of the other side of the Moon and together, with the one in $L2$, are able to cover almost the full surface of the Moon. Moreover, these two applications can be shifted to assure the communications between the Earth and inner interplanetary spacecrafts because they do not involve the usual noise produced by the clouds.

Finally, the periodic orbits about the Earth-Moon $L1$ would be ideal locations for a future manned space station as an intermediate step for the Moon intensive exploration. This station will orbit the equilibrium point, and so the communication with the Earth would be allowed, but, starting from here, another vehicle would reach the Moon and from the Moon back to the station with small costs.

In this chapter only the cost to reach the halos will be considered while the one required for the station-keeping have to take into account the perturbation of the Sun. Anyway, it has been estimated [21] that a cost around $\Delta V = 100\ m/s/year$ is enough to assure the station-keeping.

4.2 Dependence on the Poincaré section

As stated above, a point on the stable manifold associated to the final orbit must be targeted starting from a given Earth's orbit. In order to lower the dimensions of this problem, Poincaré sections are again introduced. But, as discussed in section 3.2, the location of the appropriate surface of section is not trivial. In the present section two different cut of the stable manifold will be analyzed. Departing from the same 200 km LEO the costs for the transfers to the halos around $L1$ will be evaluated. This short analysis will suggest the problem approach that will be shown in the next section.

4.2.1 Section at $x = -\mu$

Given a halo orbit with an out-of-plane amplitude A_z and its associated stable manifold that is cut, as in figure 4.5, by the surface of section $x = -\mu$ and $\dot{x} > 0$, several transfers have been studied departing from a LEO with altitude $h = 200\ km$.

These transfers have been obtained by patching together a L3BP arc and a piece of the showed stable manifold. So, the full transfer cost involves a first Δv_1 to perform the Lambert's arc, a second Δv_2 for the manifold injection and a third Δv_3 for the halo orbit injection. This latter cost is always under

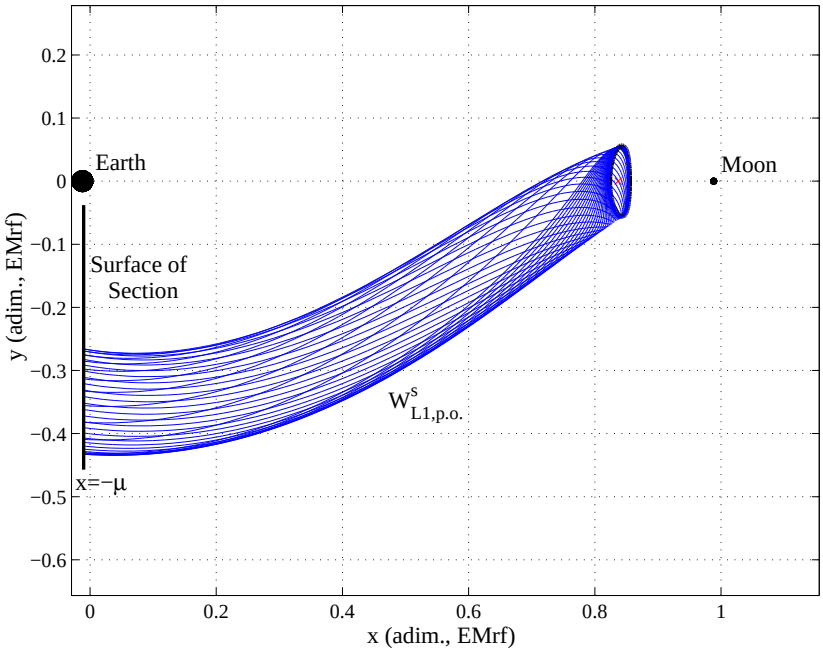

Figure 4.5: Stable manifold cut at $x = -\mu$ and $\dot{x} > 0$.

1 m/s and so it will not be taken into account. The overall cost for the transfer is:

$$\Delta v = \Delta v_1 + \Delta v_2 \tag{4.1}$$

The time of flight associated to the Lambert's arc is called Δt_L and the time that the spacecraft spends on the stable manifold, until the halo orbit injection occurs, is called Δt_W. Thus, the total time of transfer is:

$$\Delta t = \Delta t_L + \Delta t_W \tag{4.2}$$

Several results have been obtained with the given surface of section by considering eight halos with amplitude:

$$A_Z = i \cdot 1000\ km, \qquad i = 1, ..., 8 \tag{4.3}$$

and the transfer parameters are shown in table 4.1. In this problem there are no particular constraints on the out-of-plane amplitude as in the Sun-Earth system. Nevertheless, the only one is given by the lunar far side communication, but with a maximum A_z equal to 8000 km also this constraint is satisfied.

Since the manifold is sectioned at the first encounter with the plane $x = -\mu$, the very-short transfers contained in table 4.1 show high costs.

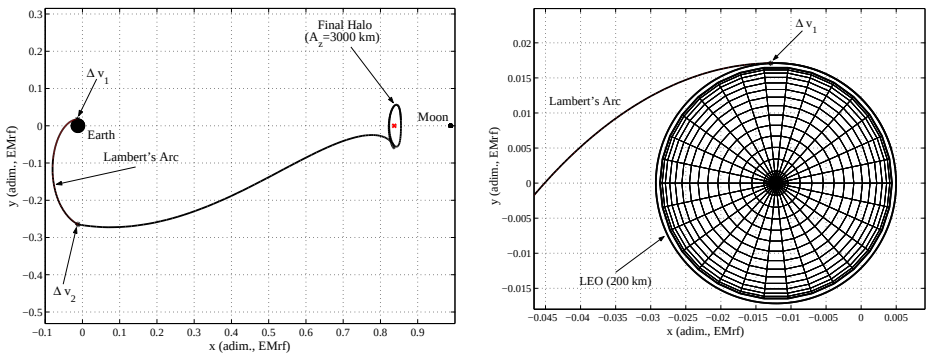

Figure 4.6: A typical transfer trajectory associated to the surface of section $x = -\mu$ and $\dot{x} > 0$ corresponding to the third row of table 4.1 (left). The starting LEO and the first leg of the Lambert's arc (right).

Moreover, it is straightforward that the more the out-of-plane amplitude increases, the more the transfer becomes expensive.

As discussed in section 4.1.1, looking for short transfers seems to involve high costs because the Moon's influence needs more time to act. If a typical five-day Hohmann transfer to the Moon is thought by this point of view, its high costs seems to be explained because in such a short time, and with the conic approximation, the trajectory is not allowed to exploit the Moon's gravitational field.

A_z (km)	Δt_L $(days)$	Δt_W $(days)$	Δt $(days)$	Δv_1 (m/s)	Δv_2 (m/s)	Δv (m/s) (m/s)
1000	0.6	16.6	17.2	2947	1146	4093
2000	0.6	16.6	17.2	2963	1148	4111
3000	0.5	16.6	17.2	2988	1156	4144
4000	0.5	16.6	17.2	3021	1156	4177
5000	0.5	16.6	17.2	3052	1162	4214
6000	0.5	16.7	17.2	3085	1168	4253
7000	0.5	16.6	17.2	3117	1175	4292
8000	0.5	16.7	17.2	3151	1182	4333

Table 4.1: Parameters of the transfer trajectories to the $L1$ halos in the Earth-Moon system with surface of section $x = -\mu$.

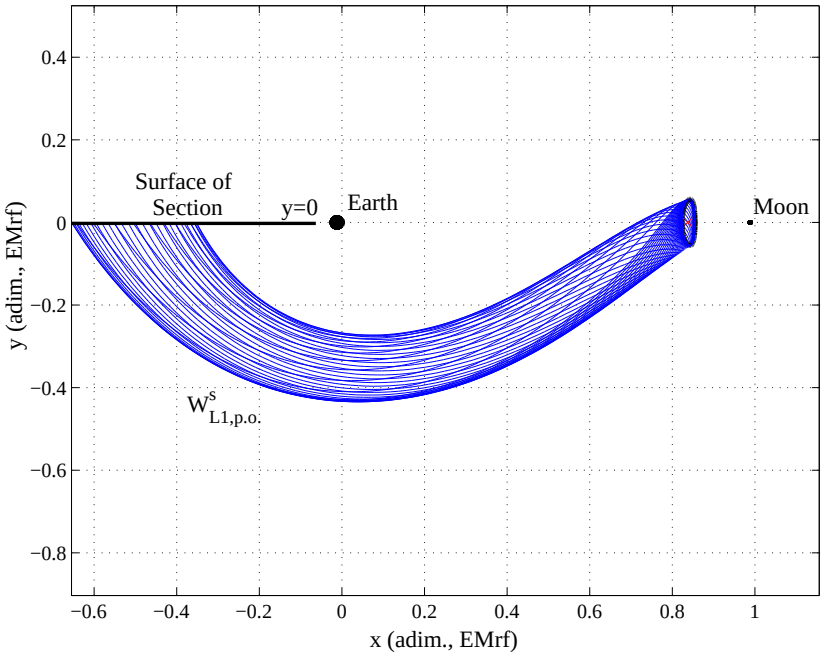

Figure 4.7: Stable manifold cut at $y = 0$ and $\dot{y} < 0$.

4.2.2 Section at $y = 0$

Figure 4.7 shows the second surface considered that is the plane $y = 0$ with $\dot{y} < 0$. The analysis has been carried out for the same halos as in the

A_z (km)	Δt_L $(days)$	Δt_W $(days)$	Δt $(days)$	Δv_1 (m/s)	Δv_2 (m/s)	Δv (m/s) (m/s)
1000	1.5	17.6	19.1	3114	636	3750
2000	1.5	17.6	19.1	3136	653	3789
3000	1.5	17.6	19.1	3179	645	3824
4000	1.5	17.6	19.1	3199	666	3865
5000	1.5	17.6	19.1	3231	656	3887
6000	1.5	17.6	19.1	3262	661	3923
7000	1.5	17.6	19.1	3248	683	3931
8000	1.5	17.6	19.1	3225	736	3961

Table 4.2: Parameters of the transfer trajectories to the $L1$ halos in the Earth-Moon system with surface of section $y = 0$.

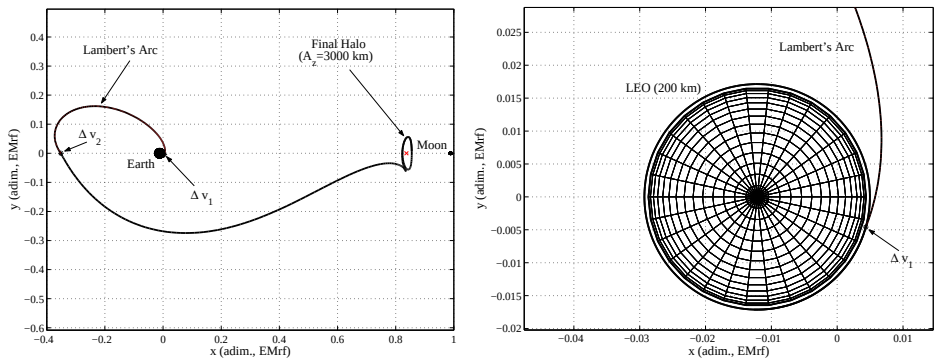

Figure 4.8: A typical transfer trajectory associated to the surface of section$y = 0$ and $\dot{y} < 0$ corresponding to the third row of table 4.1 (left). The starting LEO and the first leg of the Lambert's arc (right).

previous section and the results are contained in table 4.2. Figures 4.8 show the transfer trajectory associated to the third row of that table.

It is remarkable how in this case the costs are sensitively lower than the ones found in the previous case. Even if the times are only two days longer, the costs differ for more than 300 m/s!

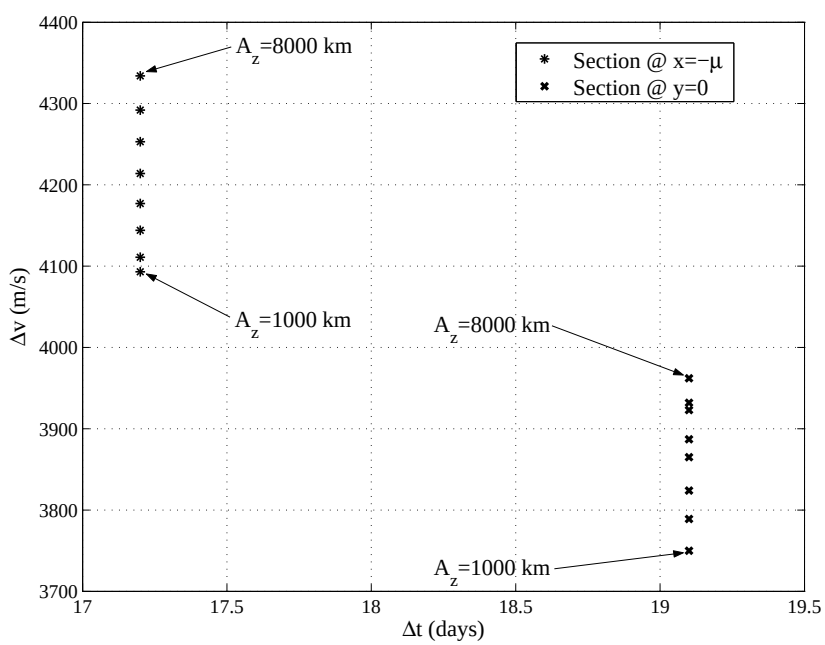

Figure 4.9: Comparison between the times and costs associated with the two sections.

If the total costs (Δv's) are plotted versus the total times of flight (Δt's), the figure 4.9 is obtained. This trade-off diagram clearly shows what has been discussed above: if the manifold extend far enough from its generating orbit, cheaper transfers to the halos in the Earth-Moon system can be obtained. The price to pay is the growth of the total time of transfer.

In addition, figure 4.9 shows a weak relation between the overall cost and the size of the final orbit. Indeed, both the tables 4.1 and 4.2 confirm that the growth of the out-of-plane amplitude increases, as a consequence, the total cost of the transfer.

4.3 Problem approach

From the analysis above, it is clear that the time of flight plays a key role for the transfers to the halo orbits in the Earth-Moon system. Hence, the problem has been formulated by removing the surface of section that fixes the time of flight. At the same time, the dimensions of the problem have been reduced by taking into account only one point, and its associated stable manifold, of the orbit at a time. So, if $\mathbf{x^i}$ is a point on the halo orbit, its associated stable manifold, after a time equal to Δt_W, can be written as:

$$W^{s,\ x^i} \quad = \quad \Phi(\mathbf{x^i}, \Delta t_W) \tag{4.4}$$

and represent a point in the six-dimensional phase space to be targeted. Indeed, a L3BP arc is again used to link an Earth's orbit with this point. By this, the overall cost and time are defined respectively as in the equations 4.1 and 4.2.

By this formulation the time of the second leg of the trajectory, the one that lies on the stable manifold, Δt_W, can be easily shifted and cheaper transfers can be found.

As shown in figure 4.9, with the range of amplitudes assumed in the previous section, $A_z \in [1000,\ 8000\ km]$, the two bounds represent extremum for the cost function. The costs relative to the intermediate orbits, indeed, is a function bounded by the costs associated to these two orbits. Known this, in the next section only the amplitudes equal to $A_z = 1000\ km$ and $A_z = 8000\ km$ will be considered for the sake of exposition.

4.4 Transfers trajectories to the $L1$ halos

This section presents several solutions that have been found with the problem applied to the orbits around the $L1$ point. For each point the solutions

are again subdivided into the ones for the $A_z = 1000\ km$ case and for the $A_z = 8000\ km$ case. Three different starting orbit have been assumed:

- LEO: a circular orbit with altitude $h = 200\ km$ in order to consider the common parking orbits achieved from the launchers. Here, the transfer starts by using the spacecraft's thrusters;

- GTO: this is the high elliptical orbit that links the LEO and the GEO. The altitudes of the pericenter and the apocenter are respectively $h_p = 200\ km$ and $h_a = 35841\ km$. This orbit has been considered because several low-cost spacecrafts (e.g. SMART-1) are launched as secondary payloads and so put in GTO orbits;

- GEO: the common geostationary orbit with altitude[2] $h = 35841\ km$. Even if this situation is of less practical interest, it has been taken into account because the geostationary orbit represents an upper bound for the altitudes of almost all the Earth's orbit.

These starting Earth's orbits have been assumed with inclination, taken with respect to the orbital plane of the Moon, equal to zero. The extension to the other inclinations could be implemented in a further step.

The problem is highly non-linear and the structure of the search space is very irregular; hence a good algorithm is required to look for feasible solutions. The one developed here is a combination of a evolutionary algorithm [31] and a sequential quadratic programming. The former looks for global solutions that are later refined by the latter algorithm. Again in a future work the best algorithm suitable for this kind of problem could be established.

4.4.1 $A_z = 1000\ km$ orbits

Table 4.3 summarizes the costs and times found for the transfer to the halos around $L1$ with amplitude $A_z = 1000\ km$. Figure 4.10 shows a typical trajectory belonging to this family with a LEO as the starting orbit.

[2]Sometimes there is a bit disagreement concerning the exact value of the altitude of a GEO. The one used in this study is equal to $h = 35841\ km$.

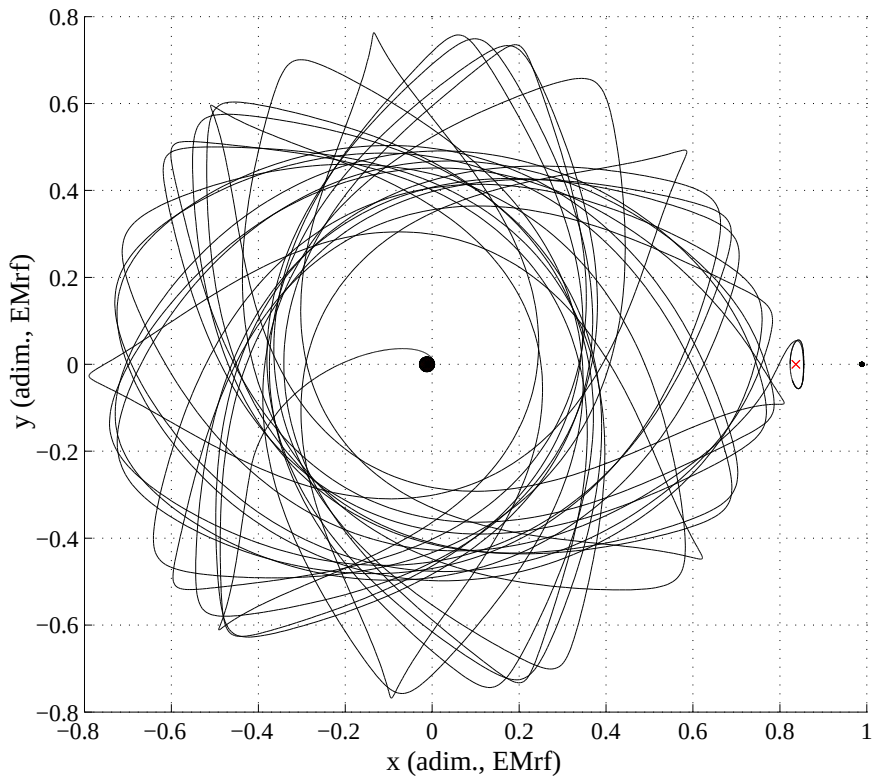

Figure 4.10: A typical transfer trajectory found for the transfer to the $A_z = 1000\ km$ $L1$ halo departing from the LEO. This trajectory requires a total cost equal to $\Delta v = 3104\ m/s$ and a time of flight $\Delta t = 553\ days$.

LEO		GTO		GEO	
$\Delta v\ (m/s)$	$\Delta t\ (days)$	$\Delta v\ (m/s)$	$\Delta t\ (days)$	$\Delta v\ (m/s)$	$\Delta t\ (days)$
3103	52.7	936	52.7	1023	47.9
3104	553.2	937	553.2	1074	77.6
3111	63.6	944	63.6	1122	62.9
3122	129.2	955	129.2	1261	787.7

Table 4.3: Overall cost and time found for the transfers to the $L1$ halos with $A_z = 8000$ departing from the three given Earth's orbits.

4.4.2 $A_z = 8000\ km$ orbits

Table 4.4 and figure 4.11 summarize the features (costs and times) of the solution found for this second family. Figure 4.11 represents a "fast" solution,

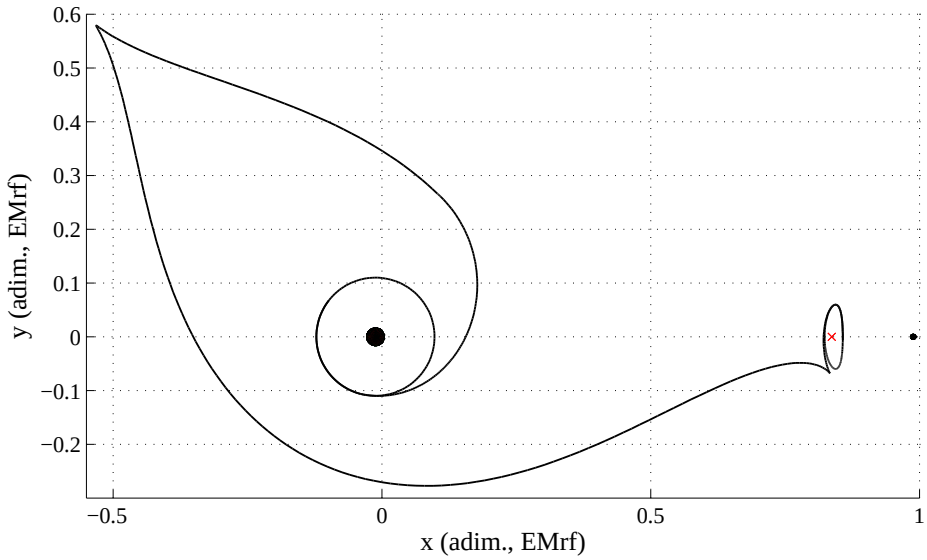

Figure 4.11: A typical transfer trajectory found for the transfer to the $A_z = 8000\ km$ $L1$ halo departing from the GEO. This trajectory requires a total cost equal to $\Delta v = 1102\ m/s$ and a time of flight $\Delta t = 27.6\ days$.

requiring around 27 days, that links a geostationary orbits with a halo about $L1$. The trajectory is drawn in the usual synodic rotating system; if it is though as in the Earth-centered inertial frame, it is clear how, at the end of the second orbit, when it is at the apogee, the spacecraft does not return to the perigee but become captured by the Moon's attraction and enters in the halo orbit.

LEO		GTO		GEO	
$\Delta v\ (m/s)$	$\Delta t\ (days)$	$\Delta v\ (m/s)$	$\Delta t\ (days)$	$\Delta v\ (m/s)$	$\Delta t\ (days)$
3169	124.9	1002	124.9	1102	27.6
3181	253.9	1014	253.9	1112	149.7
3199	47.1	1032	47.1	1140	88.5
3214	88.6	1047	88.6	1187	184.3

Table 4.4: Overall cost and time found for the transfers to the $L1$ halos with $A_z = 8000$ departing from the three given Earth's orbits.

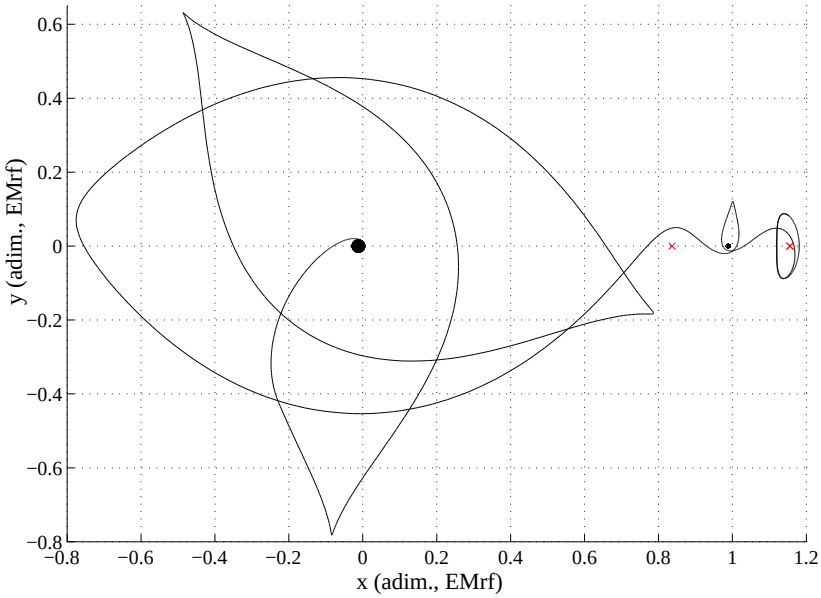

Figure 4.12: A typical transfer trajectory found for the transfer to the $A_z = 1000\ km$ $L2$ halo departing from the LEO. This trajectory requires a total cost equal to $\Delta v = 3119\ m/s$ and a time of flight $\Delta t = 77.4\ days$. The spacecraft performs also a loop around the Moon before injecting in the final $L2$ halo.

4.5 Transfers trajectories to the $L2$ halos

4.5.1 $A_z = 1000\ km$ orbits

LEO		GTO		GEO	
$\Delta v\ (m/s)$	$\Delta t\ (days)$	$\Delta v\ (m/s)$	$\Delta t\ (days)$	$\Delta v\ (m/s)$	$\Delta t\ (days)$
3104	783.9	937	783.9	1001	110.9
3119	77.4	952	77.4	1009	304.4
3120	111.6	953	111.6	1084	366.1
3127	99.9	960	99.9	1414	30.2

Table 4.5: Overall cost and time found for the transfers to the $L2$ halos with $A_z = 1000$ departing from the three given Earth's orbits.

4.5.2 $A_z = 8000\ km$ orbits

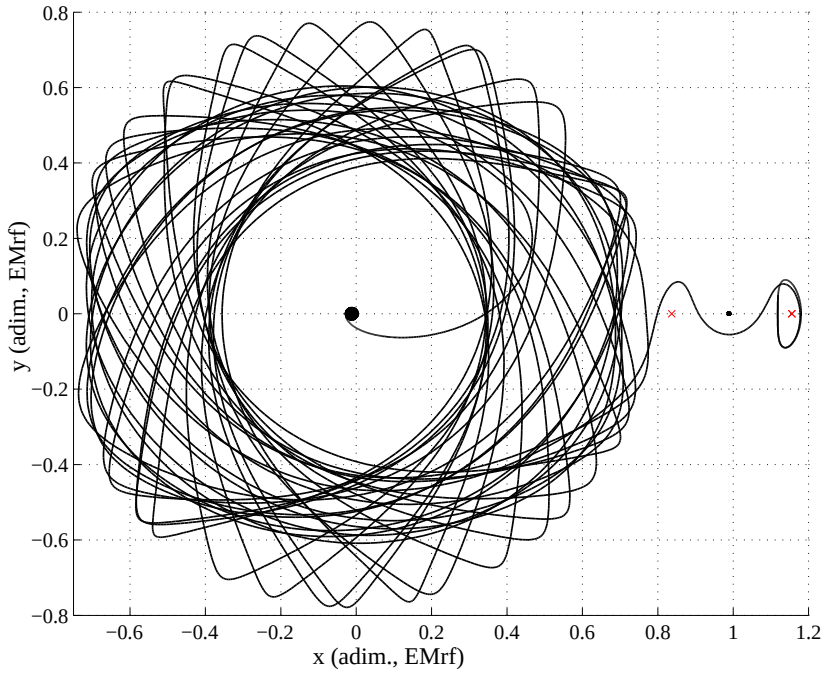

Figure 4.13: A typical transfer trajectory found for the transfer to the $A_z = 8000\ km$ $L2$ halo departing from the LEO. This trajectory requires a total cost equal to $\Delta v = 3551\ m/s$ and a time of flight $\Delta t = 764\ days$. The high time is due to the several Earth orbits performed by the spacecraft before it enters in the Moon's region.

LEO		GTO		GEO	
$\Delta v\ (m/s)$	$\Delta t\ (days)$	$\Delta v\ (m/s)$	$\Delta t\ (days)$	$\Delta v\ (m/s)$	$\Delta t\ (days)$
3154	255.1	987	255.1	1030	141.4
3156	123.1	989	123.1	1140	202.5
3193	905.6	1026	905.6	1184	99.9
3203	42.8	1036	42.8	1185	56.4

Table 4.6: Overall cost and time found for the transfers to the $L2$ halos with $A_z = 8000$ departing from the three given Earth's orbits.

4.6 Earth-Moon libration point orbits: uses for future space missions

In this chapter a method has been developed to evaluate the cost and time required to transfer a spacecraft on orbits around libration points $L1$ and $L2$ in the Earth-Moon system. The method is based on the target of a piece of stable manifold associated to a point of the final orbit starting from a LEO, GTO or GEO. The intermediate arc assuring this link is the solution of a Lambert's three-body problem formulated in section 2.7. Here follows a brief discussion about the obtained results, the applications for future space mission, the drawbacks and the implications, at system level, of these trajectories.

4.6.1 Comparison among the solutions

The results presented in the sections 4.4 and 4.5 have shown that a minimum cost around 3100 m/s is required to place a spacecraft into a $L1$ halo orbit departing from a 200 km LEO. This cost reduces down to 930 m/s if the spacecraft leaves from a GTO with 200 km apogee altitude and to 1000 m/s if a GEO is the starting orbit. These results correspond to times of transfer between 40 and 800 $days$, but the authors suspect the existence of solutions

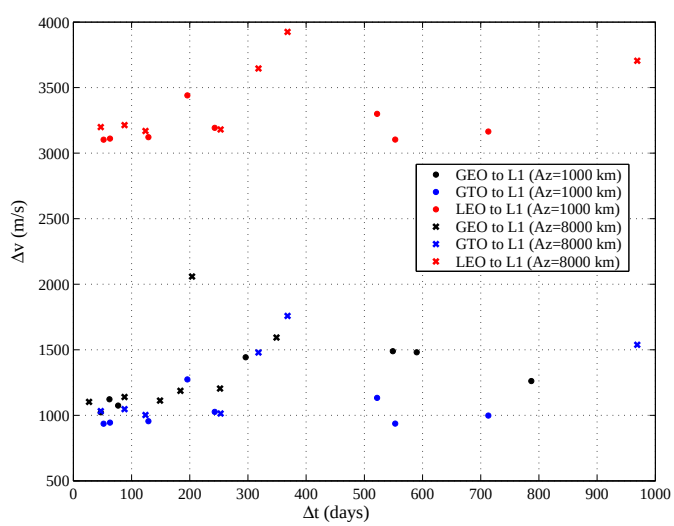

Figure 4.14: Δv vs Δt trade-off for transfers to $L1$ orbits with $A_z = 1000$ km and $A_z = 8000$ km. The transfers starting from the GTO turn out to be less expensive among the solutions found. Sometimes, transfers requiring high times do not involve low costs.

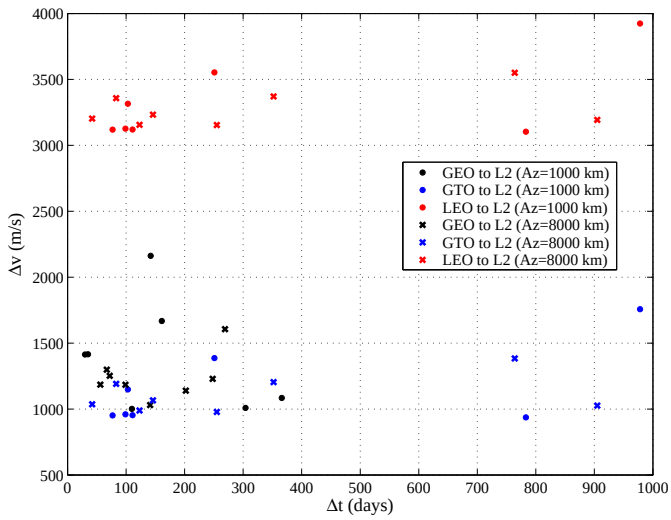

Figure 4.15: Δv vs Δt trade-off for transfers to $L2$ orbits with $A_z = 1000\ km$ and $A_z = 8000\ km$. Again the transfers departing from GTO are the less expensive. Most of the solutions have low times and costs.

with the same costs and shorter times. In fact, some transfers requiring high times do not correspond to low-cost solutions.

Even if theoretically a transfer to $L1$ is cheaper[3] than a transfer to $L2$, the results found in this frame indicate that on average the costs and times are comparable and can be assumed equal. Moreover, the dependence on the out-of-plane amplitude of the target orbit does not seem to be marked, so these costs refer to generic halos with A_z less or equal than 8000 km.

Figures 4.14 and 4.15 show the trade-off schemes for a few solutions found in this work. It would be interesting, in future studies, to characterize the whole Δv vs Δt space and the structure of the pareto-fronts for transfers to libration point orbits.

The authors want to stress that a direct comparison between a Hohmann transfer to the libration points is forbidden since the equilibria are not defined in a two-body scheme. Nevertheless, the libration points describe circular orbits in the Earth-centered reference frame and so the cost to reach them can be calculated as a common transfer between two Keplerian Earth-centered orbits. For instance, the point $L2$ draws a circular orbit with radius 444000 km around the Earth. If the Hohmann transfer is calculated between the GTO and this circular orbit, the cost is equal to $\Delta v_H = 1950\ m/s$ that is more than twice the one obtained in this study!

[3]This is due to the lower value of the Jacobi constant associated to $L2$ that corresponds to a higher energy level with respect to $L1$.

4.6.2 Uses for future space missions

This study demonstrates that halo orbits in the Earth-Moon system can be reached with reduced costs and reasonable times. This result evidences the high potential use of these points for future space missions. Indeed, it is remarkable how the performances associated with libration point orbits cannot be obtained with other Keplerian orbits since they offer the possibility to have a fixed configuration with respect to two primaries. So, all the missions requiring this constraint are potential libration point missions.

In the future, an automated sample return mission to the Moon seems to play a key role for the space activities of the next decades. The far side of the Moon has been located as the appropriate landing site for the samples collection. Thus, a direct communication with the Earth is forbidden for landers acting in this region. By this, a relay spacecraft in a $L2$ halo orbit could assure an uninterrupted communication with the landers and the Earth exploiting the Farquhar's concept described in section 4.1 (figure 4.1).

Two spacecrafts in both $L1$ and $L2$ can be used to assure the communication with the whole Moon surface and the Earth. This concept can be used also for a future manned base on the Moon. Moreover, the two spacecrafts could also monitor the surface of the Moon.

The libration point $L1$ could be viewed as a gateway for the future interplanetary missions if the following sequence is considered:

- first, with low-costs, the spacecraft is sent in a translunar trajectory by starting from an Earth orbit. Here, when it reaches the stable manifold associated to $L1$, it is forced to follow this subspace;

- on the stable manifold the spacecraft reaches the $L1$ point and proceeds by following the unstable manifold associated to the same point;

- by a small manoeuvre, the spacecraft is forced to enter into the stable manifold associated to $L2$ and then follow the unstable one in the exterior region;

- when the spacecraft is in the exterior region, the Earth-Moon $L2$ unstable manifold intersects with the stable manifold associated to $L1$ or $L2$ points of the Sun-Earth system; so, again with a small manoeuvre, it could reach the two equilibrium points of the Sun-Earth system;

- once the spacecraft is around these points, far from the Earth, another manoeuvre could place in into an interplanetary trajectory toward both the inner or outer planets.

This last manoeuvre has great effects since it is applied in a region at the boundary of the Earth's sphere of influence and the saving in Δv is due to the "soft" Earth escaping exploiting the Moon. This concept can be applied backward for the Earth return after an interplanetary journey. Anyway, these statements need to be assessed in future studies.

4.6.3 Drawbacks

The drawbacks associated to the trajectories proposed in this chapter are associated to the non-linear behavior of the three-body problem. Hence, even if the times are reasonable, the guidance on these trajectories is a delicate matter since small changes in the initial condition produce large deviation in the forward trajectory.

Moreover, these paths are defined in the Earth-Moon system where the primaries are assumed in circular orbits and "only" their two gravitational attractions are taken into account. By this, it is clear that the real trajectory requires a successive correction that takes into account the orbital eccentricities and the Sun perturbation. In a more refined step, the solar wind and the actions of other bodies may be considered too.

This refinement could establish the features involved with the launch windows that are expected not to be critical due to the short synodic period between an Earth orbit and the Moon.

4.6.4 Considerations at system level

Since the presented trajectory requires mid-times of transfer and since the authors believe that shorter solution exists, the subsystems of a potential spacecraft do not presents particular differences from the usual Earth-centered spacecrafts.

Anyway, spacecrafts in orbits about the libration points in Earth-Moon system must hold their nominal orbit for a long period. So, the propulsion subsystem must provide for an additional propellant mass fraction because of the costs associated to the stationkeeping. It has been estimated that a cost around 100 $m/s/year$ is enough to overcome the solar perturbation that breaks the periodicity of the orbits.

The guidance, navigation and control system requires accurate instrumentations in order to know the exact position of the spacecraft and calculate how exactly the spacecraft is following the nominal trajectory.

The thermal, attitude and communication subsystem do not require particular constraints associated with these trajectories. The power generation

may be provided by solar arrays and batteries with a high number of cycles if the spacecraft have to remain in orbit for a long time.

Chapter 5

Low-Energy Interplanetary Transfers Using Libration Points

This chapter studies the feasibility of interplanetary transfers that make use of the R3BP dynamics and libration points. Although the method developed in this chapter can be applied to any body-to-body transfer, the results presented here involve only transfers of practical interest (i.e. with relative short times of transfer).

Apart from a pair of lunar transfers that will be cited in the next chapter (Hiten and SMART-1), no missions are planned in order to validate this concept for interplanetary missions. This has produced a lack of works dealing with this topic, so in the state of the art only a few works, known to the authors, are presented. Then, the approach that allows to link two celestial bodies using a R3BP dynamics will be shown. Finally, the outcome of this work will be presented together with some considerations about the drawbacks and the uses of these trajectories.

5.1 State of the art analysis

The patching conic method represents the classical technique adopted for the preliminary analysis of interplanetary transfers. This method is based on the idea of joining together conic arcs, defined in different reference frames, in order to obtain a complete trajectory [3]. This method takes into account only one gravitational attraction at a time, solving, in this way, a number of two-body problems. Furthermore, when used as a first guess solution in more refined models, a patched-conics trajectory, due to the intrinsic approxima-

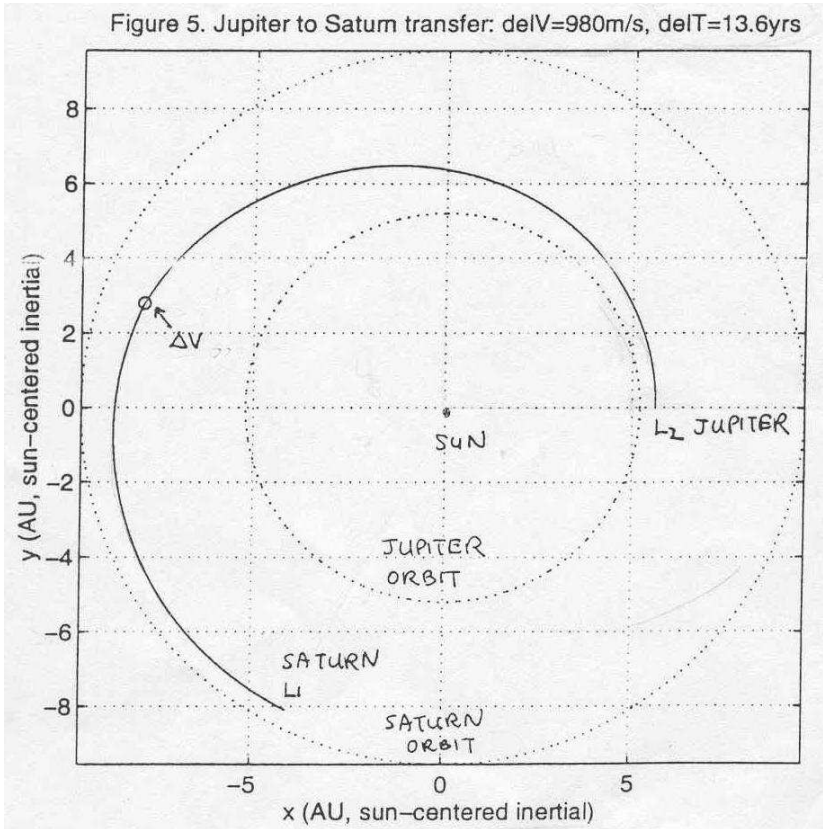

Figure 5.1: The Jupiter-Saturn low-energy transfer found by Lo and Ross [46].

tions introduced in its formulation, *forces* the energy to high levels[1].

Recently, several studies, undertaken in generic n-body systems, are showing that it is possible to lower the cost of the transfers by involving more than one gravitational attraction in the model used to design the trajectory. Apart from the reduced cost of the transfer, these techniques produced refined trajectories that can be used as good initial guesses in more complex models [49].

Lo and Ross [46] studied the complex structure provided by the invariant manifolds associated to both the libration points $L1$ and $L2$ and the periodic orbits around them. This analysis was carried out in the R3BPs with primaries the Sun and an outer planet and the full four body problem was split into two coupled R3BPs. They found that low-energy transfers can be

[1]For instance, the concept of *sphere of influence* that the patching conics method introduces, involves the trajectory to rapidly cross the regions at the boundary of the spheres in order to assure a good level of approximation. By this, the spacecraft is induced to have high relative velocities and so high energy levels

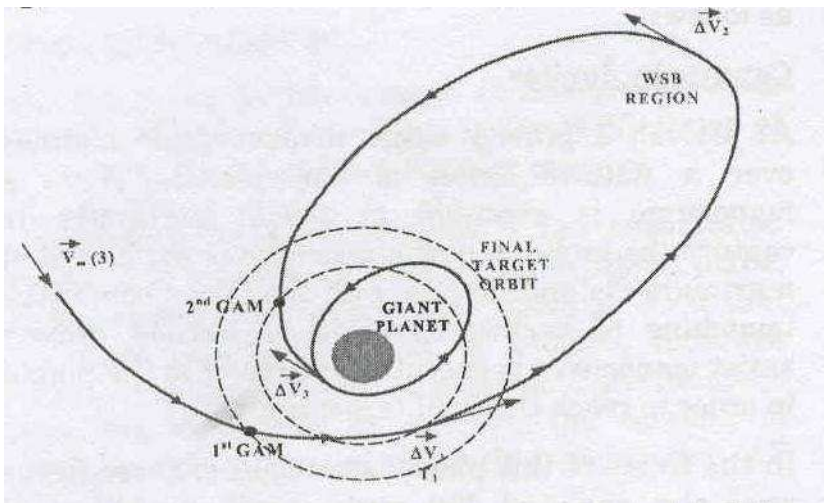

Figure 5.2: An interplanetary WSB trajectory over a four-body scheme [11].

obtained if the manifolds intersect in the configuration space. Here, a small ΔV performs the step from one manifold to another and the spacecraft is captured by the arrival planet. Figure 5.1 shows a Jupiter-Saturn transfer obtained by linking the unstable manifold of the Sun-Jupiter $L2$ and the stable manifold of the Sun-Saturn $L1$. The intermediate impulse is $\Delta V = 980\ m/s$ and the time of transfer is $\Delta t = 13.6\ years$. The Hohmann transfer between the same planets require a $\Delta V = 2700\ m/s$ and $\Delta t = 9.9\ years$ [46].

This work was performed assuming the planar R3BPs where, since the Jacobi constant is three dimensional, the manifolds associated to the orbits separate different regimes of motion. Later, Gómez et al [28] extended these results to the spatial (3D) problem and showed that the invariant manifolds associated to the periodic orbits still act as separatrices for two types of motion: orbits inside the invariant manifolds "tubes" are transit orbits and those outside the tubes are non-transit orbits (see section 1.4.2 and figure 1.7). Moreover, they developed a numerical algorithm for constructing orbits with any prescribed finite itinerary and applied this method for a tour of the Jupiter's moons.

In order to explain the basics of the Moon's capture in a WSB lunar transfer (see section 6.1), Lo and Ross [47] observed that the invariant manifold of the Earth-Moon $L2$ is strictly connected with those associated to $L1$ and $L2$ in the Sun-Earth system. Thus, they proposed a lunar $L1$ gateway for future interplanetary missions.

Castillo et al [11], under ESA contract, studied the feasibility of WSB interplanetary trajectories to both inner and outer planets. They noted that

in the case of inner planets, the WSB trajectories neither improve the performances (ΔV) of the transfers nor give any flexibility in the choice of the final orbit about the arrival planet. This is due to the lack of moons about these planets that forbids to fly over a four-body dynamics, which gives the possibility to save propellant mass as in the case of the Sun-Earth-Moon system. For giant planets, the presence of moons (figure 5.2) allows the WSB trajectories to give a wide flexibility in the final orbit but again the saving in propellant mass fraction is negligible.

Topputo [70] proposed a method to compute low-energy interplanetary transfers among inner planets where a two-body conic arc links the non-intersecting manifolds. Later, Topputo et al [71] developed this concept from an optimization point of view. Finally, Lo et al [49] have recently undertaken a series of studies aimed to demonstrate a strict relation between the invariant manifolds and low-thrust trajectories.

5.1.1 Motivations for further studies

The patched-conics method is the only technique used for the analysis of the interplanetary paths of the past space missions. Since the space activity begun, this tool has been adopted from the designers because it involves analytical (i.e. conic) formulation of the full trajectory, even if a number of planets are encountered. Moreover, in this latter case, the hyperbolic swing-by trajectories allow a reduction of the overall cost of the mission.

Nevertheless, the matter is that spacecrafts travelling in the solar system are not included in a multiple two-body environments at a time, but they*feel* several gravitational attractions all acting simultaneously. Thus, sometimes the patched-conics trajectory represents the consequence of a "rough" representation of the full solar system dynamics. This aspect involves high energy levels associated to these transfers in order to overcome this approximation: the spheres of influences, that are the regions where the approximation is more critical, must be crossed rapidly to have accurate solutions and these high velocities turn out in high energy levels. By the patching-conics technique, the elevated Δv involves a reduction of the mass of the payload since an high fraction is required by the propellant needed to assure the total velocity change.

This chapter considers the possibility to lower the cost of the transfers by exploiting the gravitational attractions within the solar system. It is known that this technique involves high times of transfer that sometimes lead to unfeasible solutions. Hence, here the interest is focused on transfers of practical interest (i.e. "low" times of transfer) that are achievable among inner planets.

5.1.2 Space applications

The transfers analyzed in this chapter are those passing through the libration points of several Sun-Planet systems and then ballistically captured by the arrival planet[2]. It is clear that they involve all the missions that do not have any particular constraint on the time of flight.

As an example, a *cargo* mission to Mars or Venus, with the aim to bring several payloads and instruments on these planets, useful for future man activities, must have reduced costs in order to maximize these masses. An interplanetary and impact trajectory with these planets can be easily achieved by passing through the libration points of the Sun-Mars or Sun-Venus system.

Moreover, these trajectories are useful also to orbit one of the inner planets, as the common interplanetary missions do. As will be shown later in the chapter, unstable captured or stable Keplerian orbits can be obtained by adding small costs on the transfer trajectory.

Finally, by the technique of the manifolds, the transport of the "material" (i.e. comets, asteroids, NEOs, ...) within the solar system can be easily explained and estimated.

5.2 Problem formulation

The problem is formulated with the use of the planar R3BP. This choice lowers the dimensions of the problem and allows the establishment of transit trajectories with the use of only one Poincaré section (see figure 1.7). Anyway, the final transfer is full 3D since an analytical ephemeris model [16] has been adopted.

Let a and b be respectively the generic departure and arrival planets and, without any loss of generality, let a be inner to b. The following description can be easily implemented for the opposite case only by exchanging $L1$ with $L2$ and vice versa. Let $A_{x,a}$ and $A_{x,b}$ be respectively the semi-amplitudes of two Lyapunov orbits, one around $L2$ in the Sun-a system and the other around $L1$ in the Sun-b system. In order to obtain the best intersection between the manifolds associated to these orbits, the sideral plane (section 1.1) has been introduced.

On this plane, as shown in figure 5.3, $W^{u,\ ext}_{L2,p.o.}$ (Sun-a system) and $W^{s,\ int}_{L1,p.o.}$ (Sun-b system) are computed, both previous obtained in the respective synodic frames. The superscripts ext and int means respectively that only the exterior and interior branch of the manifolds have to be computed (see equation 1.23). Propagations stop when manifolds develop respectively for an

[2]With an abuse of language, sometimes they are called WSB transfers.

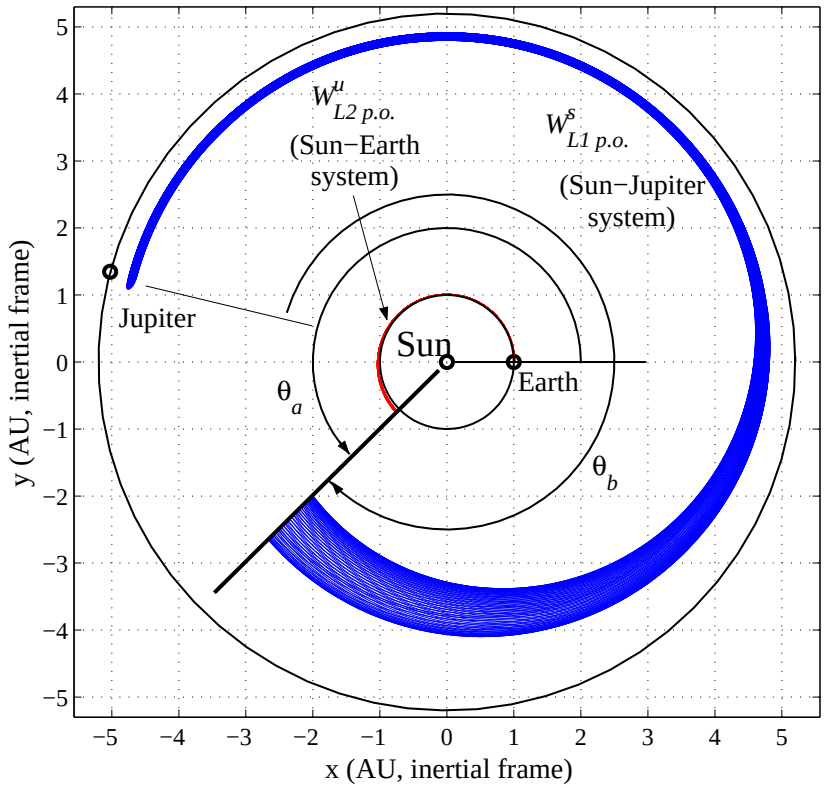

Figure 5.3: Sideral plane and invariant manifolds for the Earth-Jupiter transfer ($a = Earth$, $b = Jupiter$).

angle of θ_a and θ_b, when angles measurement starts from the corresponding planet (figure 5.3). This stoping condition is easy to obtain when manifolds are described in polar coordinates $(r,\ \theta)$ instead of the rectangular ones. Using θ as a parameter, indeed, the surface of section can be easily shifted by varying its value and a sort of fluctuant section can be obtained.

Let $\gamma_a = \gamma_a(r, \dot{r})$ be the curve produced by the section of $W^{u,\ ext}_{L2,p.o.}$ corresponding to the angle $\theta = \theta_a$ and $\gamma_b = \gamma_b(r, \dot{r})$ the section of $W^{s,\ int}_{L1,p.o.}$ when $\theta = \theta_b$. Now, points within these curves, intended in the four dimensional phase space, correspond to the transit trajectories, discussed in section 1.4.2, that approach the planet by passing through the small neck allowed by the forbidden regions (figure 5.4).

Once a transit orbit is built and propagated, it can be translated in the 3D ecliptic frame by taking into account the real eccentricity and inclination of planetary orbits given by the ephemeris model. Figure 5.5 represents the trajectory in the 3D absolute sun-centered reference frame.

From figure 5.5, it is clear that now the problem has become the link of

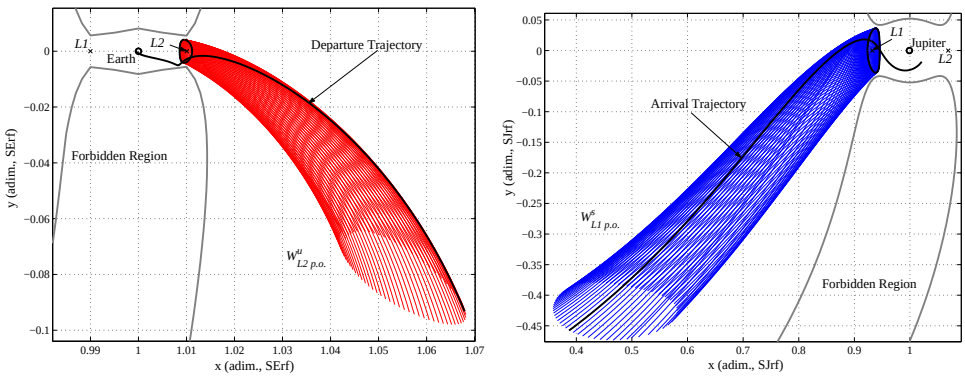

Figure 5.4: Departure (left) arrival (right) transit trajectories within the invariant manifolds tubes for the Earth-Jupiter case.

A and B that are the terminal points of the two trajectories. These links have been done by using a two-body Lambert's arc. Hence, the full four-body problem is split into two R3BP (at departure and arrival) and an intermediate 2BP that assures the connection of the manifolds. This technique represents an extension of the one proposed by Lo and Ross (section 5.1) and overcomes the problem of non-intersecting manifolds.

Two intermediate deep space maneuvers, called Δv_1 and Δv_2 are then required to realize the link of the conic arc in the phase space with the stable

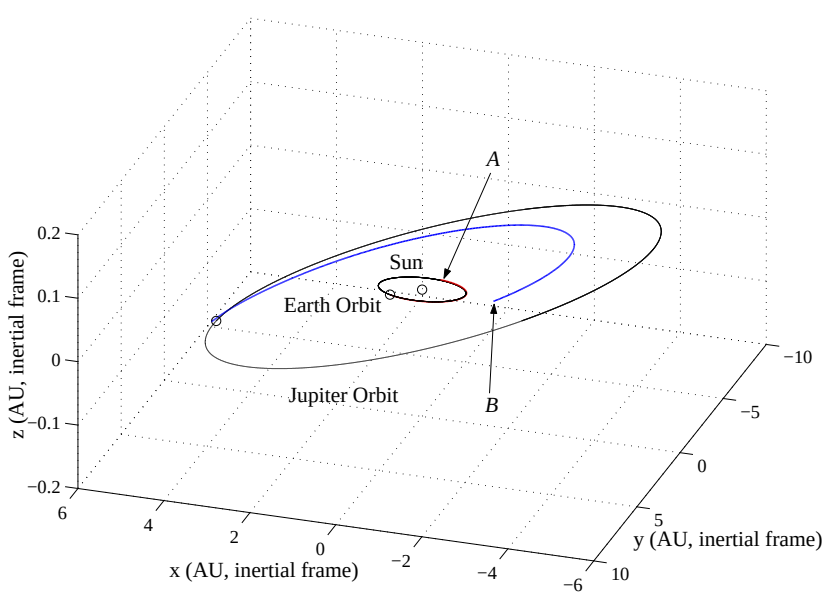

Figure 5.5: Transit trajectories in the Sun-centered inertial frame.

and unstable transit trajectories. The total Δv associated to the conic link can be tuned changing the dimensions of the source periodic orbits with a consequent change of the energy associated to the transit orbits.

5.3 Results for the multi-burn case

Here the *patching manifold approach* described in the previous section is applied to the design of some representative transfers from the Earth to Venus, Mars and Jupiter. The results are compared in terms of total Δv and time of flight Δt to the corresponding classical Hohmann transfers. The problem has been solved considering three different cases:

- a powered capture into a circular orbit around the target planet (*circularized trajectory*);
- a slightly perturbed trajectory near the target planet that closes the Hill's curve and remains captured (*permanent captured trajectory*);
- a pure ballistically captured trajectory. In this case the capture is allowed only for a finite time (*free captured trajectory*).

In the first case one additional maneuver, Δv_e, must be considered. In particular in the following, Δv_s and Δv_e indicate respectively the cost necessary to depart from a circular orbit of radius r_s around planet a and the cost for the insertion into a circular orbit of radius r_e around planet b. The values r_s and r_e are not imposed a priori but computed simply propagating forward and backward in time the starting and arriving legs of the transfer, which are uniquely specified by the Poincaré section, and taking the closest point to the corresponding planet. The costs of the multi-burn and of the Hohmann transfers are then calculated as the total Δv necessary to transfer the spacecraft between the two circular orbits of radius r_s and r_e.

Finding a solution with the problem formulated above is a very difficult task. This is due to the high non-linearities influencing the R3BPs involved and to some parameters, as the two amplitudes of the periodic orbits, that play a key role. Thus, the solution of interplanetary transfers passing through libration points requires a more detailed study and a more refined approach. Here, in order to validate the proposed concept, only few solutions will be shown because the computational time required to this problem is extremely high.

The performances of these trajectories will be compared with the classical bicircular Hohmann transfer, between the two orbits r_s and r_e, with cost Δv_H and a time of transfer equal to Δt_H.

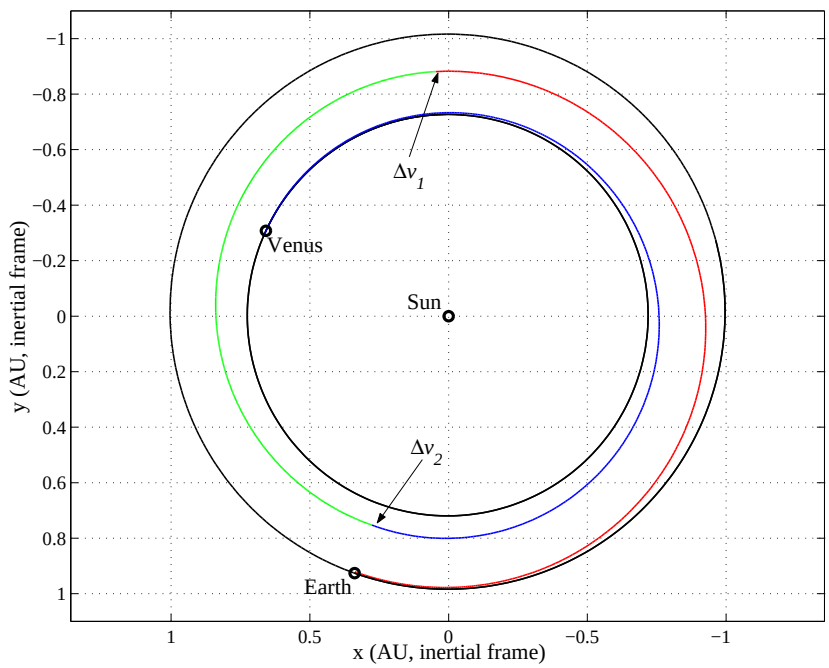

Figure 5.6: Earth-to-Venus direct transfer. The Sun-Earth $L1$ unstable manifold (red) is linked with the Sun-Venus $L2$ stable manifold (blue) by the intermediate conic arc (green).

5.3.1 Earth to Venus direct transfers

Table 5.1 summarizes the options found for the Earth-Venus transfer. These solutions require a cost that is less than the Hohmann transfers and the time of flight is almost three times. The full interplanetary trajectory is shown in figure 5.6 where the first deep space maneuver is performed after $180\,deg$ to decrease the altitude of the aphelion down to the terminal point of the stable

Departure (MJD)	Δv (m/s)	Δt $(days)$	Δv_H (m/s)	Δt_H $(days)$	r_s (km)	r_e (km)
2504	4126	448	5105	145	225630	349480
3650	4245	483	4845	145	175045	282766
5809	4109	780	5140	145	568140	188880

Table 5.1: Parameters of the Earth-to-Venus transfers.

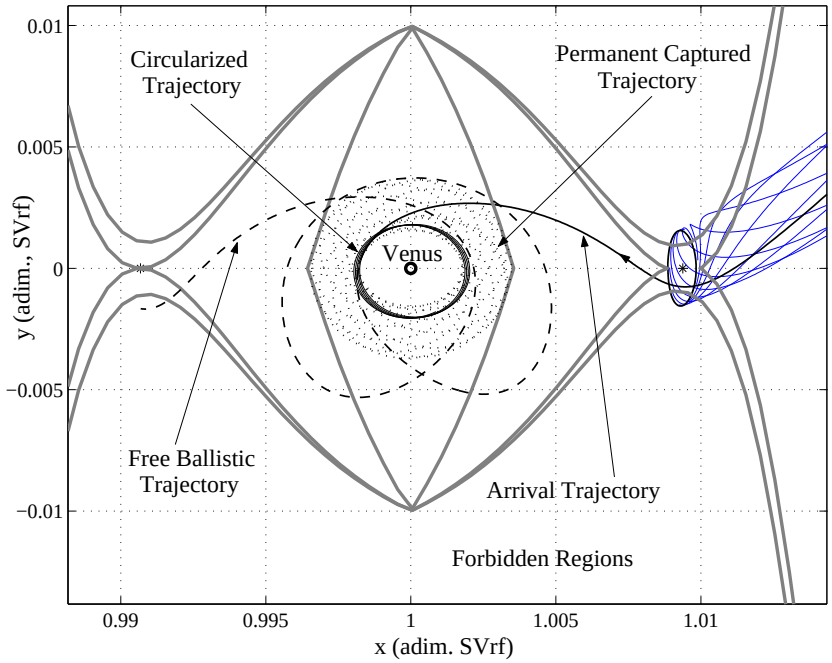

Figure 5.7: Options for the injections around Venus: free captured trajectory (dashed), permanent captured trajectory (dotted) and circularized trajectory (solid).

manifold of the Venus-Sun system. A second burn is required to insert the spacecraft into the transit orbit reaching Venus and a final burn injects the spacecraft in the circular orbit around Venus.

Figure 5.7 shows the three different option allowed at Venus arrival. For instance, the cost corresponding to the solution in the second row of table 5.1 can be lowered down to $\Delta v_{cap} = 4149\ m/s$ if the spacecraft is put in a permanent captured trajectory. This condition is obtained by reaching the value of the Jacobi constant C_1 that close the Hill's curves. If the trajectory is left free to evolve, the total cost is further less ($\Delta v_f = 4085\ m/s$) but the time around Venus reduces to $\Delta t_f = 116\ days$.

5.3.2 Earth to Mars direct transfers

For the Earth-Mars case, two solutions are illustrated in table 5.2. The first leads to a transfer cheaper than the Hohmann one with again a time of transfer almost three times longer. The second solution has a total cost higher than the Hohmann; but this solution have been intentionally showed to demonstrate that if permanent capture trajectories are considered, the

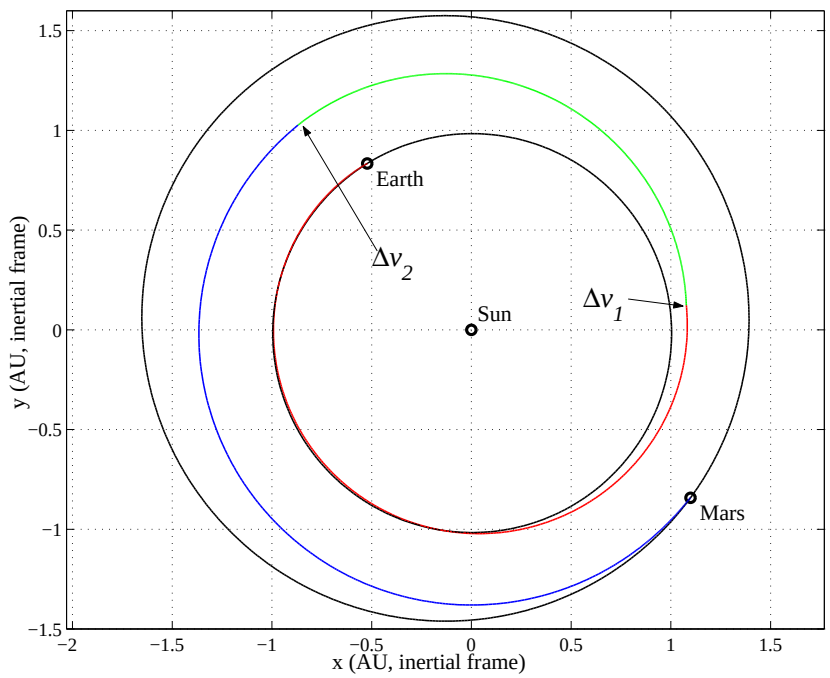

Figure 5.8: Earth-to-Mars direct transfer. The Sun-Earth $L2$ unstable manifold (red) is linked with the Sun-Mars $L1$ stable manifold (blue) by using the intermediate Lambert's arc (green).

final cost turns out to be cheaper anyway. Indeed, in this case the total cost required to have the unstable captured trajectory, dotted in figure 5.9, is equal to $\Delta v_{cap} = 4731\ m/s$ that is almost 400 m/s less than the one associated to the Hohmann transfer.

Figure 5.8 shows the full interplanetary path that is again obtained by joining with the Lambert's arc (green) the unstable departure (red) and the stable arrival trajectories (blue). The three options at Mars arrival are in figure 5.9 where the low circular Mars orbit ($r_e = 34830\ km$), the permanent

Departure (MJD)	Δv (m/s)	Δt ($days$)	Δv_H (m/s)	Δt_H ($days$)	r_s (km)	r_e (km)
3327	3702	860	4566	246	380090	34830
3365	5469	844	5142	258	48000	202000

Table 5.2: Parameters of the Earth-to-Mars transfers.

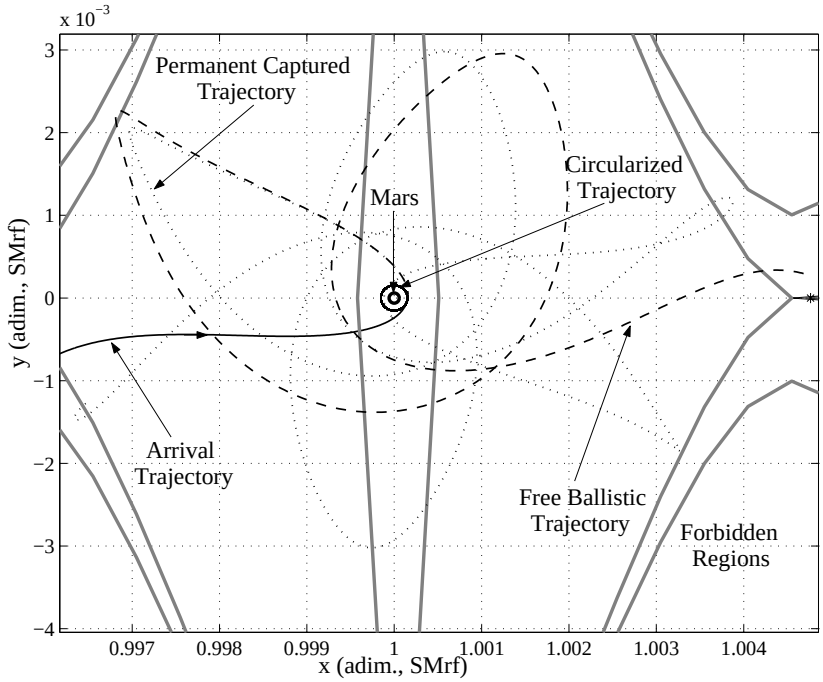

Figure 5.9: Options for the injections around Mars: free captured trajectory (dashed), permanent captured trajectory (dotted) and circularized trajectory (solid).

captured and the free captured trajectories have been shown.

Finally, the reader has to observe that a small error is introduced when the Sun-Mars problem is considered. The Mars orbits, in fact, has an eccentricity equal to $e = 0.093$ while the eccentricities of the Earth and Venus are respectively $e = 0.017$ and $e = 0.007$. So, when the Sun-Mars system is analyzed from the *circular* R3BP point of view, the Mars orbit is forced to be circular and the final parameters (lengths, time, velocities) contain a small error since the equations of motion (equations 1.6) are dimensionless with respect to these quantities.

5.3.3 Earth to Jupiter direct transfers

One solution is presented for the transfer trajectory to Jupiter with its terminal leg illustrated in figure 5.10. In this case only the permanent captured option has been considered since the circularized orbits are quite expensive. The total cost is $\Delta v = 11732\ m/s$ and the time of transfer is $\Delta t = 3868\ days$. This transfer is clearly unfeasible due to its long time, but the attention is again pointed out on the reduced cost with respect to the Hohmann transfer

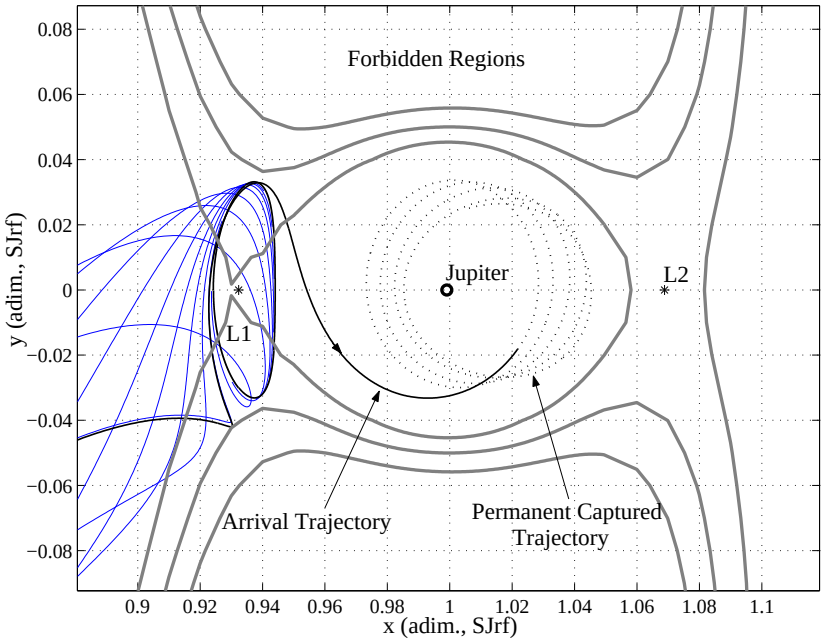

Figure 5.10: Permanent captured trajectory around Jupiter.

that is $\Delta v_H = 12321\ m/s$ and has a time of flight equal to $\Delta t_H = 940\ days$ (again one third of the time achieved with the patching-manifolds method).

5.4 Interplanetary transfers through libration points: uses for future space missions

The solutions found in this frame have shown that it is possible to reach Venus, Mars and Jupiter by following the stable and unstable manifolds associated to the Sun-Planet systems. Nevertheless, these trajectories have great implications at all the mission levels. Here, some discussions are made according to the authors' point of view.

5.4.1 Remarks and comparison among other techniques

The patching conics method has proven to be a powerful tool to the design of interplanetary trajectories since it involves an analytical formulation that is the exact solution of the two-body problem. When these conics are assumed as first guess solutions for interplanetary transfers, they provide accurate results also in a full n-body problem. This result occurs since the formulation

of a patched conics trajectory implicitly involves high energy levels and high velocities at the boundaries of the spheres of influence.

When these velocities reduce, and so the energy level do, other phenomena, as the ballistic capture, can be appreciated when more than one gravitational attraction acts on the spacecraft. If a trajectory is designed with these principles, the total cost may be reduced if compared with a patched conic path.

In this chapter, the possibility to design interplanetary transfers, with orbits defined in a three-body system, has been evaluated. Three planets (Venus, Mars and Jupiter) have been considered as the targets for these interplanetary missions. Mercury is not taken into account in this study since its orbit cannot be approximated as circular and so it does not respect the hypothesis of the restricted problem. The outer planets have been discarded since the transfer time grows with the period of the target planets. Thus, their assumption would have led to really unfeasible solutions.

In the sections above, solutions found from the Earth-Venus and Earth-Mars transfer have demonstrated that these planets could be reached with a reduced cost. In particular, a transfer to Venus, when compared with the same starting and arrival orbits around the Earth and Venus, costs around 1000 m/s less than a Hohmann transfer. But, the time of transfer raises up to three times than the Hohmann one: the best solution requires around 450 *days* to reach Venus.

The costs associated to a transfer to Mars by exploiting the invariant manifolds trajectories are again less than the Hohmann costs. The best solution requires a cost that is around 800 m/s less than the Hohmann transfer and the time of flight here is about 850 *days*. Nevertheless, the authors want to point out that the solutions found in the Sun-Mars system are affected by a small error due to the eccentricity of the Mars' orbit ($e = 0.09$) that is not totally negligible.

The solution showed for the Jupiter transfer is clearly unrealistic since it requires more than 3800 *days* to reach Jupiter and the saving is only about 600 m/s. By this, the authors believe that this technique is not employable for a transfer to Jupiter because these high times repeat in any solution found in this study. But, this solution has been intentionally showed since it demonstrates the powerful of a captured trajectory in the Sun-Jupiter case (see figure 5.10).

Hence, the following discussions concern only the two cases of "practical" interest: a transfer to Venus and a transfer to Mars.

The costs associated with these two missions can be further reduced if the spacecraft is placed in unstable permanent captured trajectories around the arrival planet. This saving can be in the range $100 \div 300$ m/s depending on

the altitude, over the target planet, of the manoeuvre that closes the Hill's curves.

By this discussion it follows that the most important problem associated to the trajectories through the libration points is the high transfer time. In other words, all the saving in Δv is payed in Δt. So, if the cost reduces to levels that require 15÷20% less than the Hohmann transfer, the time of flight has a variation equal to 300% than the Hohmann time.

Between Venus and Mars, the results seems to be better for the transfers to Venus since in this case the times are reasonable and the saving is more advantageous.

5.4.2 Uses for future space missions

The uses of such trajectories for future space applications concern all the missions requiring a maximization of the payload mass without any restriction on the transfer time; meaning for transfer time a period of one and half year to reach Venus and more than two years to reach Mars.

It is obvious that the future missions following these interplanetary paths will not be manned missions because of the strong constraint on the time of transfers due to the slow dynamics. These high times could not represent a problem for the future long-time projects aimed to explore the two planets considered.

As an example, the construction of a future base on Mars will require many preparatory cargo missions with the purpose to bring as much payload as possible on the Red planet. Or, a manned journey on Mars will require preparatory cargo missions in order to send instrumentations useful for the *in-situ utilization resources* to allow the man survival against those hostile conditions. These examples of cargo missions can be done by following interplanetary trajectories through libration points. The only request is that the trip must be two years long.

Since these trajectories are not only orbiting paths, but also impact paths with the planets, the technique showed in this chapter could be useful to design automated missions, such as the Mars sample return, that require a landing on the target planet. This application is very energy expensive since it requires a take-off phase from Mars that involves a lot of propellant mass. Thus, the interplanetary transfer cost may be reduced by following the developed three-body trajectories.

Other than missions on the surface of the planet, these trajectory may be applied also to orbit the target planet. It has been shown, indeed, that the final orbits can be either Keplerian or unstable captured trajectories around the planet. In the latter case the cost further reduces and, theoretically,

the spacecraft will remain permanently around the planet. These unstable trajectories are similar to high elliptic (figure 5.9) or circular orbits (figure 5.7 and 5.10). So, if the instrumentations and payload on the spacecraft do not require stable orbits around the planet (i.e. fixed distance, constant apocenter and pericenter distance, ...), the unstable captured trajectories may be used to reduce the total cost of the mission.

Another future application for the three-body interplanetary trajectories concerns the multi-moon tours. If the manifolds are computed in the Planet-Moon systems, indeed, they intersect each other and this intersection allows a direct transfer between the two coupled R3BPs, that is without the intermediate conic arc. This leads to great savings in Δv and, at the same time, with reasonable times of transfer. By this technique, a tour of the Jovian moons [42] and transfers among the moons of Uranus [71] have been studied. Nevertheless, even if the visits of several moons could be designed by the invariant manifolds technique, the question of how two reach the giant planets remains a patched conics problem.

Finally, an interesting application of the invariant manifolds technique involves the prediction of the motion of space "objects" (comet and asteroids) subject to a chaotic dynamics. Here the authors refer to the Near Earth Objects (NEOs) that can be viewed in the R3BP frame with the Sun and the Earth as primaries.

5.4.3 Drawbacks

The most important drawback of the interplanetary trajectories through libration points is the transfer time. As discussed above, it affects the uses of these trajectories. So, high times means, for instance, high reliability of the whole spacecraft, and so the risk of failures increases. But high times involve also high operational costs and this directly reflects into economical costs.

Another important drawback is represented by the launch windows. In fact, since the full interplanetary path is made of three different legs, when the starting date is slightly changed, it is difficult to reproduce the performances of the nominal path. Sometimes this leads to unfeasible high-cost solutions due to the high non-linearities of the manifold legs. This statement is confirmed by numerical experiments carried out within the developed model.

Due to these high non-linearities, another important weak feature of these trajectories becomes evident: the designed paths must pass through the Hill's region to approach the planet. A two-body interplanetary trajectory is designed with so an elevated energy level that the forbidden regions vanish and small corrections allow the planet approach. The invariant manifolds within the three-body problem are low-energy trajectories and so the for-

bidden regions appears. Now, since the spacecraft has to follow a transit trajectory through the small neck allowed (see figure 5.7), it is evident that small changes in the trajectory implies the loss of the transit property and so the planet could not be reached so long. Also this aspect is confirmed with numerical experiments.

Finally, it is clear that these trajectories are weak with respect to the perturbations of the other bodies and this statement requires again the comparison with a two-body trajectory. In fact, a conic trajectory taken as a first guess solution in a refined model does not require great corrections. On the contrary, the authors expect that a patched manifolds trajectory requires robust algorithms for its correction under other gravitational attractions and perturbations (i.e. solar wind). Moreover, other effects, as the orbital eccentricity of the planets, are not included into the model and need to be corrected.

5.4.4 Considerations at system level

The subsystems of a potential spacecraft using these trajectories are again conditioned by the high times and by the features of these trajectories.

The guidance, navigation and control system will require sophisticated instrumentations and robust algorithms in order to follow the nominal designed paths. By the authors point of view, this instrumentation is not yet available nowadays.

The power generation could be done by using the common solar arrays since for Mars and Venus this is expected to be the best solution. Nevertheless, due to the high times, the degradation of the arrays must be kept in mind and, concerning the batteries, an elevated number of cycles will be needed.

The propulsion is chemical and, due to the multi-burning technique, liquid restartable engines will be necessary. The thermal, communication and attitude subsystems do not present particular differences with respect to the same subsystems of an interplanetary spacecraft designed with the classical method. Finally, the authors want to point out that the reliability of these components is important since the whole mission depends on them.

Chapter 6

Low-Energy Lunar Transfers Using Libration Points

The possibility to have low-energy transfers to the Moon is presented in this chapter. These transfers are different from the usual conic paths to the Moon since they are defined in the R3BP model. They differ also from the WSB transfers since the approach undertaken here aims to directly (through $L1$) reach the Moon by targeting a point on the interior $L1$ stable manifold.

This chapter starts with a detailed analysis of the state of the art with a special emphasis on the WSB and targeting methods. Then, the necessity to compute new trajectories to the Moon lead to the this new approach. In the end the results are presented with several discussions on the uses of these trajectories for future space missions.

6.1 State of the art analysis

The Hohmann transfer represents the classical technique adopted to go to the Moon. Typically, a Hohmann transfer takes only a few days, depending on the altitude of the initial parking orbit. It requires two large rocket thrusts, one parallel to the motion to leave the Earth and the other anti-parallel to the motion to capture the probe around the Moon. The size of these burns, measured by the velocity boost ΔV, depends again on the altitudes of the Earth and Moon orbits [3]. For instance, the cost required to go from a circular Earth parking orbit of altitude $h_E = 167\ km$ to a circular orbit around the Moon with height $h_M = 100\ km$ is almost $\Delta V = 4000\ m/s$ and the time of flight is around $\Delta t = 5\ days$ [4]. As for the interplanetary transfers, discussed in the previous chapter, the full Hohmann path is obtained again by patching together two different two-body problems (the Earth-Spacecraft at

departure and the Moon-Spacecraft at arrival) and only one gravitational attraction is taken into account at each leg. The nature of this transfer involves a hyperbolic excess velocity relative to the Moon which determines the ΔV required to put the spacecraft into an orbit about the Moon. Among the conic trajectories, there are also the bi-parabolic and the bi-elliptic transfers, but the former has almost the same total ΔV as the Hohmann transfer, while the latter has a higher cost. Both these two transfers require a time that is longer than the Hohmann one.

In order to reduce the cost associated to the Hohmann transfers, in the past several authors have approached this problem from a different point of view. Since the two-body nature involves only conic trajectories, the idea has been to wide the dynamical model and involve two or more gravitational attractions simultaneously acting upon the spacecraft. In this way, several techniques have been developed to analyze the low-energy ballistic transfers to the moon.

First, D'Amario and Edelbaum [15] developed a method to find optimal impulse transfers in the circular restricted three-body problem (i.e. the natural extension of the two-body problem). This technique was based on the combination of a multiconic method with the primer vector theory and an accelerated gradient method of trajectory optimization. The important feature of their algorithm was that, thanks to the multiconic approximation, both the state transition matrix and the primer vector were found analytically without additional integrations or differentiations. As mentioned in section 4.1, this method was applied to the determination of optimal two and three-impulse transfers between the Earth-Moon $L2$ and circular orbits about the Moon.

Then, based on the previous study, the work of Pu and Edelbaum [56] was aimed again to find two and three optimal impulse trajectories but in a Sun-Earth-Moon environment where the three bodies all had a significant influence on the motion of the spacecraft. Also in this case the state transition matrix was calculated analytically. They applied this technique to analyze trajectories between the Earth and the $L1$ libration point.

One decade later, exploiting the intrinsic nature of the same model, Belbruno and Miller [4] described a method to obtain Earth-to-Moon transfer trajectories with no hyperbolic excess velocity at Moon arrival. The so called Belbruno-Miller trajectories were the first to demonstrate that a celestial body could capture another body with negligible mass. Nevertheless, this capture was unstable and required another amount of energy to be stabilized. Their technique was based on the concept of *weak stability boundaries* (WSB) that are regions in the phase space where the gravitational attractions of the Sun, Earth and Mood tend to balance.

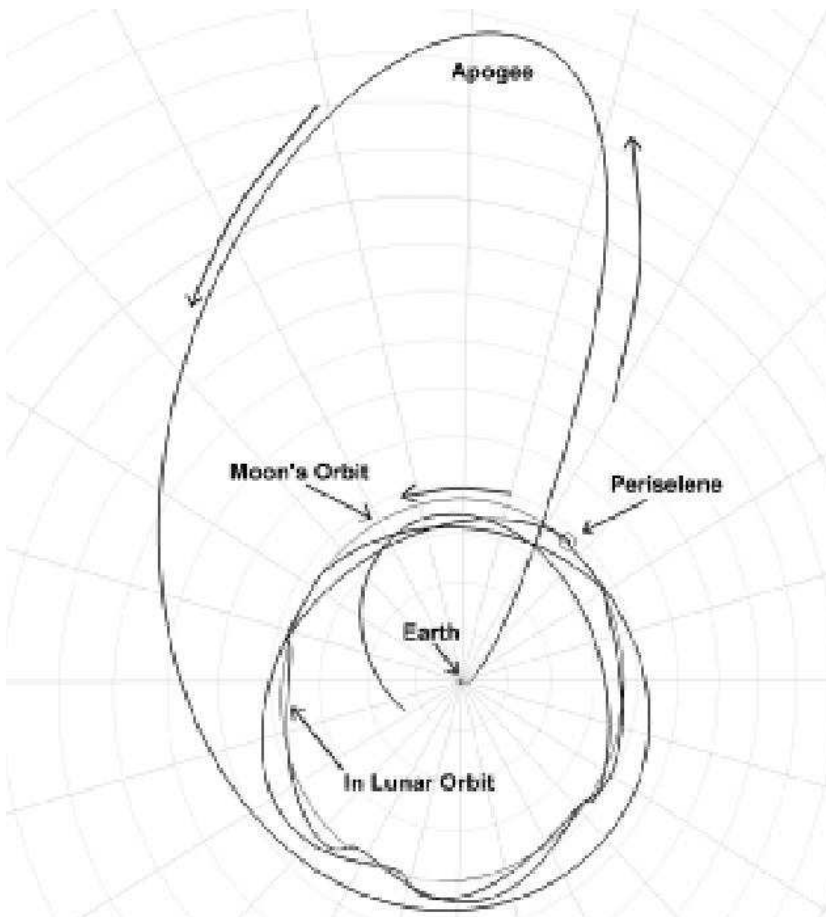

Figure 6.1: A typical Belbruno-Miller trajectory [5].

The idea, briefly described here, was to leave from a given point near the Earth and fly-by the Moon to gain enough energy to go at a distance of approximately four Earth-Moon distances from the Earth ($1.5 \cdot 10^6$ km). In this region, due to the high sensitivity to initial conditions, resulting in a chaotic dynamics, small changes make large deviations in the motion of the spacecraft. So, a small amount of energy (ΔV) was used to put the spacecraft into a ballistic lunar capture trajectory that led to an unstable ellipse. Here, another maneuver was performed to put the spacecraft into a lunar circular orbit (figure 6.1). The new technique showed to be more economical than the Hohmann transfer although time of flight was more than ten times longer. For instance, a WSB transfer between the two circular orbits mentioned above ($h_E = 167$ km and $h_M = 100$ km) has a total cost of $\Delta V = 3838$ m/s that is 153 m/s less than the Hohmann transfer. This is not a substantial saving

when the ΔV is translated into the propellant mass fraction Δm_p through the rocket equation. This small difference, together with the high transfer times, led to consider the WSB trajectories as useful only for recovery or emergency conditions. Indeed, this technique was successfully used to save the Hiten spacecraft [80] which reached the Moon after a launch failure.

After the discovery of these alternative trajectories, several studies were undertaken in order to analyze the WSB transfers from an optimization point of view. In these works, the purpose was to further reduce the cost associated with the WSB lunar transfers. But, the chaotic dynamics characterizing these trajectories did not allow the use of a deterministic approach (e.g. a gradient method) to this problem.

Biesbroek [8] studied the WSB transfers, from a dedicated GTO Earth orbit to a dedicated Moon orbit, by applying an optimization method based on genetic algorithms. He analyzed the possibility to use a WSB transfer trajectory for the LunarSat mission after that a trade-off study carried out by Seefelder [64] showed the feasibility of a lunar mission departing from a GTO[1]. Biesbroek found that such a global approach is very suitable with highly non-linear problems like the WSB transfer to the Moon where small changes in the parameters cause great difference in the final trajectory and performances. The total cost associated with these transfers, computed in a 30 days launch window, was between 1170 m/s and 1325 m/s.

Another study based on a global optimization approach was performed, in a previous ESA contract, by Bellò Mora et al [7]. They developed a software tool for constructing WSB transfer to the Moon using a systematic approach [6]. They first observed a link between the Belbruno-Miller trajectories and the R3BP: the Earth-Sun WSB region, located at almost four Earth-Moon distances from the Earth, is around the zero velocity curve connecting the two libration points $L1$ and $L2$ in the Sun-Earth system. Furthermore, the passage through this region guides the spacecraft to a dynamical state close to the zero velocity curves of the Earth-Moon system. This means that with a WSB trajectory the minimum possible energy needed to reach the Moon from *outside* and the limiting state that allows the capture corresponds to the Jacobi constant value C_2 (that is the Jacobi constant evaluated in the point $L2$ of the Earth-Moon system). Thus, a WSB transfer can be viewed as a Sun-Earth-Spacecraft and an Earth-Moon-Spacecraft problem, that are two coupled R3BPs. The authors studied both transfers from LEOs and from GTOs and they found approximately the same results as in Belbruno and Biesbroek.

[1]This is an important result since no lunar mission has been executed using a GTO as the initial orbit

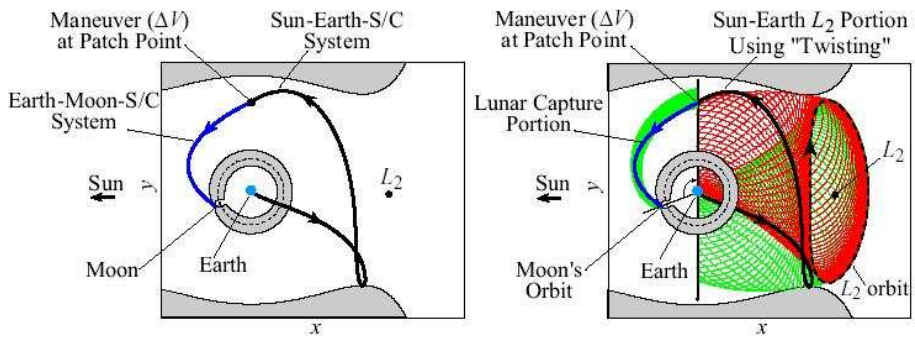

Figure 6.2: The explanation of the capture mechanism provided by Koon et al [44].

Vasile and Finzi [74] proposed a hybrid technique to optimize WSB transfers using a combination of a heuristic and a deterministic method. A modified evolutionary program was employed to assure a first guess condition to a gradient based algorithm. This work showed that WSB transfers make easily accessible some orbits, such as high eccentric polar orbits about the Moon, with reduced cost.

All the previous works were aimed to analyze the performances and the applicability of the WSB transfers from a numerical and an optimization standpoint, but they did not treat the nature of the capture that is the most important dynamical feature of a WSB trajectory. On the contrary, Koon et al [44] gave a deep explanation, based on the dynamical system theory, of the Moon's capture mechanism found from Belbruno. Using two coupled planar circular R3BP, they showed that the full WSB trajectory could be separated into two "deterministic" legs: the first was a piece of the unstable manifold of a $L2$ Lyapunov orbit in the Sun-Earth system, while the second, the one that allows the Moon's capture, was a leg of the stable manifold associated to a $L2$ Lyapunov orbit in the Earth-Moon system (figure 6.2). When these two manifolds intersect in the configuration space, a small ΔV performs the step from the first manifold to the second. An approximated value of this cost can be found by analyzing the Poincaré sections of the two manifolds. Beyond this case, with such approach Koon et al provided an additional structure of the phase space and characterized different regimes of motion in the region near the libration points $L1$ and $L2$.

The studies above deal with the problem to transfer a spacecraft from an Earth parking orbit to an orbit about the Moon by taking into account the gravitational attraction of the Sun, Earth and Moon. In a WSB trajectory, the action of the Sun is relevant because, during the transfer, the spacecraft

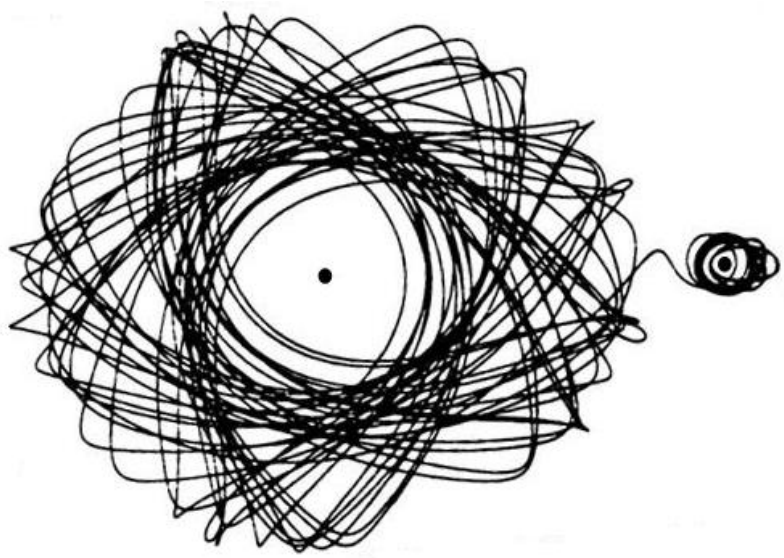

Figure 6.3: The Earth-Moon transfer found from Bolt and Meiss [9].

is far from the Moon and the Earth. Moreover, the Moon is approached from the exterior region of an Earth-Moon problem (figure 6.2).

Looking for a *direct* Earth-to-Moon transfer, the Earth-Moon-Spacecraft circular R3BP may be considered as the model for the trajectory design. Such an approximate system is very useful for the preliminary analysis of the trajectory that is later refined through more precise models which include effects like the eccentricity, the Sun and other planets, the solar wind, etc. Thus, the mission analyzed in this "simple" model could take advantage of the dynamical features provided by two primaries acting upon the spacecraft. Furthermore, the smallest energy level that allows the transfer corresponds to the Jacobi constant at $L1$ (C_1), that is lower than the level of a WSB. This is due because in a WSB transfer the Moon is approached from the exterior, so the minimum energy value needed to open the Hill's curves is C_2. In the Earth-Moon system the transfer is direct, through $L1$, so the minimum energy value is C_1 that is higher (i.e. lower energy) than C_2.

In this frame several studies have been carried out in order to exploit the chaotic dynamics of the R3BP. Typically, this chaotic dynamics produces highly irregular behavior and the sensitive dependence on initial conditions prevents long-term prediction of the state of the system. However, the inherent exponential sensitivity of chaotic time evolutions to perturbations can be exploited to guide trajectories to some desired final state by the use of a carefully chosen sequence of small perturbations to some control parameters. These perturbations can be so small that they do not significantly change the

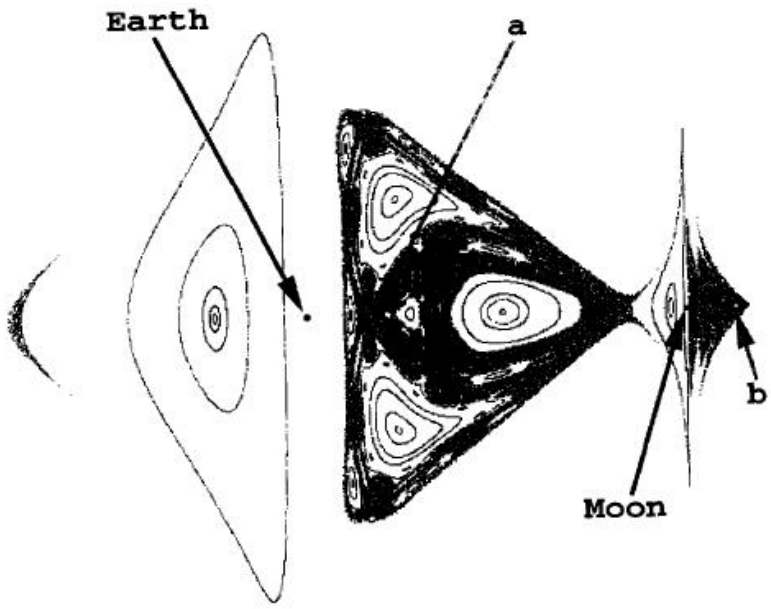

Figure 6.4: The Poincaré section of the Bolt and Meiss trajectory [9].

system dynamics, but enable this intrinsic dynamics to drive the trajectory to the desired final state. This process has been called *targeting*.

Bolt and Meiss [9] applied the targeting to find short orbits in the planar R3BP with the Earth and the Moon as primaries. They reduced the 4D phase space of the planar problem on a 2D Poincaré section. Here, with the appropriate choice of a starting and a target point, they were able to find a low energy transfer between two orbits at an altitude of almost $h_E = 60000\ km$ and $h_M = 14000\ km$ respectively above the Earth and the Moon (figure 6.3). They obtained a ballistic capture that was asymptotic to a Moon-orbiting invariant torus. Strictly speaking, this kind of capture is more rigorous than the one found from Belbruno, which requires an additional maneuver, because it aims to insert into a stable Moon's orbit. The overall ΔV required by this transfer is 750 m/s with a time of flight equal to $\Delta t = 2.05\ years$. In contrast, the total boost required for a Hohmann transfer between the same orbits is $\Delta V = 1220\ m/s$ but with an interval time of only $\Delta t = 6.6\ days$. This means that the cost of the Bolt and Meiss trajectory is about 38% less than the Hohmann transfer. This result is remarkable since a typical WSB trajectory requires an overall ΔV that is "only" 18% less than the Hohmann transfer between the same orbits [4].

Nevertheless, this transfer has two weak key features. The first is the altitudes of the departure and arrival orbits that are chosen according to

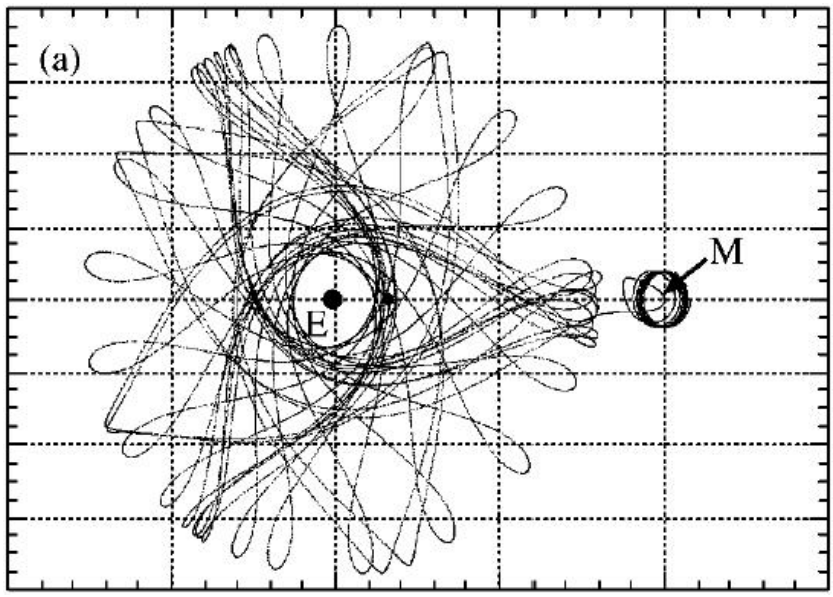

Figure 6.5: The Earth-Moon transfer trajectory found from Schroer and Ott [63].

the chaotic regions on the Poincaré section (figure 6.4). Since the phase space close to the primaries is characterized by an *ordered* dynamics[2] and since the targeting method uses the highly nonlinear dynamics that occurs in the medium region, the starting and ending points turn out to be far from both the Earth and the Moon (points `a` and `b` in the figure 6.4). This is the reason why the study of Bolt and Meiss does not treat the leg close to the Earth. The second aspect is obviously the time needed for the transfer that is an intrinsic consequence of the targeting method. This happens because in chaotic Hamiltonian systems, beside the coexistence of interwoven chaotic and quasi-periodic regions, the phase space is divided into layered components which are separated from each other by Cantori. Typically, a trajectory initialized in one layer of the chaotic region wanders in that layer for a long time before it crosses the Cantori and wanders in the next region [50]. This leads to transfers that are only of academic interest but they are not employable for real lunar missions.

In order to reduce the high transfer times, another approach was suggested by Schroer and Ott [63] who applied a modified targeting procedure to the same Hamiltonian system assumed in Bolt and Meiss. The authors found short orbits that "quickly" lead to the Moon arrival orbit. Through this method they were able to find a transfer between the same departure

[2]Sometimes the regions of ordered dynamics are called *islands* in the chaotic *see*. This concept is clearly shown in figure 6.4.

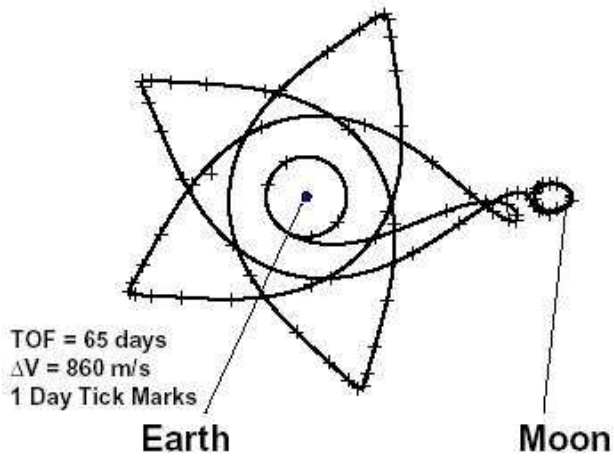

Figure 6.6: The Earth-Moon transfer computed by Ross [61].

and arrival orbits used by Bolt and Meiss with a time of flight equal to $\Delta t = 377.5$ *days* and with the same ΔV (figure 6.5).

In the same Hamiltonian system (planar and circular R3BP with Earth and Moon as primaries) and with the same starting and departure orbits, Macau [50] found a chaotic Earth-Moon transfer that requires a cost slightly higher ($\Delta V = 767$ m/s) than the two previous works, but with a time of transfer equal to $\Delta t = 284$ *days*. Using the Hill's equation to describe the motion of the spacecraft, he introduced again a surface of section transverse to the flow so the continuous time system was translated to a discrete time Poincaré map. With this method, Macau found a considerable shorter transfer time and, different from the two previous studies, it was necessary to apply just two impulsive thrusts to achieve the transfer.

Ross [61] compared these three studies based on the targeting with his approach to the Earth-Moon transfer problem. He analyzed the planar and circular R3BP with the invariant manifolds technique and reduced the dimension of the problem to two with the use of an appropriate Poincaré section. Using these dynamical channels, Ross was able to find a transfer between the same orbits around the Earth and the Moon ($h_E = 60000$ km and $h_M = 14000$ km) that requires a ΔV equal to 860 m/s and a transfer time of $\Delta t = 65$ *days*. By this technique, the spacecraft is placed on a trajectory near one of the resonances which is linked to capture tubes.

Finally, the mission analysis of the recent ESA's SMART-1 [62] was designed by combining the low-thrust propulsion with the Moon's perturbations acting upon the spacecraft. The designers used Moon's resonances to raise the pericenter and the apocenter of the elliptic Earth's orbit, Moon swing-

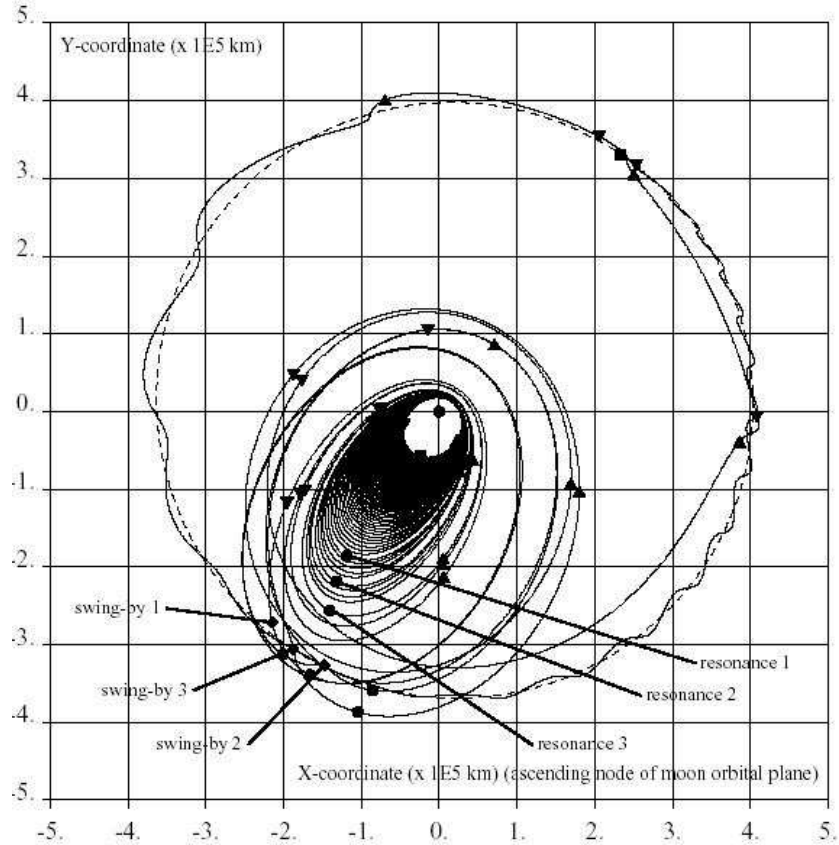

Figure 6.7: The SMART-1's transfer trajectory to the Moon [62].

by's to increase the energy level and the lunar capture to orbit the Moon. The combination of these four different *building blocks* produced the singular transfer path shown in figure 6.7.

6.1.1 Motivations for further studies

The state of the art analysis has evidently shown that the Hohmann transfer to the Moon is quite expensive with respect to the other possibilities developed in the last years. But, with this high cost a very short time of transfer is associated and so only two missions (i.e. Hiten and SMART-1) have employed these innovative techniques to reach the Moon. For instance, all the manned missions to the Moon of the Apollo program were designed using a two-body approach [3] since there was the strong constraint on the time of flight.

Nevertheless, since the Moon is the *key* of the future space activities, there

will be several missions requiring a maximization of the payload mass without any constraint on the time of flight (e.g. lunar sample return missions, cargo missions, ...). Thus, the costs (Δv) must be lowered by considering other possibilities that involve reasonable times.

It has been shown that the WSB transfer need a total cost that is 18% less than the Hohmann Δv, but the time of flight is more than ten times longer. So, from the authors point of view, the Belbruno-Miller trajectories do not give a particular advantage for transfers to the Moon since the longer times turn out to be a marked drawback for the other features of the mission, such as the mission operations and control, the reliability of the instrumentation and the scientific results. Hence, if viewed as the intersection of two manifolds, the WSB transfers seems to be of less practical interest.

The costs of the lunar transfers have been further reduced with the targeting method which reduces again the Hohmann cost down to 38%. But, this method has again associated high times because the trajectories need a lot of time to exploit the dynamics of the system. Moreover, the method of targeting works well between high orbits around the Earth and the Moon, but it does not assure a link when low orbits are considered.

By these two approaches (i.e. the manifolds technique and the targeting method), it is clear that a *combined* method is still missing or a technique that, departing from a low orbit about the Earth, targets a piece of the interior manifold that assures the Moon arrival. Here, this technique is investigated as a new possible way to reach the Moon

6.1.2 Space applications

Since the technique proposed for the Earth-to-Moon transfers is a combination of the manifolds and targeting methods, it will have a natural "high", if compared to the Hohmann, time of transfer. But, in this chapter, among all the solutions, only trajectories with a reasonable time will be considered.

Anyway, these kind of transfers are not suitable for manned missions to or around the Moon because they present intrinsic high times. Nowadays, the two-body patched trajectory continues to be the best solution for manned missions.

The proposed trajectories, could be appropriate for cargo missions to the Moon. As an example, if a permanent lunar base will be developed, many missions will be planned in order to bring the modules on the Moon before the man arrival. These missions, without any particular constraint on the time, would follow a path that exploits the dynamics of the Earth-Moon system in order to maximize the mass of the payload modules.

In addition, another mission that is being planned for the next decade

is the lunar sample return. Also this mission would not have particular time constraints and it would maximize the mass of the samples to bring back to the Earth. Its path could be again a non-linear trajectory within the Earth-Moon frame; more precisely a Moon-impact and an Earth-impact trajectories.

Finally, the developed technique could be applied also for the "common" missions that aim to orbit the Moon. Here, following the manifolds, an additional manoeuvre will be required to place the spacecraft in a Keplerian orbit around the Moon.

6.2 Problem approach

The minimum energy required to reach the Moon, departing from the Earth, is the one corresponding to a value slightly lower than C_1, that is the Jacobi constant (equation 1.9) corresponding to the $L1$ point. With greater values, indeed, Hill's curves close and the motion is allowed only in the region around the Earth (figure 1.2).

Thus, assuming $C \leq C_1$, transfers to the Moon can occur through the small neck opened at $L1$. But, even if these transfers may occur theoretically, designing a trajectory crossing this region is very difficult in a chaotic regime like the R3BP. To overcome these difficulties, the invariant manifold theory is again considered. This is a clear example of the power of the manifolds since they provide for *additional structure* within the restricted problem frame.

Figure 6.8 shows a piece of the interior stable manifold associated to $L1$ (W^s_{L1}) and the corresponding exterior unstable manifold (W^u_{L1}). As can be seen, even if the transit region is very thin, these two trajectories represent *transit orbits* between the forbidden region. So, if a spacecraft is on the W^s_{L1}, the system, by itself, will bring it from a region close to the Earth to the region close to the Moon by simply exploiting the intrinsic dynamics. From another point of view, the Moon captures the spacecraft using its gravitational field.

One has to point out that this kind of capture is different to both the "Belbruno-Miller trajectories" and to the "Koon et al patched manifolds" since there the Moon approach occurs from the exterior (i.e. from $L2$). The two invariant manifolds considered here allow a Moon transfer from the interior and with the smallest energy possible! Strictly speaking, this approach is also different to the "targeted trajectories" since there the trajectory was continuously perturbed in order to reach the target. Here, the trajectory the consequence of the system evolution.

Thus, the matter is to put a spacecraft on the interior stable manifold associated to $L1$ and wait for the natural evolution of the system. Unfortu-

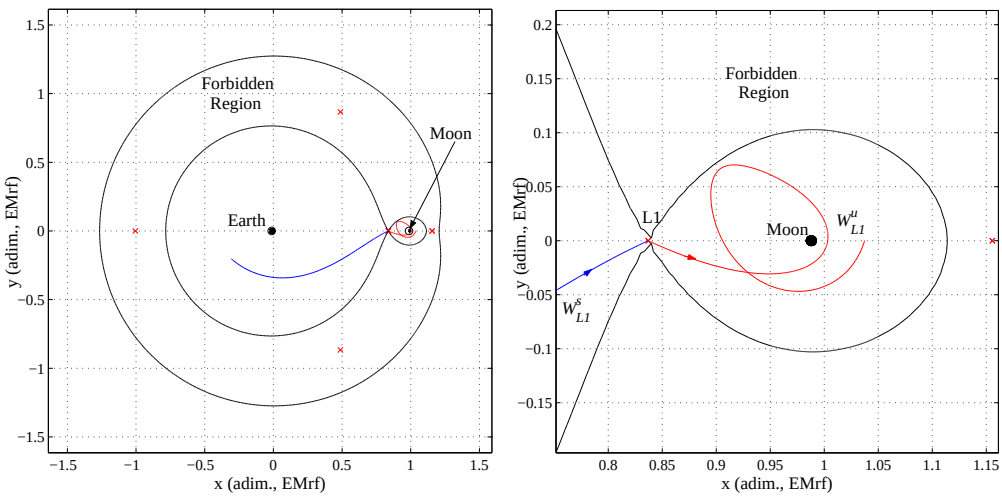

Figure 6.8: The stable (blue) and unstable (red) manifolds associated to the point $L1$ in the Earth-Moon system (left). The two are transit trajectories through the small neck opened at $L1$ (right).

nately, this manifold does not reach the Earth that is the greatest primary in this system. Figure 6.9 shows the interior leg of the $L1$ stable manifold integrated for five Moon's periods (i.e. around 140 days). This orbit, performs several loops but it is never close to the Earth. Moreover, the minimum Earth distance seems to be constant and almost equal to 0.35 Earth-Moon unit distances.

Another question arises: the trajectory shown in figure 6.8 is represented in the rotating system. If viewed in the usual Earth-centered inertial frame, this trajectory appears as a conic-like orbit. Thus, the farther points are the apogees and the closest are the perigees. Now, when the apogee is not aligned with the Earth-Moon line, the orbit is anyway perturbed by the Moon, but it remains conic. When the apogee occurs near the Earth-Moon line, the Moon "pumps" up the apogee until it captures the orbit that breaks and become non-elliptic. This is another explanation of the Moon resonance concept successfully used in the design of the SMART-1 mission.

Now, the stable manifold can be written as:

$$W^s_{L1} = \Phi(L1, t_W) \tag{6.1}$$

that is the asymptotic trajectory after a time equal to t_W and represents a point in the six-dimensional phase space. The problem has become the target, starting from an Earth orbit, of a point belonging to the stable manifold. This formulation allows again the use of the Lambert's three body problem that has proven to be a useful tool for this kind of problems.

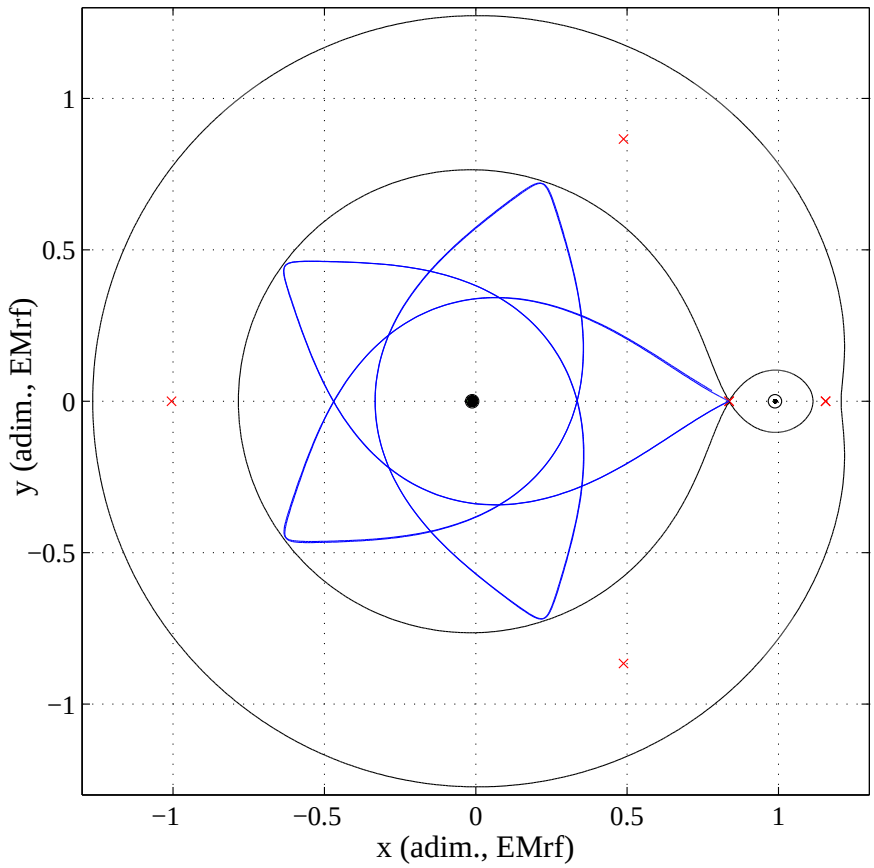

Figure 6.9: Interior leg of the $L1$ stable manifolds integrated for five Moon's periods. The overlapping of the trajectory suggests the possibility of the existence of a homoclinic orbit.

Again, a first Δv_1 places the spacecraft in a translunar trajectory starting from a low Earth orbit and a second manoeuvre Δv_2 is used to inject the spacecraft on the stable manifold.

In this chapter, the problem to reach the Moon's neighborhood, departing from an Earth orbit, will be considered. This means that the possibility to reach the point $L1$ with low costs will be analyzed. Once the spacecraft is in the $L1$ point, if no additional manoeuvres are performed, it will orbit the Moon with unstable trajectories near the exterior unstable manifold (red) shown in figure 6.8.

At $L1$, since the two gravitational forces balance, small changes in the velocity vector produce large deviations in the final trajectory. So, with very small cost, free fall trajectories to the Moon could be easily implemented for the missions that require a Moon landing. This concept is the one studied

by Broucke [10] and, thanks to the mirror image theorem, leads also to trajectories from the Moon to $L1$.

If a stable orbit around the Moon is needed, again with small changes the spacecraft could be placed in a path asymptotic to a Moon Keplerian orbit as done by Bolt and Meiss [9]. Both these two aspects are pretty interesting and could be further analyzed in a successive and more refined study.

In figure 6.10 the unstable manifold W^u_{L1} has been integrated for twelve Moon's periods. The trajectories fill the whole Moon's neighborhood with orbits that are close to the classical two-body Keplerian ones. It is clear that, theoretically, the spacecraft remains forever captured by the Moon and bounded by the forbidden regions.

The trend of the altitudes, above the Moon's surface, of these orbits, with respect to the time, is shown in figure 6.11. This altitude has a periodic trend and a mean value, with twelve Moon's period, equal to$h_M = 21600\ km$ (dashed line).

This mean "virtual" orbit has been taken as the arrival orbit in order to compare the costs found here with the Hohmann transfers. Hence, while the

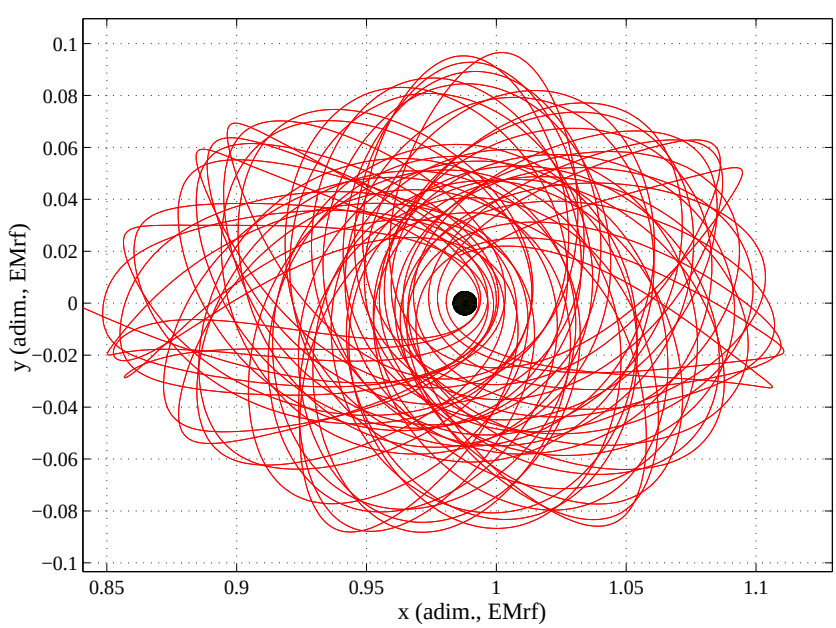

Figure 6.10: Interior leg of the $L1$ unstable manifolds integrated for twelve Moon's periods. The spacecraft fills the whole Moon's neighborhood with unstable orbits that are close to the two-body Keplerian orbits.

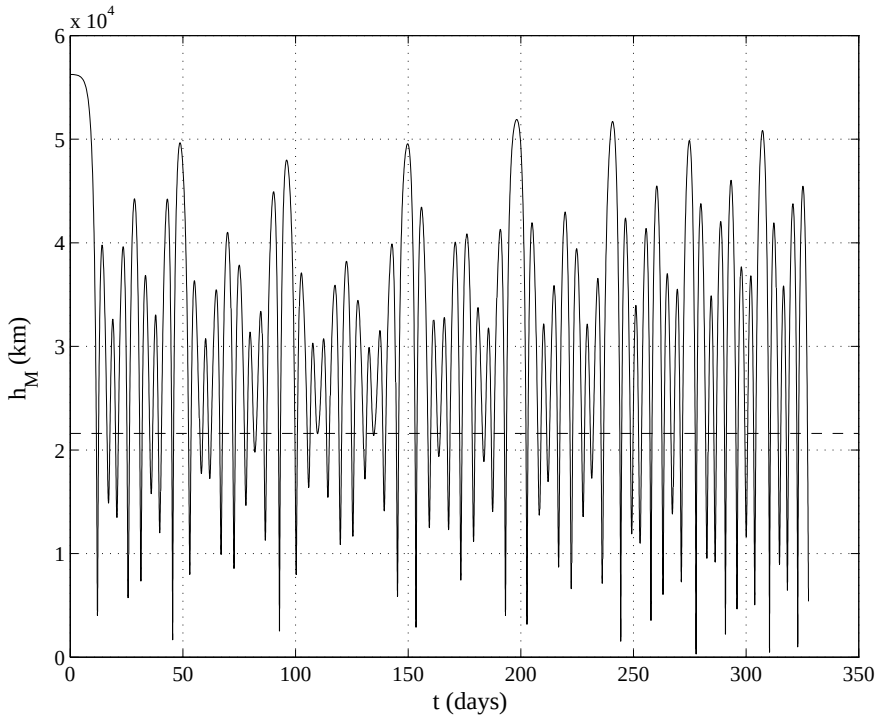

Figure 6.11: Altitude, with respect to the Moon, versus time of the unstable manifold plotted in figure 6.10. The dashed line represents the average altitude equal to $h_M = 21600\ km$.

departure orbit around the Earth is fixed for the two kind of transfers, the arrival condition is the mean orbit for the Hohmann transfer and an unstable trajectory fluctuating around it for the computed transfers.

Based on the concept above, an algorithm has been developed to target pieces of the stable manifold and so inject the spacecraft around the Moon. The results found are summarized in the next sections.

6.3 Transfer trajectories from LEO and GTO

In this section the following orbits have been taken as the starting orbits for the transfers to the Moon:

- LEO: this is the same orbit considered in chapter 4 to simulate the usual parking orbits achieved by the launchers. The LEO considered here is a circular orbit with an altitude equal to $h = 200\ km$ above the Earth's surface;

LEO		GTO	
Δv (m/s)	Δt $(days)$	Δv (m/s)	Δt $(days)$
3081	49.0	914	49.0
3085	119.6	918	119.6
3091	47.7	924	47.7
3172	118.5	1005	118.5

Table 6.1: Overall cost and time found for the transfers to the Moon departing from the LEO and GTO.

- GTO: it is again the same as in chapter 4 ($h_p = 200$ km and $h_a = 35841$ km) and it has been assumed to simulate the launch of the spacecraft as a secondary payload for a mission to a geostationary orbit.

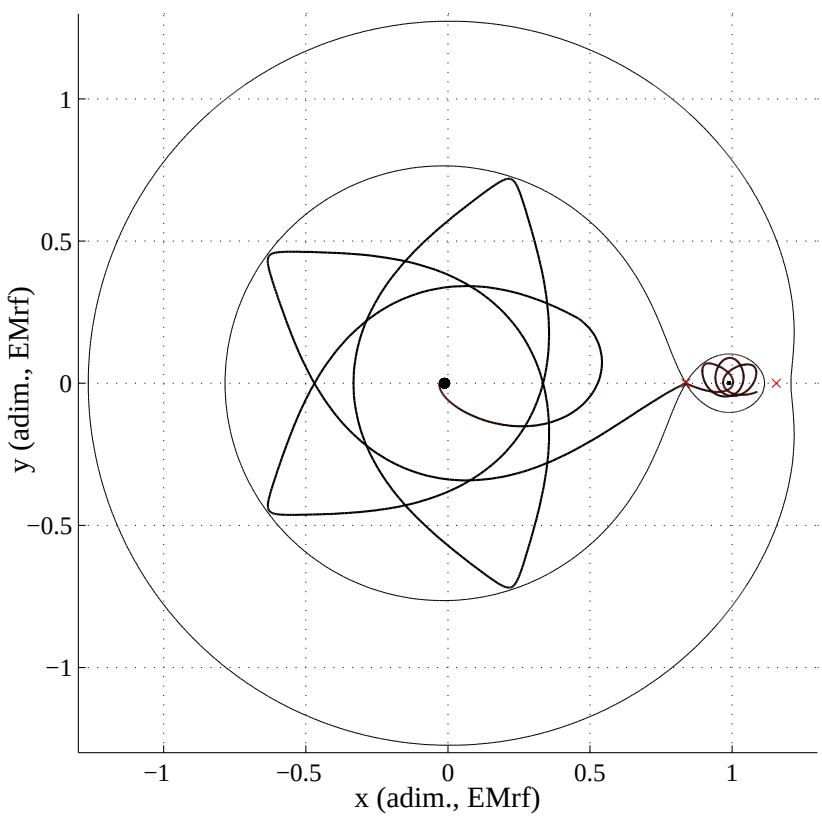

Figure 6.12: An Earth-to-Moon transfer departing from a LEO. This solution requires a cost equal to $\Delta v = 3244$ m/s and a time of transfer $\Delta t = 65.1$ $days$.

Table 6.1 contains several solutions found for the Earth-to-Moon transfer by the approach showed above. The first solution is remarkable since allows to reach the Moon with a cost equal to $\Delta v = 3081\ m/s$ and with a time of flight of "only" $\Delta t = 49\ days$. The corresponding solution obtained departing from a GTO has a cost equal to $\Delta v = 914\ m/s$ and the same time of transfer.

The Hohmann transfer from the LEO to the virtual orbit requires a cost equal to $\Delta V = 3344\ m/s$ and a time of transfer of 6.5 $days$. If this transfer starts from a GTO the cost reduces down to $\Delta V = 1177\ m/s$ with the same time.

6.4 Transfer trajectories from high Earth orbits

In order to validate the developed approach, in this section the starting orbit has been taken equal as the orbit in the works of Bolt and Meiss [9], Schroer and Ott [63], Macau [50] and Ross [61]. This is a high Earth orbit (HEO) with altitude $h = 60000\ km$ and with this assumption the generic high orbits (i.e. geostationary orbits) are taken into account. The results found by the cited authors can be found in the section 6.2, while some result found in this work are summarized in table 6.2.

The corresponding Hohmann transfer to the mean orbit require a cost equal to $\Delta V = 964\ m/s$ and a time of flight again equal to 6.5 $days$.

Figure 6.13 shows the solution corresponding to the first row of table 6.2 that is the best found in this frame. It has to be pointed out that these solutions do not consider the injection into the high Moon orbit, with altitude equal to 14000 km, assumed in the cited works. Anyway, it is remarkable how the best solution has a time of transfer that is much shorter with respect to the previous solutions to this problem.

HEO	
Δv (m/s)	Δt $(days)$
766	50.5
862	164.6
1358	427.8

Table 6.2: Overall cost and time found for the transfers to the Moon departing from the HEO.

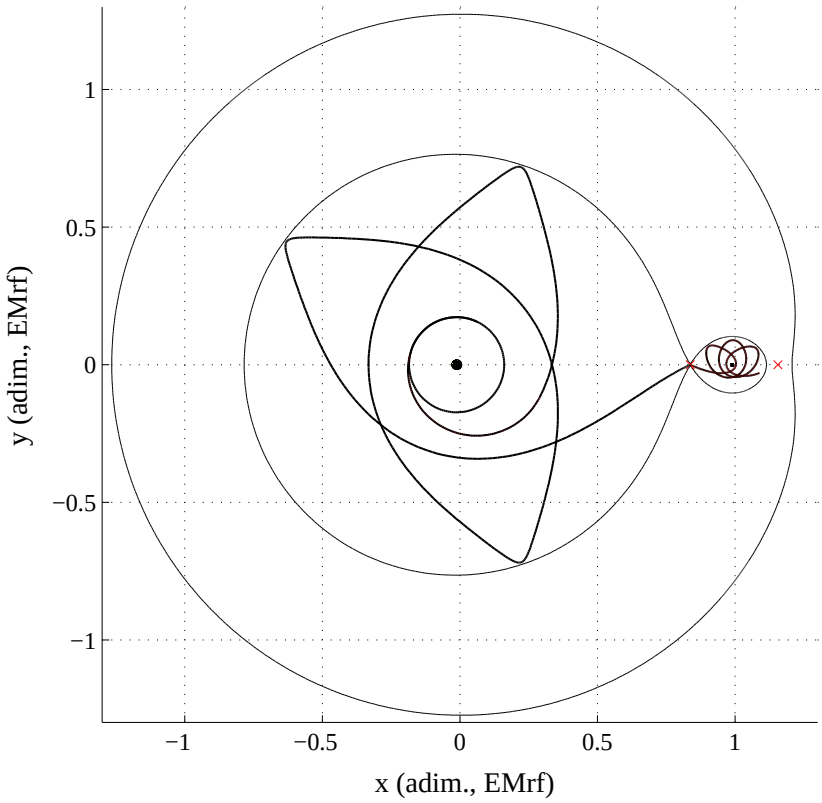

Figure 6.13: An Earth-to-Moon transfer departing from a high Earth orbit. This solution requires a cost equal to $\Delta v = 766\ m/s$ and a time of transfer $\Delta t = 50.5\ days$.

6.5 Earth-Moon transfers through $L1$: uses for future space missions

The two sections above have demonstrated that the Moon could be easily reached with a low-energy trajectory that passes through the small neck opened al $L1$. Follows a brief analysis of how these solutions collocates among the existing techniques, their drawbacks, their uses and their implications on the subsystems of the spacecraft.

6.5.1 Remarks and comparison among other techniques

A Hohmann transfer requires a cost around $\Delta v = 4000\ m/s$ to reach a low Moon orbit, departing from a low Earth orbit, and a time of flight less than a week. These trajectories are the fastest among all the other possible since

the patching conics involves a high energy level by its formulation. The Hohmann transfers are the most appropriate trajectories for manned mission to the Moon since, in this case, the constraint on the time of flight is stronger than the others on the masses of the payloads.

A WSB transfer allow a reduction equal to 18% of the Hohmann cost but the time of transfer is over four months. This is due to the singular Moon approach of these trajectory that occurs from the exterior. It has been demonstrated that the WSB transfers make easily accessible some orbits, such as high eccentric polar orbits about the Moon, with reduced cost. But, the high times have led to a generally accepted conclusion that the WSB transfer can be used only in recovery situations to overcome launch or spacecraft failures.

The transfers obtained with the targeting method reduce the ΔV cost by more than 38% but involve high times, meaning from more than two months to two years, since the method itself is based on small perturbations that require a lot of time to produce their effects. But the main drawback of these trajectories is due to the altitude of the starting and arrival orbits. This technique, indeed, since it exploits the chaotic regime far from the primaries, needs to start from high altitude orbits: in the cited works this altitude is equal to 60000 km above the Earth. This feature, together with the high times, makes these trajectories not employable for the Moon transfer by the authors' point of view.

In the two previous sections, some solutions have been computed with the developed method based on the target of a piece of stable manifold associated to the $L1$ point. This technique, by its formulation, allows to overcome the problems of the targeted trajectories because the starting orbit may be chosen a priori without any restriction. Some of these solutions are both low-energy and "low-time", meaning that the minimum cost, departing from a GTO orbit, is around $\Delta v = 900\ m/s$ and the minimum time is around $\Delta t = 50\ days$. These costs and times refer to trajectories that reach the Moon and remain forever captured into unstable Moon orbits. But, it has been demonstrated that low changes in the velocity vector, applied near the $L1$ point, lead to Keplerian stable orbits or to Moon impact trajectories. Hence, by the authors' point of view, the method described in this chapter can be used to design such missions that do not have any particular constraint on the time of flight but aim to maximize the masses of the payloads. Here the reference involves Moon orbiter or Moon landers for various applications.

6.5.2 Uses for future space missions

The uses of these trajectories are clearly the consequence of the results and features discussed above: by the developed method, low-cost and mid-time transfers to the Moon can be obtained. In the future, there could be some missions requiring a maximization of the payload masses without any strong constraint on the time of flight. Such missions are evidently not manned, but scientific, cargo or validating technology missions.

The sample return mission to the Moon is being studied in order to return back to the Earth Moon samples. This is an example of mission to the Moon, with a terminal leg that is a Moon impact trajectory, that does not require to reach the Moon in a few days, but, for instance, needs to maximize the masses of the instrumentations. Following the stable manifold associated to $L1$, a spacecraft can be easily captured by the Moon until it reaches its surface. Here, after the scientific goals, the spacecraft departure could be again divided into a first transfer to $L1$ and a leg of the $L1$ unstable manifold to allow the Earth to capture the spacecraft. The total time here does not matter. The same use can be thought for mission that have to validate new technologies.

The sample return mission is not the only use for the Moon impact trajectories, but all the scientific missions that aim to explore the Moon surface could use these trajectories. Recently, the interest in missions on the far side of the Moon is raising among the scientists. This is another example of mission that could use the developed concept to reach the Moon.

Finally, all the missions that needs to orbit the Moon in both stable Keplerian or unstable orbits could use the Moon capture mechanism explained in the previous section to lower the total cost.

One has to point out that the possibility to depart from GTO orbits has been taken into account too. This is a great advantage for all the spacecraft launched as secondary payload in GTO orbits.

All these features indicates that it is important to continue the research begun with this study in order to apply the powerful performances provided by the trajectories through $L1$ for future Moon missions.

6.5.3 Drawbacks

The trajectories proposed in this chapter are non-linear orbits within the R3BP frame. The transfers making use of these paths must provide for robust control and navigation systems since here small changes in the initial conditions make large difference from the designed and the real trajectory. Hence, even if the energy of the transfer is lowered, the spacecrafts will require

sophisticated subsystems that allow to follow the designed captured path.

Moreover, these subsystems must have a high reliability because of the time of transfer, and so the time of the whole mission, increases. This reflects also in higher costs for the control operations on the spacecraft and delays the scientific results.

Although the launch windows for such transfers need to be analyzed, it seems that it will not be a critical topic since the trajectories have been obtained in the Earth-Moon system where the time constants are fast (i.e. the system repeats the same configuration after a Moon's period) and the synodic period between an Earth's orbit and the Moon is short.

Finally, a critical role is played by the Sun since the design of these trajectories does not take into account the Sun's perturbation. This aspect is more important when the times grow because, even if it is negligible, the perturbation of the Sun could lead to unwanted trajectories when the times of flight are long. It has to be remembered that this is a chaotic regime and so small perturbations may produce large final effects. Anyway, if the problem is analyzed in the Sun-Earth-Moon system with these trajectories as first guess solution, the real transfer path could *exploit* the Sun's perturbation to reach the Moon as in the WSB transfers where it allows a cheap access to expensive Moon orbits (i.e. polar orbits around the Moon).

6.5.4 Considerations at system level

The transfers to the Moon proposed in this section do not involve particular implications on the spacecraft subsystems apart of the features associated to the high times. By this, all the subsystems must have a high reliability to assure the right effectiveness during the mission period.

The propulsion subsystem is the one that may take advantage by these transfers since it will require less propellant mass. The formulation of the problem naturally involves chemical propulsion systems. Moreover, since the trajectory is multi-burned, the spacecraft will require a liquid engine because of its restartable feature.

The power subsystem could use the common solar arrays but it must provide for a high number of battery cycles. The communication and thermal subsystems do not imply particular restriction on the spacecraft configuration.

The attitude needs to be robust with respect to Earth, Moon and Sun gravity torques. The guidance, navigation and control, as discussed above, is the most sensitive subsystem with respect to the characteristics of these trajectories. It will require high accuracy to follow the designed paths.

Chapter 7

Other mission possibilities

In this chapter, the possibility to generate the common orbital transfers around the Earth within the R3BP frame has been considered. In this frame, a few examples of orbital transfers between a low and a high Earth orbit have been considered. These transfer have been calculated in the Earth-Moon system frame to allow Moon to "assists" the spacecraft during the transfer.

7.1 Problem formulation and approach

The orbital transfers among Earth orbits are commonly calculated using the Hohmann transfer theory. In the Earth's neighborhood, this technique, that links two orbits by using an intermediate semi-elliptical arc with two burns parallel to the velocity, provides very accurate results since the Earth attraction is order of magnitudes greater than the others (i.e. the Sun and Moon attractions).

But, the point is that when the altitudes of the final orbits increase,the gravitational attraction of the Earth lowers but the attraction of the other bodies increases. So, one can think that it could be advantageous to exploit these other forces to reduce the cost of the transfer. Moreover, after a launch failure, sometimes the spacecraft does not have the propellant needed to reach the final orbit. In this case the result of the whole mission is uncertain.

Here, the possibility to use a Moon assist for the transfers between a low orbit and a high orbit around the Earth has been analyzed. The problem has been formulated as the search of an optimal Lambert's three-body arc between the two given initial and final orbits (see figure 7.1). So, the two burns strategy remains the same as in the conventional transfer, but the important feature here is to find a Moon phase that involves reduced costs. Once the location of the Moon at launch has been established, the transfer

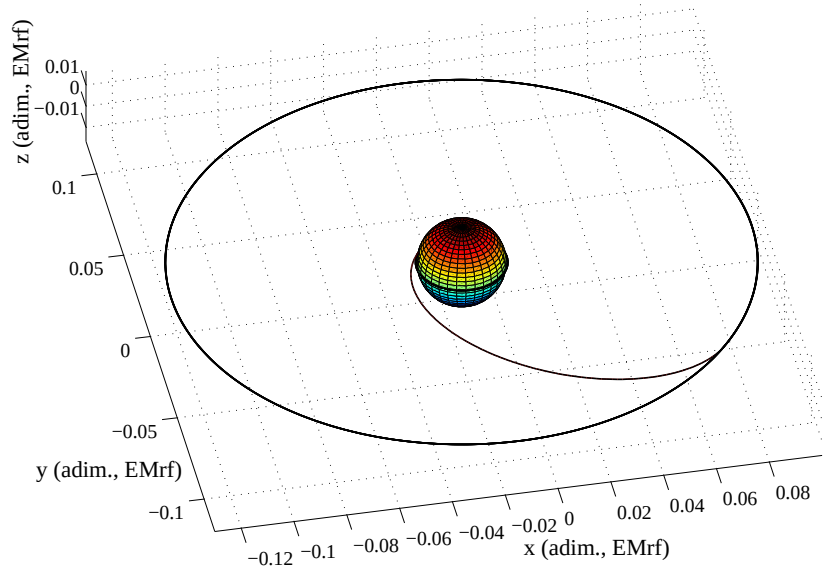

Figure 7.1: LEO to GEO transfer example.

trajectory, thanks to the Moon's influence, will be "pumped up" by simply following the dynamical evolution of the system.

Thus, if Δv_1 and Δv_2 are the two burns required to transfer the spacecraft from an orbit with altitude h_1 to another with altitude equal to h_2, the total cost of the transfer will be:

$$\Delta v = \Delta v_1 + \Delta v_2 \tag{7.1}$$

and the corresponding time will be called Δt. Given these two orbits, the problem is to find the minimum of the function:

$$min(\Delta v - \Delta v_H) \tag{7.2}$$

where Δv_H is the cost of the Hohmann transfer between these two orbits.

In this study, only circular orbits have been assumed in order to validate this idea. Anyway, the extension to generic starting and arrival orbits is not difficult. It could be done in a second and more refined step after that the problem has been assessed.

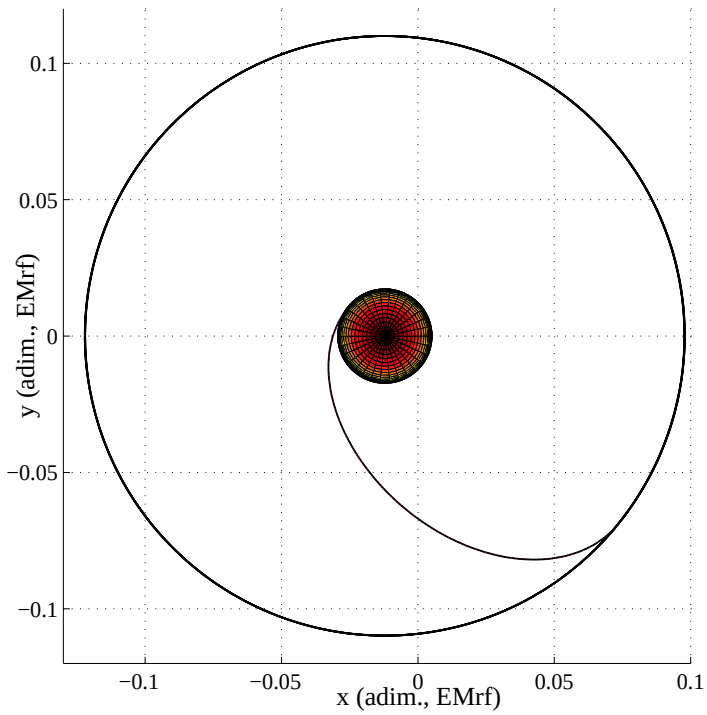

Figure 7.2: LEO to GEO 2D view transfer corresponding to the first row of table 7.1.

7.2 Transfer to the geostationary orbit

As the starting orbit, the LEO used in the previous chapters ($h = 200\ km$) has been considered; the final orbit has been fixed equal to the GEO ($h = 35841\ km$). Lower final orbits have not been considered since the Moon assists is more marked when the altitudes of the Earth orbits are elevated.

Table 7.1 shows three solutions found for this case. It is remarkable how

LEO to GEO	
$\Delta v - \Delta v_H\ (m/s)$	$\Delta t\ (days)$
-117.4	0.21
-117.6	0.21
-117.7	0.21

Table 7.1: Results for the LEO to GEO Moon assisted transfers.

up to 117 m/s can be saved if the transfer trajectory is calculated by taking into account the Moon's perturbation. This saving in Δv reflects in a saving of propellant mass or in a maximization of the payload masses. The times corresponds to the usual few hours needed to reach a GEO.

Different from the previous chapter, here the saving in Δv does not involve an increase in the time of transfer, but it remains the same as in the conic transfers. Moreover, several simulations have been done all leading to the same minimum. This means that the problem is well posed and the global optimal solution is unique.

7.2.1 Inclined geosynchronous orbits

Here the focus is the evaluation of this transfer technique when the inclination of the final orbit is different from zero. For this purpose, some geosyncronous[1] orbits have been considered. The results, summarized in table 7.2 shows that when the inclination grows, the Moon's action is not useful so long and, for perpendicular orbits, this technique furnishes results that are more expensive than the Hohmann transfer.

LEO to Geosynchronous		
i (deg)	$\Delta v - \Delta v_H$ (m/s)	Δt $(days)$
30	-44	0.20
60	+95	0.20
90	+173	0.20

Table 7.2: Results for the LEO to geosynchronous Moon assisted transfers.

7.3 Transfers to the high Earth orbits

As stated above, the power of this method seems to be more marked when high Earth orbits (HEO) are considered. Here, six different circular orbits have been assumed with altitudes from $h = 50000$ km to $h = 100000$ km (figure 7.3).

Table 7.3 shows the results found in this case. As supposed, the benefit increases with the altitudes of the final orbit up to 476 m/s for the transfer

[1] These orbits have the same radius as the GEO and the inclination different from zero. By this they are not geostationary orbits, but simply geosynchronous.

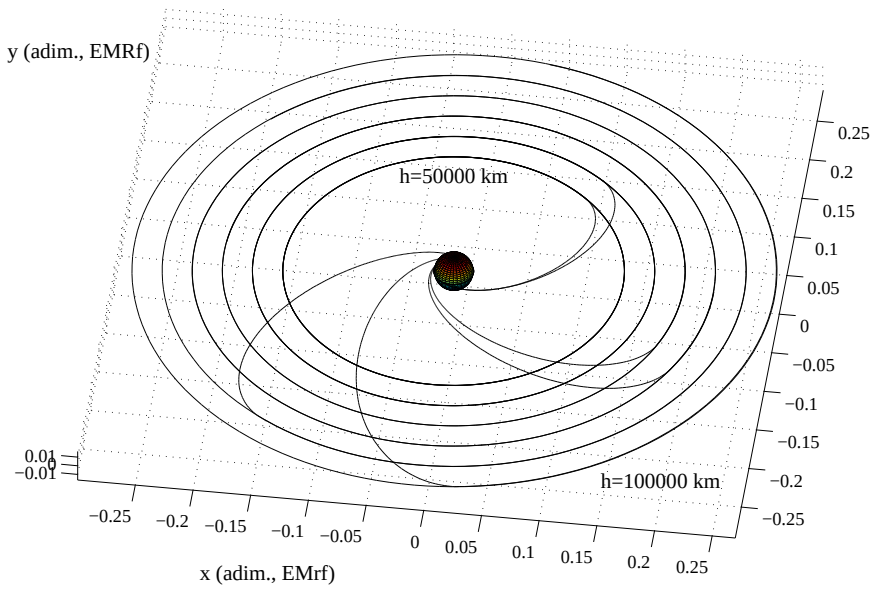

Figure 7.3: Results for the LEO to HEO Moon assisted transfers.

to the 100000 km HEO. This is an interesting result since it allows to save around 11% of Δv with the same time.

Figure 7.3 represents the six solutions in table 7.3. It can be observed that the Moon phase does not have a unique solution for the six cases but it varies with the transfer considered. Again the time remains equal to the Hohmann time of transfer.

LEO to HEO		
h (km)	$\Delta v - \Delta v_H$ (m/s)	Δt $(days)$
50000	-207	0.30
60000	-265	0.38
70000	-306	0.46
80000	-374	0.55
90000	-425	0.64
100000	-476	0.74

Table 7.3: Results for the LEO to HEO Moon assisted transfers.

7.4 Transfers between Earth orbits: uses for space missions

In this chapter, the common orbital transfer between two Earth orbits has been analyzed in the frame of the Earth-Moon restricted problem. The leading idea has been the exploitation of the Moon's perturbation for transfers to high altitude orbits.

7.4.1 Remarks

The problem seems to be well posed and the authors guess that it has a unique minimum. The solution showed in this chapter have evidently demonstrated that it is possible to lower the cost associated to these transfers by taking into account the Moon's effect. The matter is to find the appropriate Moon phase suitable for the considered transfer. Up to 476 m/s could be saved for transfers to high altitude Earth orbits; this advantage reduces to 117 m/s for transfers to geostationary orbits.

The important feature of these trajectories is that they do not involve, as in the previous chapters, an increasing on the time of transfer but give the usual conic-like 180 deg solution.

7.4.2 Uses for space missions

The application of these trajectories is obvious due to their formulation: they can be used in any transfer to a high altitude orbit; the benefit increases with the final altitude.

Most of the Earth satellites are placed in the geostationary orbit because there, the fixed position with respect to the azimuth, allows the satisfaction of a lot of mission constraints. The cost associated to these transfers could be lowered and so the mass of the payloads could be increased.

Recently, there is a great interest concerning the space debris and several studies conclude that the end-of-life spacecrafts must be placed in appropriate high-altitude belts. Since low-energy manoeuvres are needed for such transfers, the spacecraft could exploit the Moon's attraction to move in a high-altitude stable orbit by simply adopting the technique showed here.

7.4.3 Drawbacks

The usual drawbacks associated to orbits exploiting more than one gravitational attractions concern the times of transfer. Here, thanks to the devel-

oped technique, short times have been obtained, meaning that they require the same time as in the Hohmann transfer.

From the authors' point of view, the only drawback associated to these trajectories is the transfer window that has to consider the appropriate Moon phase. Thus, if a spacecraft is in the LEO orbit, it has to wait for the right Moon phase to make the transfer. This is not a particular restriction since the synodic period between the considered LEO and the Moon is expected to be very short.

Conclusions and Final Remarks

This work has been carried out in a two-month study (from April to June 2004) within the Ariadna context, under ESA contract, with the intention to assess the uses of the libration points and generic non-linear chaotic trajectories for space applications.

Some of all the potential uses of the libration points for space missions have been discussed in this report. The actual state of the art, known to the authors, has been analyzed from both the concepts and the technical point of view. Since no general methods were available for the analysis of such a missions, the authors have first developed the mathematical tool and then they have evaluated the possible missions within this scenario.

Even if both the missions on halos in the Sun-Earth system and the interplanetary transfer have been analyzed, special emphasis has been given to the Earth-Moon system: transfers to the Moon and to the halos around$L1$ and $L2$ in this frame have turned out to be quite interesting. This is because the authors believe that the powerful dynamics and the potential uses offered by these two libration points could be better exploited in the Earth-Moon system: cheap and short-time transfers have been demonstrated to exist in this frame. Later, the uses of such trajectories for future space missions have been discussed together with the possible drawbacks and some considerations at system level.

Again in this system, the outcome concerning the Moon assisted orbital transfers between two orbits around the Earth seems interesting because with the same times, cheaper transfers could be accomplished if the appropriate lunar phase is selected.

The authors believe that libration points and invariant manifolds could represent a powerful tool to carry out future space missions with unique performances. Here, the intention has been to demonstrate that such studies, aimed to assess the effectiveness of these concepts, are on the right way for a complete characterization of their potential uses. Nevertheless, in order to have a full scenario of all the features concerning specific missions, further and more intensive studies are necessary.

For instance, an observation arises: throughout the work it has been shown that as the spacecraft is in the chaotic region, just small thrusts are necessary to guide it to the desired paths. This scenario could be very useful in the case of low-thrust propelled spacecraft (e.g. by means of electric propulsion or solar sails) since in this case the intrinsic benefits due to the chaotic motion could combine together with the great savings in the propellant mass offered by the low-thrust propulsion.

Bibliography

[1] S.A. Astakhov, A.D. Burbanks, S. Wiggins and D. Farrelly – *Chaos-Assisted Capture of Irregular Moons* – Nature, Vol. 423, pp. 264-267, 2003

[2] B.T. Barden and K.C. Howell – *Formation Flying in the Vicinity of Libration Point Orbits* – Paper AAS 98-169, AAS/AIAA Space Flight Mechanics Meeting, Monterey, California, 9-11 February, 1998

[3] R.H. Battin – *An Introduction to the Mathematics and Methods of Astrodynamics* – AIAA, New York, 1987

[4] E.A. Belbruno and J.K. Miller – *Sun-Perturbated Earth-to-Moon Transfers with Ballistic Capture* – Journal of Guidance, Control and Dynamics, Vol. 16, No. 4, pp. 770-775, 1993

[5] E.A. Belbruno, R. Humble and J. Coil – *Ballistic Capture Lunar Transfer Determination for the US Air Force Academy Blue Moon Mission* – Paper AAS 97-171, AAS/AIAA Space Flight Mechanics Meeting, Alabama, 9-12 February, 1997

[6] M. Bellò Mora, F. Graziani, P. Teofilatto, C. Circi and M. Porfilio – *Study on Software Tool for Construction of Weak Boundary Transfers* – Mid Term Review, GMVSA 4070/99, 1999

[7] M. Bellò Mora, F. Graziani, P. Teofilatto, C. Circi, M. Porfilio and M. Hechler – *A systematic Analysis on Weak Stability Boundary Transfers to the Moon* – IAF-00-A.6.03, IAC 2000, Rio de Janeiro, Brazil, 2-6 October, 2000

[8] R. Biesbroek – *Study on Lunar Trajectories from GTO by Using Weak Stability Boundary Transfers and Swing-by's* – ESTEC Working Paper n. 2014

[9] E.M. Bolt and J.D. Meiss – *Targeting Chaotic Orbits to the Moon Through Recurrence* — Physics Letters A 204, pp. 373-378, 1995

[10] R. Broucke – *Traveling Between the Lagrangian Points and the Moon* – Journal of Guidance and Control, Vol. 2, No. 4, pp. 257-263, 1979

[11] A. Castillo et al – *Use of Weak Stability Boundary Trajectories for Planetary Capture* – IAF-03-A.P.31, IAC 2003, Bremen, Germany, Sept. 29 - Oct. 03, 2003

[12] J. Cobos and J. Masdemont – *Astrodynamical Applications of Invariant Manifolds Associated with Collinear Lissajous Libration Orbits* – International Conference on Libration Point Orbits and Applications, Girona, Spain, 10-14 June, 2002

[13] G. Colombo – *On the Satellites of the Earth-Moon System (in Italian)* – Atti dell'Accademia Nazionale dei Lincei. Rendiconti, Series 8, Vol. 28, pp. 169-172, 1960

[14] G. Comoretto – *WSB Transfers Optimization Using a Combination of Euristhic Methods and SQP (in Italian)* – M.S. Thesis, Politecnico di Milano, A.A. 1999-2000

[15] L.A. D'Amario and T. N. Edelbaum – *Minimum Impulse Three-Body Trajectories* – AIAA Journal, Vol. 12, No. 4, pp. 455-462, 1974

[16] P. Dysli – *Analytical Ephemerides for Planets* – Dysli, 1977

[17] D.W. Dunham and R.W. Farquhar – *Libration Point Missions, 1978-2002* – International Conference on Libration Point Orbits and Applications, Girona, Spain, 10-14 June, 2002

[18] J. Fabrega, T. Schirmann, R. Schmidt and D. Mc Coy – *Venus Express: The First European Mission to Venus* – IAC-03-Q.2.06, IAC 2003, Bremen, Germany, Sept. 29 - Oct. 03, 2003

[19] R.W. Farquhar – *Lunar Communications with Libration-.Point Satellites* – Journal of Spacecraft and Rockets, Vol. 4, No. 10, pp. 1383-1384, 1967

[20] R.W. Farquhar – *Future Missions for Libration-Point Satellites* – Astronautics & Aeronautics, Vol. 7, No. 5, pp. 52-56, 1969

[21] R.W. Farquhar – *Comments on "Optimal Control for Out-of-Plane Motion about the Translunar Libration Point"* – Journal of Spacecraft and Rockets, Vol. 8, No. 7, pp. 815-816, 1971

[22] R.W. Farquhar – *A Halo-Orbit Lunar Station* – Astronautics & Aeronautics, Vol. 10, No. 6, pp. 59-63, 1972

[23] R.W. Farquhar, D.P. Muhonen and D.L. Richardson – *Mission Design for a Halo Orbiter of the Earth* – Journal of Spacecraft and Rockets, Vol. 14, No. 3, pp. 170-177, 1977

[24] R.W. Farquhar – *Halo-Orbit and Lunar Swing-by Missions of the 1990's* – Acta Astronautica, Vol. 24, pp. 227-234, 1991

[25] F. Gabern and Á. Jorba – *A Restricted Four-Body Model for the Dynamics near the Lagrangian Points of the Sun-Jupiter System* – Discrete and Continuous Dynamical System, Series B, Vol.1, n.2, 2001, pp. 143-182

[26] F. Galgani – *Low-Energy Transfer Orbits in the Earth-Moon System (in Italian)* – M.S. Thesis, Politecnico di Milano, A.A. 1998-1999

[27] G. Gòmez and J.M. Mondelo – *The Dynamics Around the Collinear Equilibrium Points of the RTBP* – Physica D 157, pp. 283-321, 2001

[28] G. Gòmez, W.S. Koon, M.W. Lo, J.E. Marsden, J. Masdemont and S.D. Ross – *Invariant Manifolds, the Spatial Three-Body Problem and Space Mission Design* – Paper AAS 01-301, AAS/AIAA Astrodynamics Specialist Conference, Quebec City, Canada, July 30 - Aug. 2, 2001

[29] G. Gòmez, J. Masdemont and J.M. Mondelo – *Libration Point Orbits: a Survey from the Dynamical Point of View* – Libration Point Orbits and Application, Parador d'Aiguablava, Girona, Spain, 10-14 June, 2002

[30] T.A. Heppenheimer – *Steps Toward Space Colonization: Colony Location and Transfer Trajectories* – Journal of Spacecraft and Rockets, Vol. 15, No. 5, pp. 305-312, 1978

[31] C.R. Houck, J.A. Joines and M.G. Kay – *A Genetic Algorithm for Function Optimization: A Matlab Implementation* – NCSU-IE TR 95-09, 1995

[32] K.C. Howell, B.T. Barden and M.W. Lo – *Application of Dynamical System Theory to Trajectory Design for a Libration Point Mission* – The Journal of Austronautical Sciences, Vol. 45, n. 2, pp. 161-178, 1997

[33] D. Jamison – *Uses of the Trojan Libration Points of the Earth-Sun System* – Journal of Spacecraft and Rockets, Vol. 3, No. 4, pp. 595-596, 1966

[34] A.B. Jenkin and E.T. Campbell – *Generic Halo Orbit Insertion and Dispersion Error Analysis* – Paper AIAA 2002-4527, AIAA/AAS Astrodynamics Specialist Conference and Exhibit, Monterey, California, 5-8 August, 2002

[35] B.L. Jones and R.H. Bishop – *Rendezvous Targeting and Navigation for a Translunar Halo Orbit* – Journal of Guidance, Control and Dynamics, Vol. 17, No. 5, pp. 1109-1114, 1994

[36] Á. Jorba and J. Masdemont – *Dynamics in the Center Manifold of the Collinear Points of the Restricted Three Body Problem* – Physica D 132, pp. 189-213, 1999

[37] Á. Jorba and J. Masdemont – *Nonlinear Dynamics in an Extended Neighbourhood of the Translunar Equilibrium Point*– Hamiltonian System with Three or More Degrees of Freedom, Kluwer Academic Publishers, 2001

[38] O. Junge, J. Levenhagen, A. Seifried and M. Dellnitz – *Identification of Halo Orbits for Energy Efficient Formation Flying* – Proceedings of the International Symposium Formation Flying, Toulouse, France, 29-31 October, 2002

[39] J.A. Kechichian – *Computational Aspects of Transfer Trajectories to Halo Orbits* – Journal of Guidance, Control and Dynamics, Vol. 24, No. 4, pp. 796-804, 2001

[40] M. Kim and C.D. Hall – *Lyapunov and Halo Orbits about L2* – Paper AAS 01-324, AAS/AIAA Astrodynamics Specialist Conference, Quebec City, Canada, July 30 - Aug. 2, 2001

[41] W.S. Koon, M.W. Lo, J.E. Marsden and S.D. Ross – *The Genesis Trajectory and Heteroclinic Connections* – Paper AAS 99-451, AAS/AIAA Astrodynamics Spacialist Conference, Girdwood, Alaska, 16-19 August, 1999

[42] W.S. Koon, M.W. Lo, J.E. Marsden and S.D. Ross – *Constructing a Low Energy Transfer between Jovian Moons* – Proceedings of the International Conference on Celestial Mechanics, Northwestern University, Chicago, Illinois, 15-19 December, 1999

[43] W.S. Koon, M.W. Lo, J.E. Marsden and S.D. Ross – *Heteroclinic Connections between Periodic Orbits and Resonance Transition in Celestial Mechanics* – Chaos, Vol.10, n.2, pp. 427-469, 2000

[44] W.S. Koon, M.W. Lo, J.E. Marsden and S.D. Ross – *Shoot the Moon* – Paper AAS 00-166, AAS/AIAA Astrodynamics Specialist Conference, Florida, 23-26 January, 2000

[45] J. Llibre, R. Martìnez and C. Simò – *Transversality of the Invariant Manifolds Associated to the Periodic Orbits near L2 in the Restricted Three-Body Problem* – Journal of Differential Equations, No. 58, pp. 104-156, 1985

[46] M.W. Lo and S.D. Ross – *Low Energy Interplanetary Transfers using the Invariant Manifolds of L1, L2 and Halo Orbits*– Paper AAS 98-136, AAS/AIAA Space Flight Mechanics Meeting, Monterey, California, 9-11 February, 1998

[47] M.W. Lo and S.D. Ross – *The Lunar L1 Gateway: Portal to the Stars and Beyond* – AIAA Space 2001 Conference, Albuquerque, New Mexico, August 28-30, 2001

[48] M.W. Lo and M.J. Chung – *Lunar Sample Return via the Interplanetary Superhighway* – Paper AIAA 2002-4718, AIAA/AAS Astrodynamics Specialist Conference and Exhibit, Monterey, California, 5-8 August, 2002

[49] M.W. Lo, R.L. Anderson, G. Whiffen and L. Romans – *The Role of Invariant Manifolds in Low-Thrust Trajectory Design*– Paper AAS 04-288, AAS/AIAA Space Flight Mechanics Meeting, Maui, Hawaii, 8-12 February, 2004

[50] E.E.N. Macau – *Using Chaos to Guide a Spacecraft to the Moon*– IAF-98-A.3.05, IAC 1998, Melbourne, Australia, Sept. 28 - Oct. 2, 1998

[51] M. Massari, F. Bernelli Zazzera and M. Vasile – *Trajectory Optimization for a Mission to NEOs using Low-Thrust Propulsion and Gravity Assist* – AAS/AIAA Space Flight Mechanics Meeting, Ponce, Puerto Rico, 9-13 February, 2003

[52] M. Massari, F. Bernelli Zazzera and R. Walker – *Optimal Trajectory Design for SIMONE Mission Study* – IAC-03-A.P.11, IAC 2003, Bremen, Germany, Sept. 29 - Oct. 03, 2003

[53] W.W. Mendell – *A Gateway for Human Exploration of Space? The Weak Stability Boundary* – Space Policy 00, 2001

[54] M. Molina – *Periodic Orbits for a Space Station in the Earth-Moon System (in Italian)* – M.S. Thesis, Politecnico di Milano, A. A. 1993-1994

[55] B.D.A. Prado – *Traveling between the Lagrangian Points and the Earth* – Acta Astronautica, Vol. 39, No. 7, pp. 483-486, 1996

[56] C.L. Pu and T.N. Edelbaum – *Four-Body Trajectory Optimization* – AIAA Journal, Vol. 13, No. 3, pp. 333-336, 1975

[57] D.L. Richardson – *A Note on a Lagrangian Formulation for Motion about the Collinear Points* – Celestial Mechanics, Vol. 22, No. 3, pp. 231-235, 1980

[58] D.L. Richardson – *Analytic Construction of Periodic Orbits about the Collinear Points* – Celestial Mechanics, Vol. 22, No. 3, pp. 241-253, 1980

[59] D.L. Richardson – *Halo Orbit Formulation for the ISEE-3 Mission* – Journal of Guidance and Control, Vol. 3, No. 6, pp. 543-548, 1980

[60] D.L. Richardson – *A Note on a Lagrangian Formulation for Motion about the Collinear Points* – Celestial Mechanics, Vol. 22, No. 3, pp. 231-235, 1980

[61] S.D. Ross – *Trade-Off Between Fuel and Time Optimization* – New Trends in Astrodynamics and Application, Princeton University, 20-22 January, 2003

[62] J. Schoenmaekers, D. Horas and J.A. Pulido – *SMART-1: With Solar Electric Propulsion to the Moon* – 16th International Symposium on Space Flight Dynamics, Pasadena, California, 3-7 December, 2001

[63] C.G. Schroer and E. Ott – *Targeting in Hamiltonian Systems that have a Mixed Regular/Chaotic Phase Spaces* – Chaos, Vol. 7, No. 4, pp. 512-519, 1997

[64] W. Seefelder – *Lunar Mission from GTO* – RT-DA 98/05, Institute of Astronautics, Technische Universität München, 1998

[65] C. Simò, G. Gòmez, Á. Jorba and J. Masdemont – *The Bicircular Model near the Triangular Libration Points of the RTBP* – From Newton to Chaos, Plenum Press, pp. 343-370, 1995

[66] T.F. Starchville and R.G. Melton – *Optimal Low-Thrust Trajectories to Earth-Moon L2 Halo Orbits (Circular Problem)* – Paper AAS 97-714, AAS/AIAA Astrodynamics Specialist Conference, Sun Valley, Idaho, 4-7 August, 1997

[67] T.F. Starchville and R.G. Melton – *Optimal Low-Thrust Transfers to Halo Orbits about the L2 Libration Point in the Earth-Moon System (Elliptical Problem)* – Paper AAS 98-205, AAS/AIAA Space Flight Mechanics Meeting, Monterey, California, 9-11 February, 1998

[68] V. Szebehely – *Theory of Orbits: The Restricted Problem of Three Bodies* – Academic Press inc., New York 1967

[69] R. Thurman and P.A. Worfolk – *The Geometry of Halo Orbits in the Circular Restricted Three-Body Problem* – Geometry Center Research Report, GCG95, University of Minnesota, 1996

[70] F. Topputo – *Invariant Manifolds of the Restricted Three-Body Problem: A New Tool for Low-Energy Interplanetary Transfers (in Italian)* – M.S. Thesis, Politecnico di Milano, A. A. 2002-2003

[71] F. Topputo, M. Vasile and A. Ercoli Finzi – *An Approach to the Design of Low Energy Interplanetary Transfers Exploiting Invariant Manifolds of the Restricted Three-Body Problem* – Paper AAS 04-245, AAS/AIAA Space Flight Mechanics Meeting, Maui, Hawaii, 8-12 February, 2004

[72] Various Authors – *Pharos Project* – Politecnico di Milano, Aerospace Engineering Department Internal Report, 2003

[73] Various Authors – *Space Weather* – CDF Study Report, CDF 11(A)

[74] M. Vasile and A. Ercoli Finzi – *Combining Evolutionary Programs and Gradient Methods for WSB Transfer Optimisation* – XVI Congresso Nazionale AIDAA, Palermo, 24-28 Settembre, 2001

[75] S. Wiggins – *Introduction to Applied Nonlinear Dynamical System and Chaos* – Springer, New York, 1990

[76] R.S. Wilson and K.C. Howell – *Trajectory Design in the Sun-Earth-Moon System Using Lunar Gravity Assist* – Journal of Spacecraft and Rockets, Vol. 35, No. 2, pp. 191-198, 1998

Web Sites

[77] *ACE Mission* – www.srl.caltech.edu/ACE

[78] *Genesis mission* – http://genesismission.jpl.nasa.gov

[79] *Halo Orbits of the Circular Restricted Three Body Problem* – www.geom.umn.edu/˜megraw/CR3BP_html/cr3bp_halo.html

[80] *Hiten Mission* – http://nssdc.gsfc.nasa.gov/planetary/nmc_sc/hiten.html

[81] *ISEE-3 Mission* – http://nssdc.gsfc.nasa.gov/space/isee.html

[82] *MAP Mission* – http://map.gsfc.nasa.gov/

[83] *Soho Mission* – http://www.esa.int/esaSC/120373_index_0_m.html

[84] *Wind Mission* – http://www-istp.gsfc.nasa.gov/istp/wind/